MARTEC™

Smart Solutions for Engineering,
Science and Computing

TP 13907E

ELASTIC AND POST YIELD STABILITY OF FRAMING

Prepared for

Transportation Development Centre
Transport Canada

by

Martec Limited

March 2002

Smart Solutions for Engineering,
Science & Computing

Martec Limited
1888 Brunswick Street, Suite 400
Halifax, Nova Scotia B3J 3J8 Canada

tel. 902.425.5101
fax. 902.421.1923
email. info@martec.com
www.martec.com

TP 13907E

ELASTIC AND POST-YIELD STABILITY OF FRAMING

by

Claude DesRochers, Ewa Pothier, John Crocker
Martec Limited

March 2002

The contents of this report reflect the views of Martec Limited and not necessarily those of the Transportation Development Centre of Transport Canada or of the Ship Structure Committee of the U.S. Coast Guard.

PROJECT TEAM

Principal Authors:

Claude DesRochers, MASc, PEng

Ewa C.P. Pothier, BEng, EIT

E.J. Crocker, MASc, PEng

Lei Jiang, PhD, PEng

Un sommaire français se trouve avant la table des matières.

Transport Canada / Transports Canada

PUBLICATION DATA FORM

1. Transport Canada Publication No.	2. Project No.	3. Recipient's Catalogue No.
TP 13907E	9771	

4. Title and Subtitle	5. Publication Date
Elastic and Post-Yield Stability of Framing	March 2002
	6. Performing Organization Document No.

7. Author(s)	8. Transport Canada File No.
C. DesRochers, E. Pothier and J. Crocker	ZCD2450-C-310-5

9. Performing Organization Name and Address	10. PWGSC File No.
Martec Limited 1888 Brunswick St., Suite 400 Halifax, N.S. Canada B3J 3J8	HAL-9-40591
	11. PWGSC or Transport Canada Contract No. T8200-9-99572/001/HAL

12. Sponsoring Agency Name and Address		13. Type of Publication and Period Covered
Transportation Development Centre (TDC) 800 René Lévesque Blvd. West Suite 600 Montreal, Quebec Canada H3B 1X9	Fisheries and Oceans Canada 200 Kent Street Station 7W080 Ottawa, Ontario Canada K1A 0E6	Final
		14. Project Officer A. Taschereau

15. Supplementary Notes (Funding programs, titles of related publications, etc.)

Co-sponsored by the U.S. Ship Structure Committee

16. Abstract

This study investigates the stability of framing in the hulls of ice-going ships, with emphasis on the post-yield stability of angle main frames. The aim was to identify accurate and practical criteria for evaluation of post-yield stability. The approach was by an empirical analysis of the results of a parametric series of finite element evaluations.

A Canadian Equivalent Standards-compliant 3x3 bay stiffened hull panel was modelled using the finite element method. The non-linear Finite Element Analysis (FEA) study was performed using a technique developed to enable main frame parameters to be varied independently. The series was performed to load levels exceeding the calculated F_{max} ice load; load induced biaxial in-plane compressive loads were included.

Limited relationships were established for the ship configuration studied. For wide variations in span, web depth, flange thickness and flange width, angle main frames did not experience buckling below a load level of $2*F_{max}$. Only two of the parameters affect the frame stability at the load levels of interest: web thickness and material yield strength.

It was found impractical to develop realistic formulae resembling current criteria.

Where critical, non-linear FEA should be performed to determine the specific post-yield buckling response of the designed structure. Procedures/guidelines should be developed for performing the non-linear analyses.

17. Key Words	18. Distribution Statement
Post-yield stability, angle main frame, finite element analysis, FEA, single-skin icebreaker hull	Limited number of copies available from the Transportation Development Centre

19. Security Classification (of this publication)	20. Security Classification (of this page)	21. Declassification (date)	22. No. of Pages	23. Price
Unclassified	Unclassified	—	xx, 66, apps	Shipping/ Handling

Transports Canada Transport Canada

FORMULE DE DONNÉES POUR PUBLICATION

1. N° de la publication de Transports Canada	2. N° de l'étude	3. N° de catalogue du destinataire
TP 13907E	9771	

4. Titre et sous-titre	5. Date de la publication
Elastic and Post-Yield Stability of Framing	Mars 2002
	6. N° de document de l'organisme exécutant

7. Auteur(s)	8. N° de dossier - Transports Canada
C. DesRochers, E. Pothier et J. Crocker	ZCD2450-C-310-5

9. Nom et adresse de l'organisme exécutant	10. N° de dossier - TPSGC
Martec Limited 1888 Brunswick St., Suite 400 Halifax, N.S. Canada B3J 3J8	HAL-9-40591
	11. N° de contrat - TPSGC ou Transports Canada
	T8200-9-99572/001/HAL

12. Nom et adresse de l'organisme parrain		13. Genre de publication et période visée
Centre de développement des transports (CDT) 800, boul. René-Lévesque Ouest Bureau 600 Montréal (Québec) Canada H3B 1X9	Pêches et Océans Canada 200, rue Kent Station 7W080 Ottawa (Ontario) Canada K1A 0E6	Final
		14. Agent de projet
		A. Taschereau

15. Remarques additionnelles (programmes de financement, titres de publications connexes, etc.)

Coparrainée par le U.S. Ship Structure Committee

16. Résumé

La présente étude porte sur la stabilité des membrures de coques de navires de cote arctique, et plus précisément sur la stabilité post-élastique de profilés servant de membrures principales. Le but était d'établir des critères précis et pratiques d'évaluation de la stabilité dans le domaine plastique. Pour cela, les résultats d'une série d'évaluations paramétriques par la méthode des éléments finis ont été soumis à une analyse empirique.

Un panneau de coque renforcé selon un quadrillage 3 x 3 et conforme aux Normes équivalentes canadiennes a été modélisé à l'aide de la méthode des éléments finis. Pour l'analyse non linéaire par éléments finis (AEF), les chercheurs ont utilisé une technique qui permettait de faire varier indépendamment les paramètres relatifs aux membrures principales. L'analyse s'est poursuivie jusqu'à ce que les charges glacielles dépassent une force égale à la valeur F_{max} calculée; les contraintes de compression biaxiale dans le plan du panneau étaient prises en compte.

Des relations limitées ont été établies pour la configuration de navire étudiée. Pour de grandes variations de la portée, de la hauteur de l'âme, de l'épaisseur et de la largeur des ailes, les membrures n'ont pas flambé, sous des sollicitations inférieures à $2*F_{max}$. Seulement deux des paramètres étudiés ont influé sur la stabilité de la structure sous les charges étudiées : l'épaisseur de l'âme et la limite élastique du matériau.

Il s'est révélé impossible de traduire les relations observées en des formules réalistes assimilables aux critères en vigueur.

Une AEF non linéaire devrait être effectuée pour déterminer la tenue au flambement de la structure étudiée dans le domaine plastique. Des procédures/directives devraient être élaborées pour guider les analyses non linéaires.

17. Mots clés	18. Diffusion
Stabilité dans le domaine plastique, stabilité post-élastique, membrure principale profilée, analyse par éléments finis, AEF, coque de brise-glace à paroi homogène	Le Centre de développement des transports dispose d'un nombre limité d'exemplaires.

19. Classification de sécurité (de cette publication)	20. Classification de sécurité (de cette page)	21. Déclassification (date)	22. Nombre de pages	23. Prix
Non classifiée	Non classifiée	—	xx, 66, ann.	Port et manutention

EXECUTIVE SUMMARY

The design of ice-going ships for operation in Canadian waters is currently controlled and regulated by the *Equivalent Standards for the Construction of Arctic Class Ships,* which includes stability criteria for scantlings that are used in ship design. However, more accurate and practical criteria continue to be developed that are valid for extreme load cases.

In the current Equivalent Standards, stability of framing is controlled by two sets of equations. The first set was developed for the purpose of controlling tripping of frames and is based on span and web ratios. The second set of rules was developed to control local buckling of frames. The two sets of rules are based on designing a structure to exceed its elastic limit before it experiences either tripping or local buckling. The equations are based on linear assumptions and are valid only up to the point of yielding.

This project is the latest in an initiative to incorporate practical and more accurate stability criteria into the Equivalent Standards, particularly in the post-yield range. The primary objective of this project was to apply Finite Element Modelling to obtain empirical performance results that could be expressed by formulae resembling those of the current Equivalent Standards.

A literature survey was undertaken to identify all current work that is relevant to post-yield structural stability of laterally loaded stiffeners on plated structures. It included all fields and was not limited to ship structures. The literature survey did not uncover any work being performed that is relevant to this project.

The present design criteria, as laid out in the Equivalent Standards, were thoroughly reviewed to understand how the equations were derived and to determine their applicability in the non-linear regime. The main results of the review were that the current stability equations could not be expected to predict the non-linear flexural-torsional buckling of stiffened panel main frames that is observed in nature as a response to a laterally applied load.

The structure used for analysis in this study is a portion of a single skin icebreaker hull. It consists of a 3x3 bay stiffened panel that is typical of an icebreaking ship hull. One bay of this panel is shown in Figure 1.

A series of linear eigenvalue buckling analyses were performed. The buckling load levels showed no correlation with those predicted using the current equations. It was concluded that this is because the response is dominated by highly non-linear phenomena. Non-linear post-yield analyses were performed to establish relationships between key parameters that describe the hull scantlings and the buckling load for main frames. The applied ice load results in two components of load: an in-plane load and a lateral load. The lateral load component of the ice load is evident. The in-plane load component is produced by the overall ship bending response and the "local-global" bending between adjacent bulkheads and decks. The global bending response produces a biaxial in-plane compressive load in the hull.

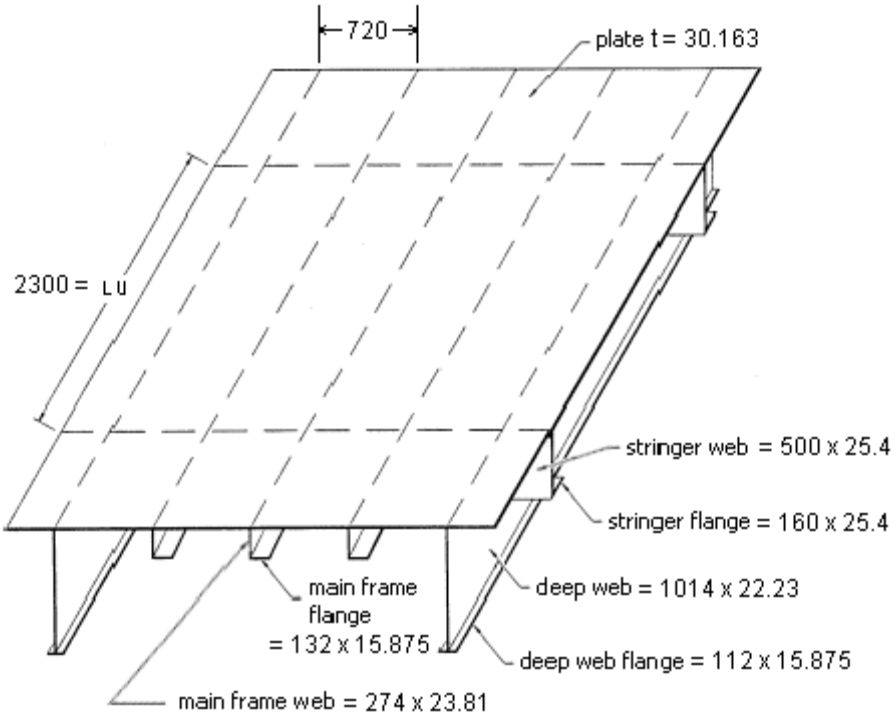

Note: Units are in millimetres

Figure 1 Elements of Stiffened Panel Construction

Key geometric parameters were selected and the panel geometry altered by varying these independently. Finite Element Analysis (FEA) was then used in a semi-empirical manner to study the response of the structure to these modifications. The study was restricted to angle section main frames, and it was expected that the most important parameters affecting the buckling load would be: span, yield stress, flange width, flange thickness, web height and web thickness.

The yield stress was manipulated so that the "strength" of the frame was unchanged as each single parameter was varied. Thus, the initiation of yield in the frame always occurred at the same value of applied lateral load.

In the non-linear solution algorithm, all of the loads and load related "initial" conditions are incrementally increased at each load step in direct proportion to each other. The effect of the in-plane load was studied by varying its "nominal" level. The nominal in-plane load is defined as the magnitude of the in-plane load at an applied ice load equal in magnitude to F_{max}. It was found that as the proportion of nominal in-plane load to lateral ice load is increased, buckling occurs at a lower overall load level.

In previous phases of this work, it was found that main frame stability is heavily affected by the magnitude of the material yield strength. Since yield strength was modified to offset the effects of varying parameters, the effect of yield strength on stability needed to be determined independently. A series of runs was completed where only the yield strength was modified. The relationship between the yield strength and the buckling load factor (BLF) was found to be linear, as can be seen in Figure 2. The panel becomes more stable in the post-yield regime as the yield strength is increased.

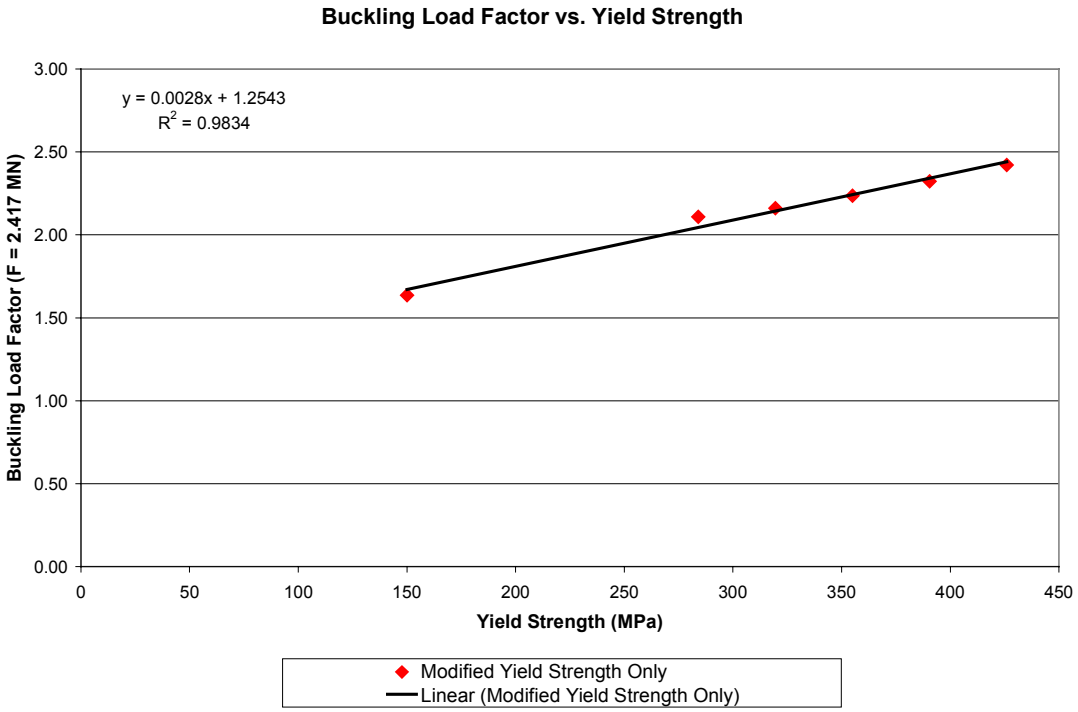

Figure 2 BLF vs. Yield Strenth

This relationship, in the form of the equation displayed in Figure 2, was used to adjust the results of the other runs to take into account the change in yield strength. It is important to note that for this particular panel, the curve does not go below F_{max} until the yield strength of the material is reduced to a value too small to be practical in design.

Linearly, under compressive loads, the buckling load of typical column-like structures depends on the inverse of span squared. Thus, as the unsupported length (or span), increases, the buckling load decreases. A similar relationship was anticipated in the case of the non-linear runs. However, this trend was not found. The results are plotted in Figure 3.

The relationship found for the effect of span on stability is rather counter-intuitive. Initially, as one might expect, the stability of the panel decreases as the span is increased. However, for spans greater than about two metres, this trend reverses and the stability begins to increase as

the span is increased. The curve in Figure 3 shows a change in buckling load as span is varied, but it appears to be bounded by a horizontal line at BLF = 2.

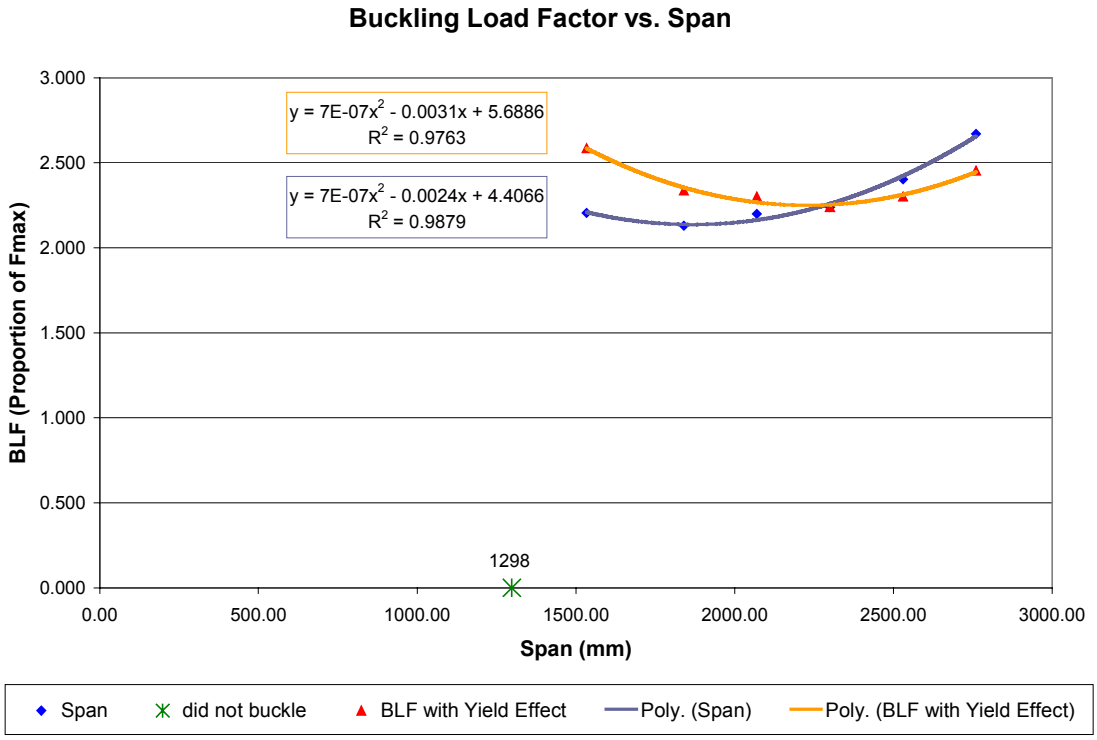

Figure 3 BLF vs. Span

Figure 3 also includes a curve with the yield strength effect described above accounted for (using the linear equation found in Figure 2). It can be seen that the effect of changing the yield strength is minimal.

Analysing the results of the non-linear FEA for the varying web depth, flange thickness and flange width series of analyses, the curves of BLF vs. dimension of the parameter were found to be similarly bounded by a horizontal line at BLF = 2. That is, regardless of the dimensions of the span, web depth or flange, the main frames do not experience buckling below a load level of $2^* F_{max}$.

An exception to this bounding phenomenon was found in the web thickness series of non-linear analyses. The post-yield buckling load level for these runs is plotted versus the web thickness in Figure 4. As can be seen from the figure, there is a linear dependence of buckling load on frame web thickness. The stability of the panel increases as the web thickness is increased. Again, the comparison of the results from the actual analyses and the results with the yield strength effect accounted for is shown in the figure. It can be seen that the effect of changing the yield strength is again minimal.

Therefore, in summary, only two parameters affect the frame stability at the load levels of interest: web thickness and material yield strength.

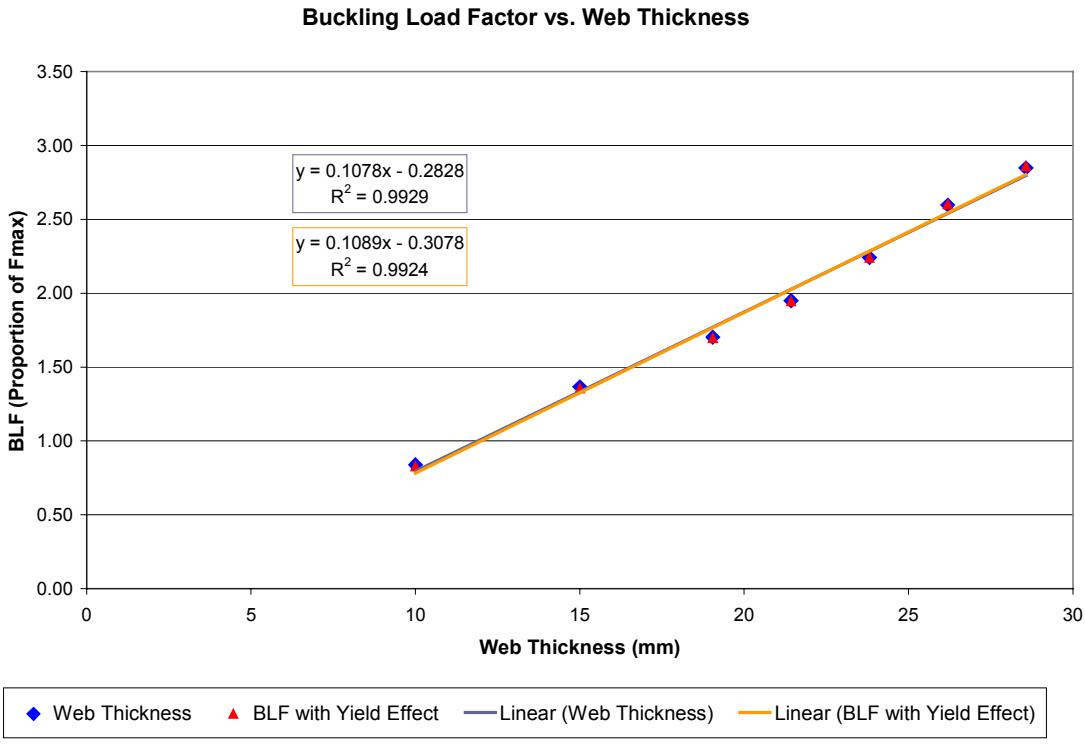

Figure 4 BLF vs. Web Thickness

It must be understood that all of the information generated in this study is based on one ship configuration (i.e., displacement and power). Scantling dimensions have been varied extensively for this ship and there is a high level of confidence that the relationships defined for this ship are accurate and that post-yield buckling will not be a problem except for frames with very thin webs. However, whether this will hold for all ships of varying displacement and power has yet to be determined and was beyond the scope of this project.

Upon completion of this study, it appeared that it would not be practical (or perhaps even possible) to identify analytical relationships that would accurately predict post-yield buckling because the response is too complicated. It is quite possible that the approach taken in the future will be that ship designers will use formulae only to provide an initial design that will then be verified and optimized by non-linear FEA.

It is therefore recommended that designers use the current Equivalent Standards rules for developing ship scantling sizes. Based on the results of this and previous phases of this study, main frames designed using the current rules for ship design show no trends toward post-yield buckling below F_{max}. In fact, most designs fail above 2* F_{max}.

It is also recommended that, where critical, non-linear FEA be performed to determine the specific post-yield buckling response of the designed structure. It is further recommended that procedures be developed for performing the non-linear analyses.

SOMMAIRE

La conception des navires de cote arctique admis dans les eaux canadiennes est actuellement réglementée par les *Normes équivalentes pour la construction des navires de cote arctique*, qui définissent des critères de stabilité visant les échantillonnages utilisés dans la conception des navires. Parallèlement à ces normes, des travaux se poursuivent en vue d'élaborer des critères plus précis et plus pratiques pour les cas de charges extrêmes.

Dans les Normes équivalentes actuelles, la stabilité des membrures est déterminée par deux ensembles d'équations. Les premières, qui régissent le déversement des membrures, sont fondées sur le rapport de la portée à l'âme. Les deuxièmes régissent le flambement local des membrures. Dans les deux cas, la structure doit être conçue de façon qu'elle ne puisse déverser ou flamber localement, à moins d'avoir atteint sa limite élastique. Les équations sont fondées sur des hypothèses linéaires et elles ne sont valides qu'en deçà de la limite élastique.

La présente étude est la dernière d'une série d'études qui visaient à incorporer dans les Normes équivalentes des critères de stabilité pratiques et plus précis, notamment dans le domaine plastique. L'objectif principal assigné à cette étude était d'utiliser la modélisation par éléments finis pour obtenir des données de comportement empirique qui pourraient être traduites en des formules semblables à celles des Normes équivalentes actuelles.

Une recherche documentaire a d'abord été entreprise, dans le but de recenser tous les travaux en cours s'intéressant à la stabilité structurelle post-élastique de raidisseurs fixés à des plaques, lorsque soumis à une pression latérale. Tous les types de structures, et non seulement les structures navales, intéressaient les chercheurs. Mais ils n'ont trouvé aucune recherche pertinente.

Les chercheurs ont ensuite examiné attentivement les critères de conception énoncés dans les Normes équivalentes, afin de comprendre comment les équations avaient été établies et de déterminer leur applicabilité à des analyses en régime non linéaire. L'examen a mené à une constatation cruciale, à savoir que les équations actuelles de stabilité ne peuvent prédire le flambement non linéaire par flexion et torsion des membrures principales d'un panneau renforcé, tel qu'il est observé dans la nature en réponse à l'application latérale d'une charge.

La structure utilisée pour l'analyse était un panneau renforcé selon un quadrillage de 3 x 3 représentant une partie de coque de brise-glace à bordé simple. La figure 1 montre un carré de ce panneau.

Une série d'analyses linéaires de flambement aux valeurs propres ont été effectuées. Aucune corrélation n'a pu être établie entre les résultats obtenus et les valeurs prédites selon les équations actuelles. Cette absence de corrélation a été attribuée au fait que les réponses sont fortement dominées par un phénomène non linéaire. Des analyses non linéaires dans le domaine élastique ont donc été réalisées afin d'établir des rapports entre les principaux paramètres qui décrivent les échantillonnages de la coque et la charge de flambement des membrures principales. La charge glacielle appliquée produit deux types de contraintes : une contrainte dans le plan du panneau et une pression latérale. La composante latérale de la

charge glacielle est manifeste. Quant à la composante qui agit dans le plan du panneau, elle résulte de la flexion globale de la coque et de la flexion «mi-locale, mi-globale» se produisant entre les parois et les ponts adjacents. La réponse de flexion globale engendre une charge de compression biaxiale dans le plan de la coque.

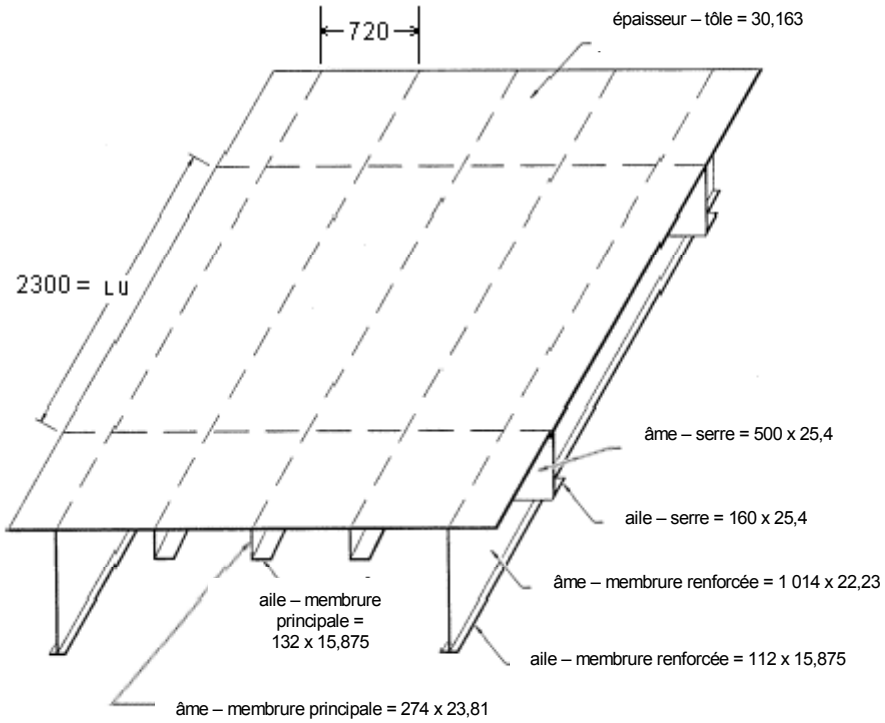

Figure 1 Panneau avec raidisseurs
(Nota : les mesures sont exprimées en millimètres)

Des paramètres clés relatifs à la géométrie du panneau ont été choisis et on a fait varier ceux-ci de façon indépendante. La méthode d'analyse par éléments finis (AEF) a alors été utilisée de façon semi-empirique pour étudier l'effet de ces variations sur la structure. L'étude a porté uniquement sur des membrures principales en forme de profilés. On s'attendait à ce que les paramètres suivants aient la plus grande influence sur la charge de flambement : la portée, la limite élastique, la largeur des ailes, l'épaisseur des ailes, la hauteur de l'âme et l'épaisseur de l'âme.

La limite élastique était établie de façon à garder la «résistance» de la membrure constante pendant que chaque paramètre variait. Ainsi, la membrure commençait toujours à flamber à la même valeur de charge latérale.

Dans l'algorithme de résolution non linéaire, toutes les charges et les conditions «initiales» reliées aux charges sont augmentées progressivement et en proportion directe les unes des autres. L'effet de la charge dans le plan du panneau a été étudié en faisant varier la valeur «nominale» de cette charge, laquelle est définie comme la valeur de la charge dans le plan du panneau sous une charge glacielle égale à F_{max}. À mesure que le rapport de la charge nominale

à la charge latérale (pression de la glace) augmentait, la charge globale menant au flambement diminuait.

Les phases antérieures du programme de recherche avaient révélé que la stabilité des membrures principales est fortement tributaire de la limite élastique du matériau. Comme, dans la présente étude, on modifiait la limite élastique pour compenser les effets de la variation des paramètres, il fallait mesurer de façon indépendante l'effet de la limite élastique sur la stabilité. Une série de cycles d'essais ont été réalisés, dans lesquels seule la limite élastique était modifiée. La relation entre la limite élastique et le facteur de charge de flambement (FCF) s'est révélée linéaire, comme on peut le voir à la figure 2. Ainsi, à mesure que la limite élastique augmente, le panneau est plus stable en régime post-élastique.

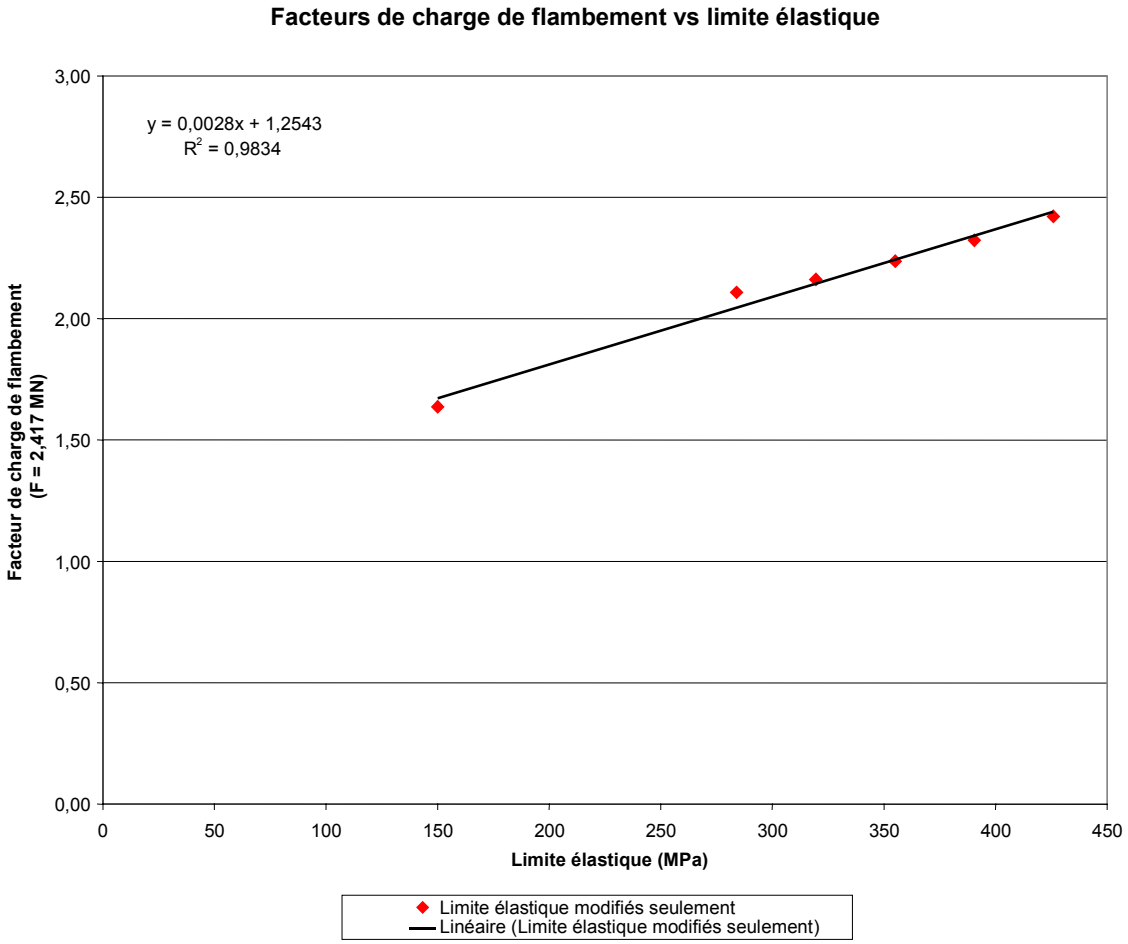

Figure 2 FCF vs limite élastique

Cette relation, exprimée par l'équation montrée à la figure 2, a été utilisée pour rajuster les résultats des autres cycles d'essais, de façon à prendre en compte la variation de la limite élastique. Il est important de noter que pour ce panneau en particulier, la courbe ne descend

sous F_{max} que lorsque la limite élastique du matériau est réduite à une valeur trop faible pour être envisagée dans la pratique.

En régime linéaire, sous des charges de compression, la charge de flambement de structures types en forme de colonnes varie en fonction inverse de la portée au carré. Ainsi, à mesure que la portée (longueur non soutenue) augmente, la charge de flambement diminue. Une relation semblable était attendue dans le cas des cycles d'essai en régime non linéaire. Toutefois, cela ne s'est pas avéré. Les résultats sont présentés à la figure 3.

La relation établie entre la portée et la stabilité défie plutôt l'intuition. Au départ, comme on peut s'y attendre, la stabilité du panneau diminue à mesure que la portée augmente. Toutefois, lorsque la portée dépasse les deux mètres, environ, cette tendance s'inverse et la stabilité se met à augmenter en même temps que la portée. Ainsi, la courbe de la figure 3 montre la variation de la charge de flambement en fonction de la portée, mais elle semble être limitée par une horizontale à FCF = 2.

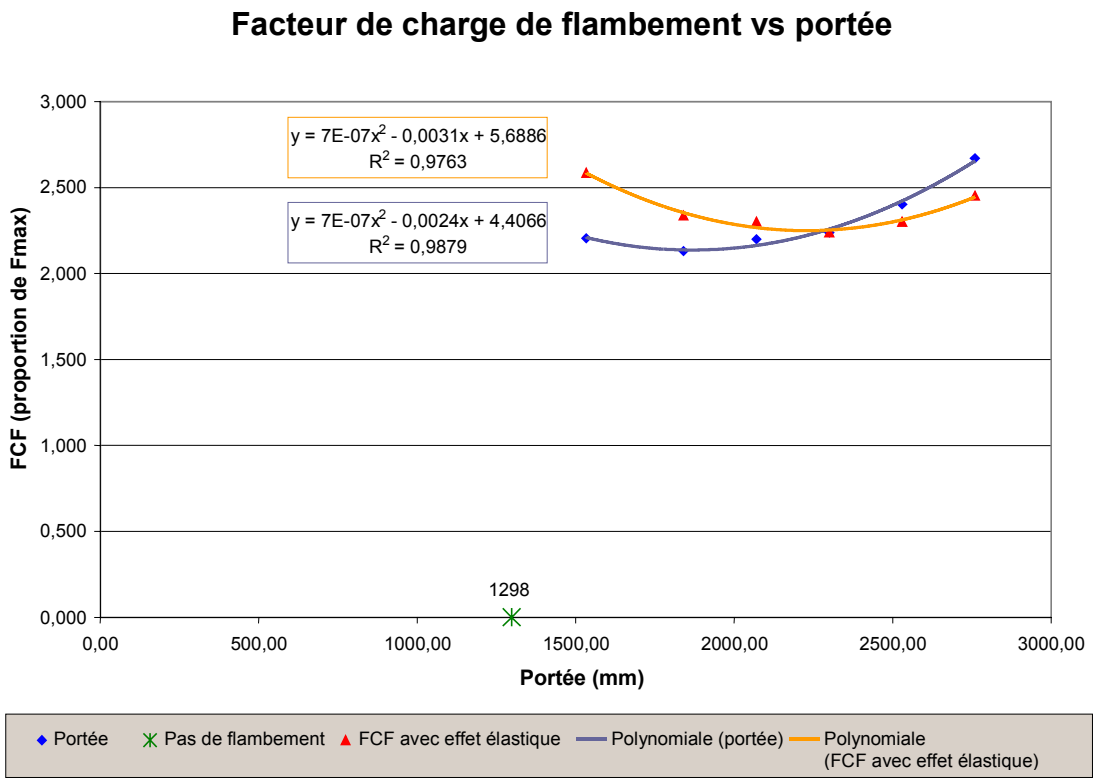

Figure 3 FCF vs portée

La figure 3 comprend également une courbe dans laquelle l'effet de la limite élastique décrite ci-dessus est pris en compte (à l'aide de l'équation linéaire reproduite à la figure 2). Il est facile de constater que la variation de la limite élastique a peu d'effet.

L'analyse des résultats des AEF non linéaires portant sur des hauteurs d'âmes et des épaisseurs et largeurs d'ailes variables a donné des courbes de FCF en fonction des dimensions des paramètres qui étaient limitées elles aussi par une horizontale à FCF = 2. C'est dire que, peu importent la portée, la hauteur de l'âme ou les dimensions des ailes, les membrures principales ne flambent pas sous des charges inférieures à $2*F_{max}$.

Une exception à ce phénomène de limitation a toutefois été constatée dans la série d'analyses non linéaires de l'épaisseur de l'âme. La figure 4 montre la charge de flambement post-élastique en fonction de l'épaisseur de l'âme, telle qu'établie lors de ces essais. Comme on peut le voir, la charge de flambement et l'épaisseur de l'âme de la membrure définissent une fonction linéaire. La stabilité du panneau augmente en raison directe de l'épaisseur de l'âme. Encore une fois, la figure permet de comparer les résultats des analyses réelles et les résultats obtenus lorsque la limite élastique est prise en compte. Et on peut voir, encore une fois, que la variation de la limite élastique du matériau produit peu d'effet.

Donc, pour résumer, deux paramètres seulement influent sur la stabilité des membrures sous les charges étudiées : l'épaisseur de l'âme et la limite élastique du matériau.

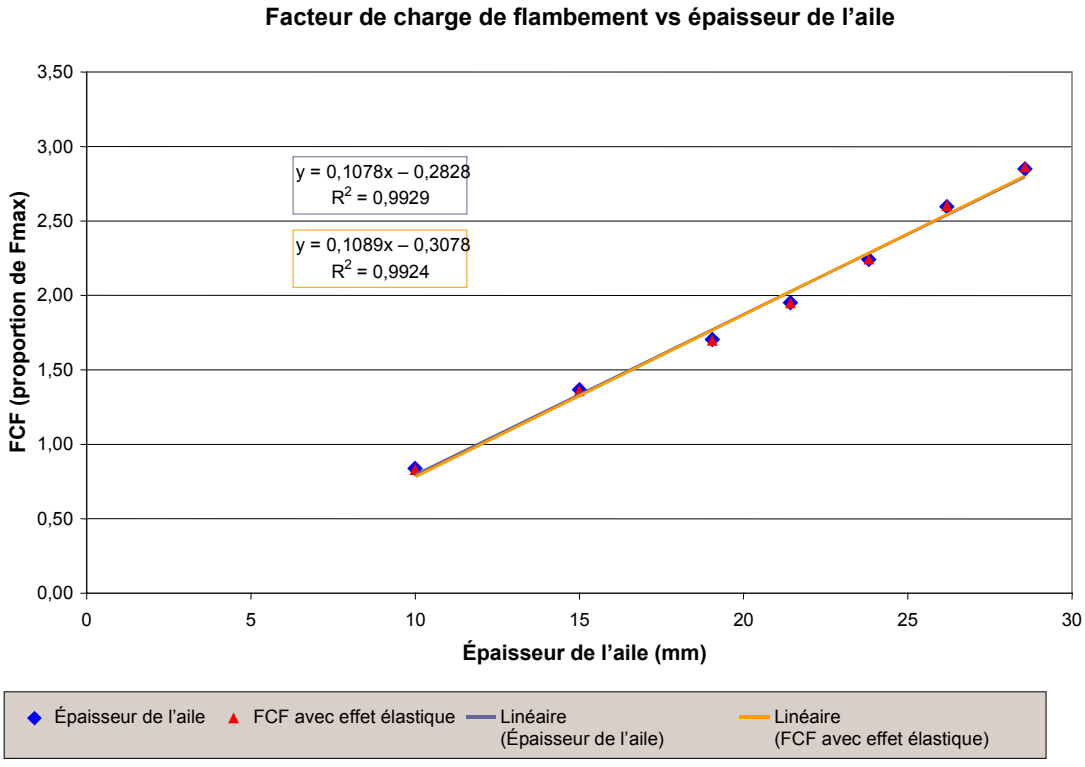

Figure 4 FCF vs épaisseur de l'aile

Il convient de noter que toutes les données générées au cours de cette étude sont fondées sur une seule configuration de navire (aux chapitres du déplacement et de la puissance). Des variations importantes des échantillonnages ont été étudiées pour ce navire et il est permis d'établir, avec un niveau de confiance élevé, que les relations définies pour ce navire sont

exactes et que le flambement post-élastique n'est pas un risque significatif, sauf dans le cas des membrures à âme très mince. Toutefois, il reste à déterminer si ces conclusions valent pour tous les navires affichant d'autres valeurs de déplacement et de puissance, ce qui dépassait la portée de ce projet.

Au terme de la présente étude, il est apparu qu'il serait difficile (voire impossible) de définir des relations analytiques permettant de prédire avec justesse le flambement post-élastique, parce que cette réponse est trop complexe. On peut penser que dans l'avenir, les architectes navals auront recours à des formules uniquement pour leurs travaux de conception initiale et qu'ils peaufineront ensuite leurs études à l'aide d'AEF non linéaires.

Il est donc recommandé que les concepteurs utilisent les Normes équivalentes en vigueur pour définir les dimensions des pièces de construction des navires. Selon les résultats de la présente étude et des phases antérieures de ce programme, les membrures principales conçues à la lumière des règles actuelles de conception des navires n'ont pas tendance à flamber dans le domaine plastique sous des charges inférieures à F_{max}. De fait, la plupart flambent sous des charges supérieures à $2*F_{max}$.

Il est également recommandé que, dans des cas critiques, une AEF non linéaire soit effectuée pour déterminer la tenue au flambement dans le domaine plastique propre à la structure étudiée. Il est en outre recommandé d'élaborer des procédures pour la réalisation des analyses non linéaires.

TABLE OF CONTENTS

LIST OF FIGURES

LIST OF TABLES

GLOSSARY OF ABBREVIATIONS AND ACRONYMS

ASPPR	Arctic Shipping Pollution Prevention Regulations
BLF	BLF
CAC	Canadian Arctic Class
DNV	Det Norske Veritas
Equivalent Standards	Equivalent Standards for the Construction of Arctic Class Ships
F_{max}	Maximum Applied Ice Load According to Eqiv. Stds.
FE	Finite Element
FEA	Finite Element Analysis
H_p	Horizontal Length of Ice Print
H_w	Web Height (Web Depth)
HW/TW	Web Ratio
LDC	Load Displacement Control
L_{DL}	Length of the Design Ice Load
LF	Load Factor
LU	Unsupported Length (Span)
LU/TW	Span Ratio for Flat Bars
LU/WF	Span Ratio
MN	Meganewton
MPa	Megapascals
MW	Megawatts
P	Load
P_a	Average Pressure on Ice Print outside Localized Higher Pressure Area
P_{av}	Average Pressure on Ice Print inside Localized Higher Pressure Area
S	Frame Spacing
TDC	Transportation Development Centre
V_p	Vertical Extent of the Design Ice Load
WF	Flange Width
Δ	Displacement in thousands of Tonnes
δ_x	Displacement in global *x* direction
δ_y	Displacement in global *y* direction
δ_z	Displacement in global *z* direction
θ_x	Rotation about global *x* direction
θ_y	Rotation about global *y* direction
θ_z	Rotation about global *z* direction
σ_T	flexural-torsional buckling stress
ϵ	Strain
[K]	Stiffness Matrix
$[K_G]$	Geometric Stiffness Matrix
{n}	Buckling Mode Shape
$\{\lambda\}$	Eignevalue Function

1. INTRODUCTION AND OBJECTIVES

This project represents Phase IV of an initiative to incorporate practical and more accurate stability criteria into the *Equivalent Standards for the Construction of Arctic Class Ships* [1], a document developed to control and regulate the design and manufacture of ice-going ships for operation in Canadian waters (hereinafter referred to as "Equivalent Standards"). The Equivalent Standards are the follow-on refined version of the previous *Arctic Shipping Pollution Prevention Regulations* (ASPPR)[2].

The present stability criteria in the Equivalent Standards were developed with the underlying philosophy that premature buckling will result in a structure that does not achieve its strength potential. Therefore, an efficient design would buckle at a design load level slightly higher than that required to cause structural failure by yielding or rupture. This would mean that for an acceptable design, a structure would never experience buckling, provided design loads were not exceeded. Traditionally, the design stresses have been yield stresses and the structure was designed such that, at a load level of sufficient magnitude to cause yielding, the structure should not buckle.

The Equivalent Standards have deviated from tradition and permit yielding of structural components at load levels corresponding to extreme, low-probability, ice interaction forces. The philosophy behind this is that the occurrence of these “extreme” loads is quite rare and a certain amount of permanent distortion should be tolerated provided that the structural integrity of the ship is not compromised. The structural integrity of the ship would be compromised if stresses exceeded the ultimate strength of the materials or if buckling (i.e., loss of stability) of structural members occurred.

By permitting yielding to occur, the formation of plastic hinges in framing is allowed to develop. This permits the utilization of plastic shear and bending capacities to carry incremental load. If instabilities are prevented throughout this process, then the potential to use the full plastic shear and bending capacity of frames can be achieved and a substantial reserve loading capacity is realized. Thus, the full plastic strength can be used to support the rare occurrence of extreme ice interaction loads. This will result in permanent damage to the ship but the overall structural integrity will be maintained, the underlying philosophy being that a ship can now be designed for no damage during “normal” loads but for some damage during “extreme” loads. This type of design will result in lighter and less expensive ships.

In the current Equivalent Standards, stability is controlled by two sets of equations. The first set was developed for the purpose of controlling tripping of frames and is based on span and web ratios as follows:

$$\frac{LU}{WF} \leq 300\ x\ N / V \qquad \text{for Angles}$$

$$\frac{LU}{WF} \le 395\ x\ N / V$$

or

$$\frac{HW}{TW} \le 155\ x\ N / V$$ for Tees

or

$$\frac{LU}{WF} \le \frac{395\ x\ N}{V\left(1-\left(155\ x\ N\ x\ TW\ /(HW\ x\ V)\right)^2\right)^{.75}}$$

$$\frac{LU}{TW} \le 710\ \ x\ \ N / V$$

or

$$\frac{HW}{TW} \le 168\ \ x\ \ N / V$$ for Flat Bars

or

$$\frac{LU}{TW} \le \frac{710\ \ x\ \ N}{V\left(1-\left(168\ \ x\ \ N\ \ x\ \ TW\ \ /(HW\ \ x\ V)\right)^2\right)^{1/2}}$$

where LU = Unsupported Length (Span)
WF = Flange Width
HW = Web Height (Depth)
TW = Web Thickness
N = 1 when $\partial \ge 85°$
N = $(1-\cos\partial)$ when $\partial < 85°$
V = $\sqrt{\frac{f_y \times Z_p}{Z_p^{AF}}}$

The second set of rules was developed to control local buckling of frames as follows:

$$\frac{HW}{TW} \le \frac{K}{\sqrt{\sigma_y}}$$ where: K = 1000 for Tee and Angle Sections

K = 282 for Flat Bars and
K = 155 for Outstand
σ_y = yield strength

The two sets of rules are based on designing a structure to achieve its elastic limit before it experiences either tripping or local buckling. The equations are based on linear assumptions and are valid up to the point of yielding. Details on the derivation of these equations are contained in the literature review in Section 5.

Section 2 of this report provides a description of the physical structure being modelled and defines some important terms. It also provides the panel dimensions used in the study. Section 3 presents the software used to complete the work and outlines the hardware on which the work was produced. A benchmark analysis was completed to verify the performance of the software and hardware to be used. A brief description of the benchmark analysis and its findings is included as Section 4.

Section 6 describes the panels selected for study and the modelling considerations involved in producing an acceptable model. The source of the applied loads is also presented.

Section 7 describes the procedure used to determine the load level at which an instability occurs. Because the structures studied do not generally experience a bifurcation type of buckling, the exact load level at which an instability is determined to be present is somewhat subjective.

The primary objective of this project was to apply Finite Element Modelling to obtain empirical performance results that could be expressed by formulae resembling those of the current Equivalent Standards. The present design criteria, as laid out in the Equivalent Standards, were thoroughly reviewed to understand how the equations were derived.

The next step was to determine whether the linear finite element (FE) representation of the buckling modes and load levels could be accurately represented by similar, simplified equations. The linear analyses and results are described in Section 8. The philosophy behind this approach is that once the linear applicability of the equations is established, then the possibility of extending the linear equations into the non-linear regime can be evaluated. The key parameters determined to be relevant for this study and the non-linear analyses and results are described in Section 9.

Section 10 presents a summary of the results, the conclusions drawn from the study and recommendations on how to proceed from this point.

Because of limited resources, this project did not encompass studying the entire range of main frame types (i.e., angles, tees, and flat bars). From previous studies [3, 4] it was determined that angle sections exhibit more of a propensity to non-linear buckling. Consequently, the project focused on the post-yield stability of angle main frames.

2. DESCRIPTION OF STRUCTURE AND DEFINITION OF TERMS

2.1 General Description of Structure

The structure used for analysis in this study was a portion of an icebreaker hull. It consisted of a stiffened panel that is typical of an icebreaking ship hull. The nominal dimensions used were taken from the work carried out in [4]. The single hull scantlings were chosen to conform to the Equivalent Standard strength and stability criteria for a CAC 3 ship.

Figure 2.1 shows a sketch of a ¼ finite element model of an icebreaking ship. This particular model of the *MV Arctic* was created for the Phase I [3] work, with the arrow identifying the midbody area of the model as the chosen region of study. The same area of an icebreaking ship will be modelled in the current project as a 3x3 bay stiffened panel, part of which is shown in Figure 2.2. This figure contains a sketch of one bay of the panel with the main structural components identified by name. As shown in Figure 2.2, the type of structure considered has three levels of support: main frames, stringers and deep web frames (sometimes referred to as "webs"). The panel is described in detail in Section 2.2.

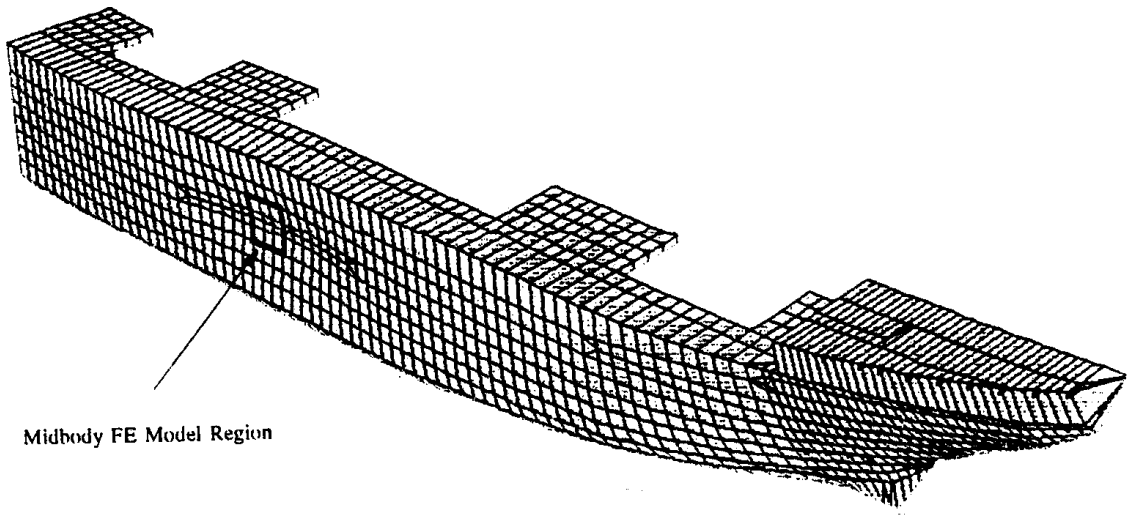

Figure 2.1 Sketch Showing 1/4 Model of an Icebreaker

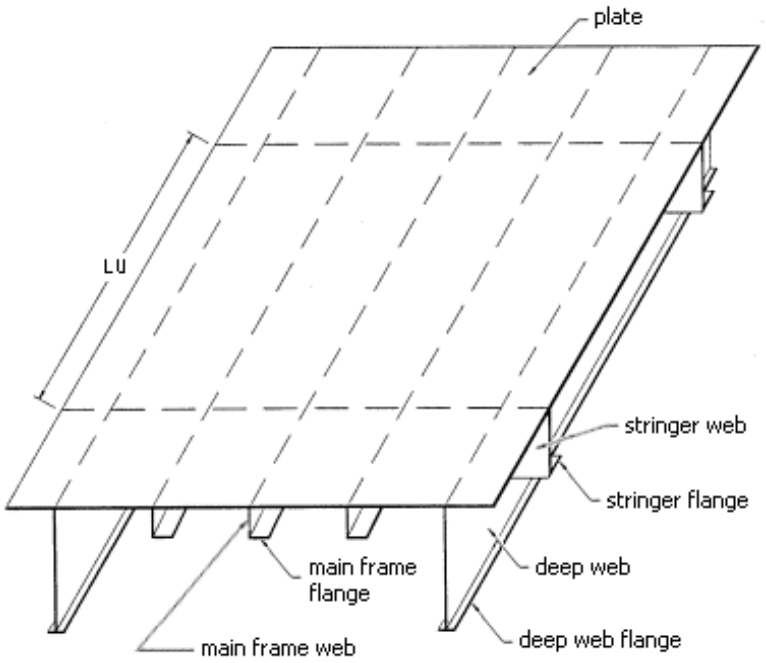

Figure 2.2 Elements of Stiffened Panel Construction

The panel design is based on a ship configuration as follows:

Displacement	12.00	kilotonnes
Power	15.00	megawatts
Material Yield Strength	355.00	megapascals
CAC	3	
Hull Area	Midbody	
Arctic Class Factor	0.6	
Area Factor for panel location	0.5	

2.2 Geometric Terms and Panel Dimensions

The stiffened panel used for this study was a panel design employing both transverse and longitudinal stiffeners, including stringers (parallel to the water line) as well as deep webs and main frames (perpendicular to the stringers). The individual elements of the panel construction, along with their dimensions, are illustrated in Figure 2.3. Dimensions are shown for the main frames as calculated for the base model, but these vary considerably among the different FE models. The main frames shown in Figure 2.3 are angle main frames.

The dimensions of the stringers, web frames and hull plating were taken from the panel designs determined from the study in [4]. The main frames were redesigned for a single hull configuration according to the Equivalent Standards. Table 2.1 lists the scantling dimensions and design criteria for each of the geometries considered.

Figure 2.4 shows a sketch of typical main frame cross sections. The variable names used to identify the dimensions are those defined in the Equivalent Standards.

This study consisted of an investigation of angle main frames only. The dimensions of the main frames varied from model to model and are listed in Table 2.1.

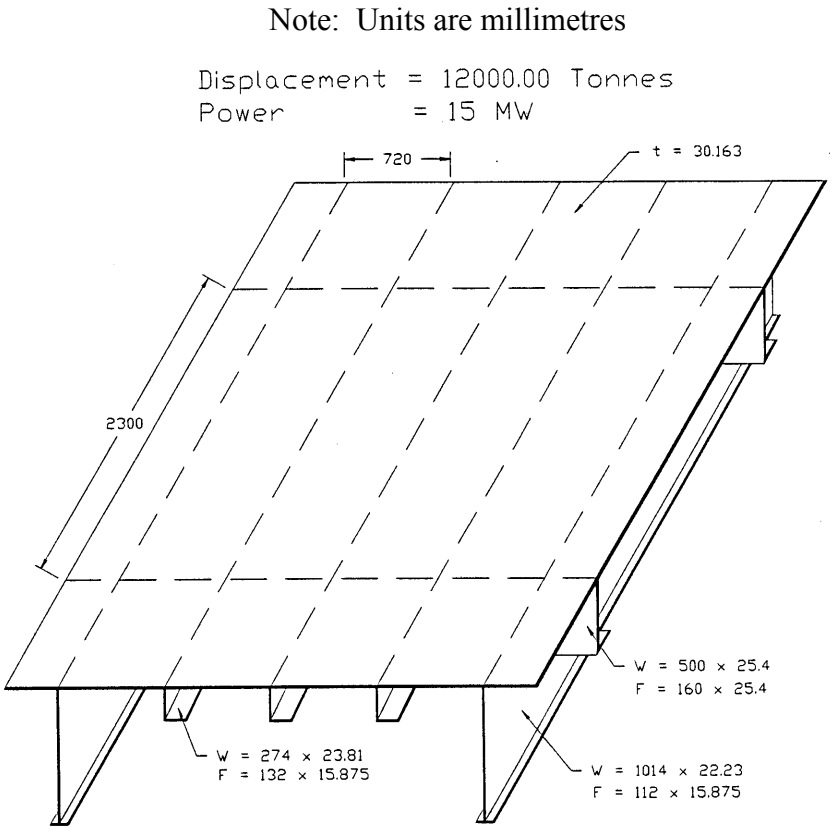

Figure 2.3 3 x 3 Bay Model (Showing the Centre Bay) with Angle Main Frames

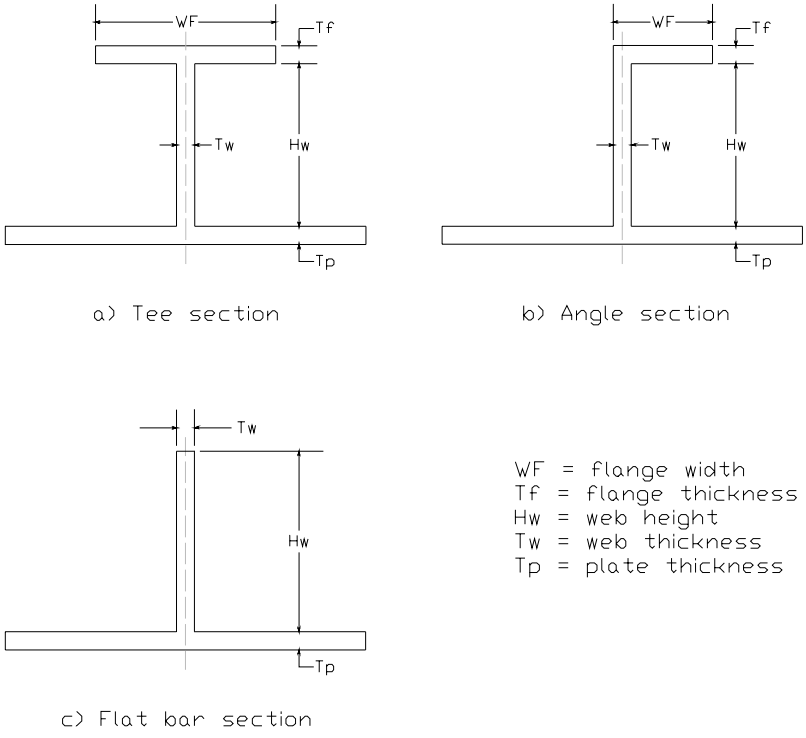

Figure 2.4 Main Frame Section Dimensions

Table 2.1 Scantling Dimensions Used in Study

Variable Dimensions:

Model Name	Run ID	Model Description	Span (mm)	Mainframe Dimensions (mm)				
				Frame Web Depth	Frame Web Thickness	Frame Flange Width	Frame Flange Thickness	Yield Stress (Mpa)
sep20_webs	**IV-1**	"Run 4" panel config.	2300	274	23.81	132	15.875	355
dec20_ip15	**-**	1.5 x in-plane load	2300	274	23.81	132	15.875	355
dec20_ip20	**-**	2.0 x in-plane load	2300	274	23.81	132	15.875	355
dec13_5x5_red	**-**	no in-plane load	2300	274	23.81	132	15.875	355
oct31_p10y	**-**	yield strength: +10%	2300	274	23.81	132	15.875	390.5
oct31_p20y	**-**	yield strength: +20%	2300	274	23.81	132	15.875	426.0
oct31_m10y	**-**	yield strength: -10%	2300	274	23.81	132	15.875	319.5
oct31_m20y	**-**	yield strength: -20%	2300	274	23.81	132	15.875	284.0
nov21_m577y	**-**	yield strength: -57.7%	2300	274	23.81	132	15.875	150.0
oct23_p10spy	**IV-2**	span: +10%	2530	274	23.81	132	15.875	390.5
oct11_p20spy	**IV-3**	span: +20%	2760	274	23.81	132	15.875	426
oct23_m10spy	**IV-4**	span: -10%	2070	274	23.81	132	15.875	319.5
oct11_m20spy	**IV-5**	span: -20%	1840	274	23.81	132	15.875	284
nov3_m33spy	**IV-6**	span: -33%	1533.3	274	23.81	132	15.875	236.7
nov22_m436spy	**IV-7**	span: -43.6%	1298	274	23.81	132	15.875	200.3
oct27_p25wfy	**IV-8**	flange width: +25%	2300	274	23.81	165	15.875	340.1
oct27_p50wfy	**IV-9**	flange width: +50%	2300	274	23.81	198	15.875	328.3
nov21_p894wfy	**IV-10**	flange width: +89.4%	2300	274	23.81	250	15.875	315.5
oct27_m25wfy	**IV-11**	flange width: -25%	2300	274	23.81	99	15.875	374.4
oct27_m50wfy	**IV-12**	flange width: -50%	2300	274	23.81	66	15.875	400.8
oct25_p20dw	**IV-13**	web depth: +20%	2300	328.8	23.81	132	15.875	286.8
nov3_p30dw	**IV-14**	web depth: +30%	2300	356.2	23.81	132	15.875	261.4
nov29_p46dw	**IV-15**	web depth: +46%	2300	400	23.81	132	15.875	228.4
nov3_m10dw	**IV-16**	web depth: -10%	2300	246.6	23.81	132	15.875	402.2
oct26_m20dw	**IV-17**	web depth: -20%	2300	219.2	23.81	132	15.875	463.0
nov8_p20tf	**IV-18**	flange thickness: +20%	2300	274	23.81	132	19.05	341.9
nov14_p50tf	**IV-19**	flange thickness: +50%	2300	274	23.81	132	23.813	325.6
nov28_p89tf	**IV-20**	flange thickness: +89%	2300	274	23.81	132	30	308.6
nov10_m20tf	**IV-21**	flange thickness: -20%	2300	274	23.81	132	12.7	370.5
nov14_m50tf	**IV-22**	flange thickness: -50%	2300	274	23.81	132	7.938	400.1
nov14_p10tw	**IV-23**	web thickness: +10%	2300	274	26.191	132	15.875	353.3
nov8_p20tw	**IV-24**	web thickness: +20%	2300	274	28.57	132	15.875	351.7
nov14_m10tw	**IV-25**	web thickness: -10%	2300	274	21.429	132	15.875	356.6
nov10_m20tw	**IV-26**	web thickness: -20%	2300	274	19.048	132	15.875	358.2
nov21_m37tw	**IV-27**	web thickness: -37%	2300	274	15	132	15.875	360.9
nov28_m58tw	**IV-28**	web thickness: -58%	2300	274	10	132	15.875	363.8

2.3 Description of Post-Yield Buckling

Buckling is a phenomenon that results from a "load-generated" loss of lateral stiffness of a structure. Buckling can be thought of as the point where a complete loss of lateral stiffness occurs as a result of induced stresses from an applied load.

In a column, axial compressive stresses generate an internal moment as a result of infinitesimal displacements (either geometric imperfections or displacements resulting from a lateral component of the applied load). This internal moment results in a decrease in the resistance of the structure to lateral displacement (or its lateral stiffness). In a finite element buckling analysis, the original structure has an overall stiffness matrix that includes a lateral stiffness component. In addition to this, a stiffness component is developed as a result of the applied load. This stiffness component is referred to as geometric stiffness. When the magnitude of the geometric stiffness (negative) equals the magnitude of the original lateral stiffness (positive), the structure has zero lateral stiffness, resulting in an unstable structure. The load magnitude at this point is commonly referred to as the buckling load.

Typical displacement and strain response curves for different types of buckling are shown in Figure 2.5.

For **Linear Buckling**, the structure behaves linearly prior to buckling (i.e., small displacements and no yielding). Generally, large displacements and material yielding occur during the buckling process, resulting in permanent deformations. Figure 2.5 shows the expected response for an elastic perfectly plastic material.

For **Linear Elastic** buckling, large displacements occur during buckling with no yielding. The structure returns to its original shape after the load is removed with no associated inelastic strain effects (plasticity). A typical return path is indicated in Figure 2.5; however, this path depends largely on the structure. When the load is removed, the structure returns to its original state (prior to buckling) with no permanent deformations.

The most general type of buckling is **Non-linear Plastic Buckling** (also referred to in this study as **Post-Yield Buckling**). As shown in Figure 2.5, both large displacements and yielding occur before the structure buckles. Permanent deformations result. At the buckling load, the structural stiffness has changed significantly from the original stiffness. While the structure does not have sufficient lateral stiffness to prevent buckling, this may not have occurred completely as a result of stiffness degradation due to compressive forces. The structure may have yielded in tension and buckled as a result of a complex combination of internal loads.

This is the phenomenon that is of interest in this study. It has been found through inspection of ice-damaged vessels that structural failure is often the result of buckling. This is even though substantial yielding has occurred in the hull plating. Therefore, large displacements (membrane stresses become apparent in plating at deflections between t/2 and t) and plasticity are occurring prior to buckling.

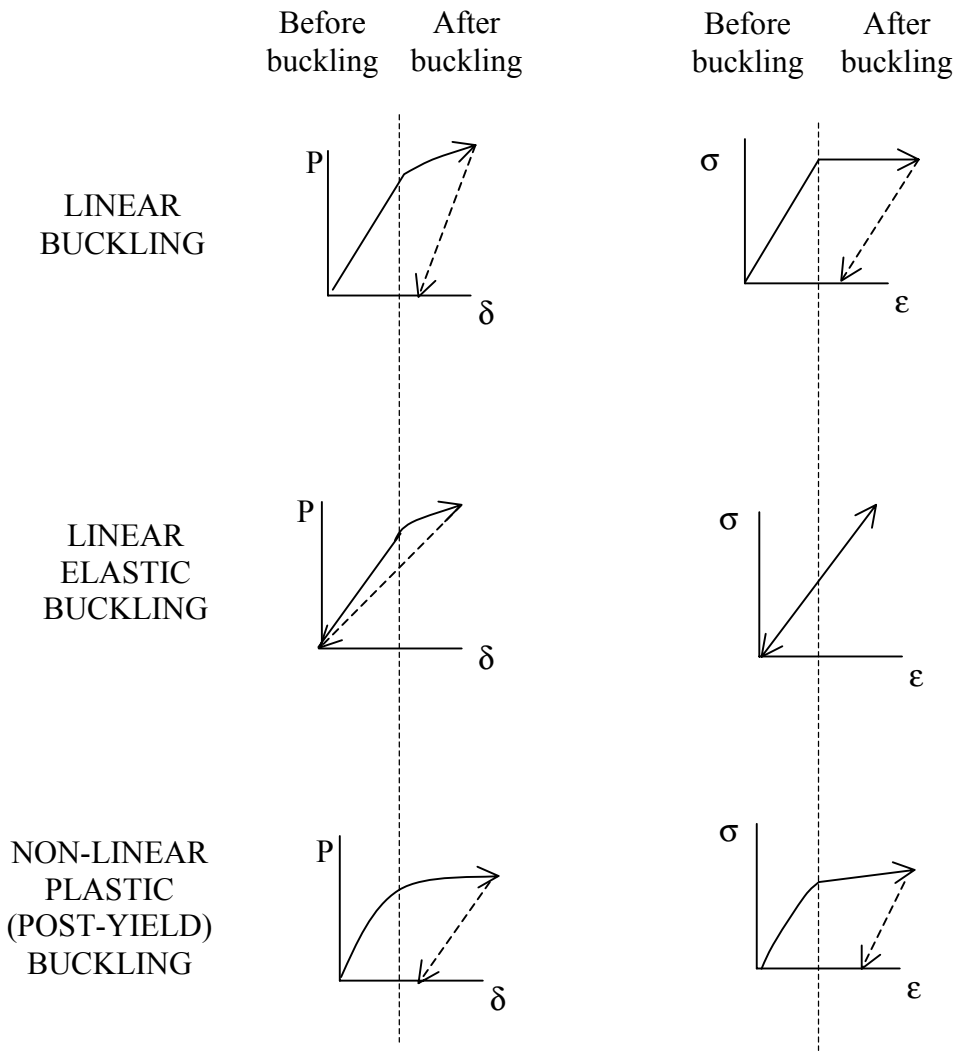

Figure 2.5 Displacement and Strain Response for Different Types of Buckling

3. COMPUTER CONFIGURATION

3.1 Software

The FE program MAESTRO/DSA [5, 6] was used to perform all the analyses carried out in this project. MAESTRO is an FE-based ship design package that includes a module called DSA (Detailed Stress Analysis), which is provided to perform detailed stress analysis of local ship areas. The FE solver used by DSA is a program called VAST [7]. MAESTRO (with DSA) is used by Lloyds, Det Norske Veritas, American Bureau of Shipping and Bureau Veritas. It is also used by several navies, including the Canadian, UK and Dutch navies.

MAESTRO/DSA incorporates full non-linear capability as well as eigenvalue buckling that can be performed at a selected step during a non-linear analysis. MAESTRO/DSA has undergone considerable verification testing that indicates that it produces results similar to other major non-linear codes such as ANSYS [8] and ADINA [9]. To check the capabilities, a selected run from the previous phase of the project was repeated using MAESTRO/DSA. The results of this study are presented in Section 4. MAESTRO/DSA was found to perform well when compared to the results from the parametric study performed in Phase III [4], and can accurately produce the same results as ANSYS and ADINA. As described in Section 4, MAESTRO/DSA has an optional "bubble function" that can be invoked to improve the bending characteristics of the 4 node shell element. This produces results that are more accurate than the previously generated ADINA results.

Some of the figures showing colour contour plots of the results were generated using the pre/post-processing program, HyperMesh [10]. The plots that show the load displacement curves and shear force difference curves were generated using Microsoft Excel [11].

3.2 Hardware

The FE analyses carried out in this study were executed using personal computers. The minimum configuration employed was a Pentium III 450 MHz processor, with 128 MB RAM and 10 GB hard drive, running Windows 95. Full non-linear static runs typically took 12 hours to execute. During the project, several personal computers were employed such that more than one run could be performed in parallel.

4. BENCHMARK ANALYSIS

A benchmark analysis was performed to ensure that MAESTRO/DSA could be used to accurately predict post-yield buckling of complex stiffened panel structures. The validation is based on producing the same results as the validated ADINA runs conducted in the previous phase.

Non-linear finite element analysis (FEA) is a complex procedure that requires both a theoretical and practical understanding of non-linear FE procedures and assumptions and also of the anticipated physical response of the structure that is being analysed. The accuracy of the results produced depends on both the capabilities of the program being used and the skills of the analysts conducting the work. The benchmark analysis was performed to verify that the FE code and computer platform to be used for this study could provide accurate results.

To perform the code validation, it was decided to reproduce the analysis results for a selected run from the Phase III study. The model chosen is identified in Phase III as "Run 4". This is an ASPPR-compliant design employing angle main frames.

In Phase III, ADINA was used to perform the FE analyses and the results were considered accurate. For the benchmark analysis, the Run 4 results were reproduced using MAESTRO/DSA and compared to those from the ADINA run. The results of the benchmark analysis showed some small differences when compared to the ADINA results, but the differences were minor and insignificant.

The two plots in Figure 4.1 compare the results of the benchmark test run using ADINA and MAESTRO/DSA. It can be seen that MAESTRO/DSA produces virtually the same results as ADINA when the "non-enhanced" 4 node shell element is utilized. However, it is felt that increased accuracy can be obtained when bubble functions[1] are incorporated to enhance the in-plane bending properties of the 4 node shell element. The enhanced element produces slightly different results but it is felt that these would be slightly more accurate, as the bending characteristics are better represented. The conclusion reached was that MAESTRO/DSA can produce slightly more accurate results than the previous ADINA results, and MAESTRO/DSA was determined to be capable of producing accurate results for all further analysis work on this project. It was also concluded that the results from the "old" and "new" runs matched well enough such that the differences would not be taken to indicate trends.

[1] *Bubble functions are numerical element enhancement shape functions that allow the in-plane bending characteristics of the 4 node shell element to be more accurately represented. They allow slightly more flexibility, which provides a numerical representation that more closely replicates "real life" response.*

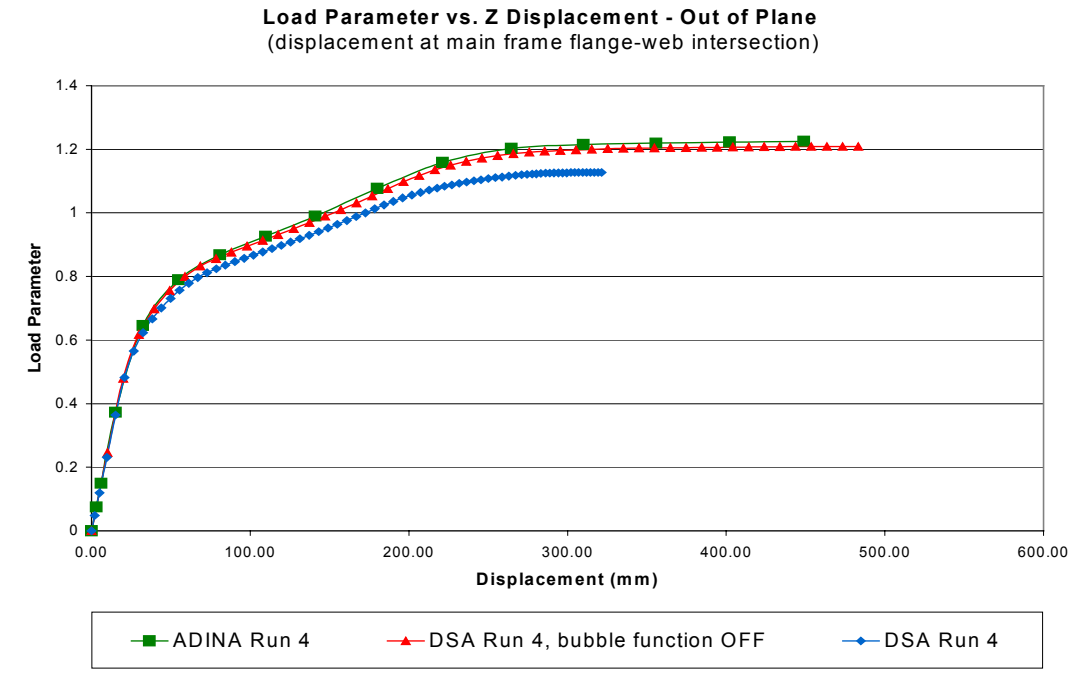

Out-of-plane (Z) Displacement Results

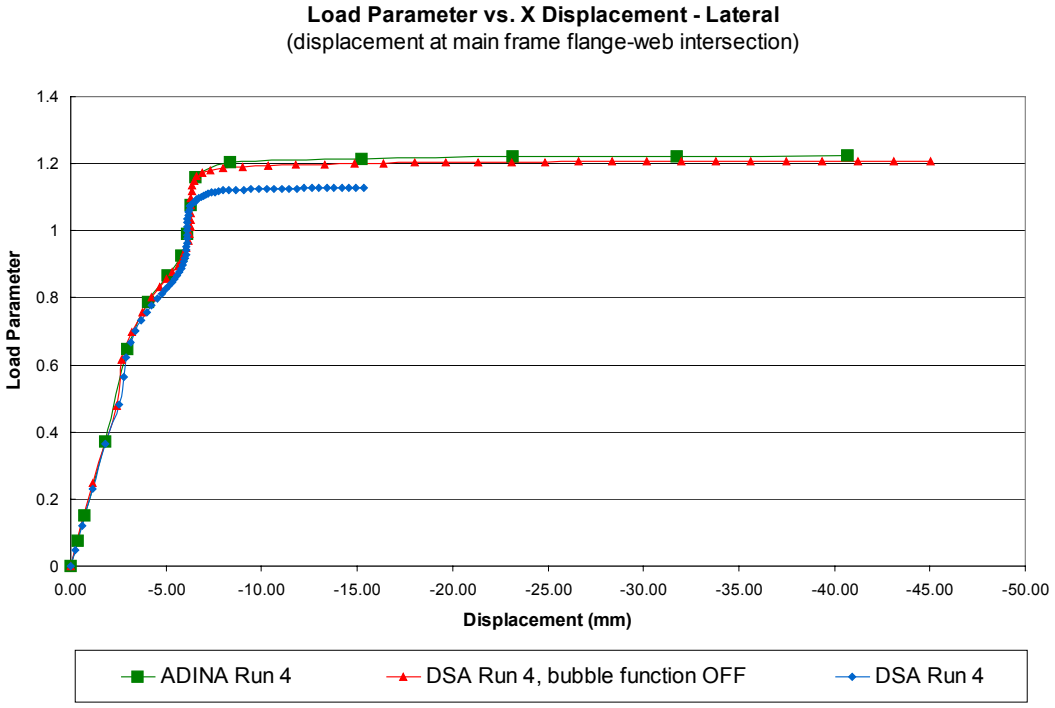

Lateral (X) Displacement Results

Figure 4.1 Load Displacement Curves Comparing ADINA and MAESTRO/DSA Run 4 Results

5. LITERATURE STUDY AND REVIEW OF EQUIVALENT STANDARDS EQUATIONS

5.1 Literature Review

A literature survey was undertaken to identify all current work that is relevant to post-yield structural stability of laterally loaded stiffeners on plated structures. It included all fields and was not limited to ship structures. Martec had undertaken a literature search on similar subject matter in 1996; therefore, this search concentrated on information that had been produced since 1996.

A general internet search of the libraries listed in Table 5.1 was performed using a combination of relevant keywords using the libraries listed in Table 5.1. Several papers were identified as having potential and were requested/printed and reviewed.

The general results of the literature survey are:

- Any formulations found in the literature are based on linear elastic response to compression of frames. In all formulations reviewed, elastic buckling will not occur if the flange is in tension.
- To the best of our knowledge, there is no work being conducted on post-yield buckling of laterally loaded frames/stiffened panels.

5.2 Review of Equivalent Standards Stability Equations

The stability equations presented in the Equivalent Standards were reviewed in detail to determine their basis and their applicability in the non-linear regime. Several textbooks [12-17], which were referenced from the Equivalent Standards, were also reviewed. These books were originally used as the basis for the formulation of the existing stability equations.

Dr. Lei Jiang of Martec performed the review and wrote a short note, which is included as Appendix A.

Table 5.1 Literature Search Sources

American Bureau of Shipping (ABS) http://www.eagle.org	**American Society of Mechanical Engineers (ASME)** http://www.asme.org
Applied Science and Technology (AST) Index (available at DalTech, Dalhousie University)	**Bureau Veritas Publications** 17 bis, place des Reflets La Défense 2 92400 Courbevoie- France http://www.bureauveritas.com
Canada Institute for Scientific and Technical Information (CISTI) National Research Council Canada (NRC) 1500 Montreal Road (M-55) Ottawa, ON, K1A 0S2 http://www.nrc.ca/cisti	**Det Norske Veritas (DNV) Publication List** Veritasveien 1 1322 Høvik, Oslo, Norway http://www.dnv.com
Edison Welding Institute (EWI) 1250 Arthur E. Adams Dr. Columbus, OH 43221 USA http://www.ewi.org	**Elsevier Publications** Publisher Database Search Performed by TDC Library Staff Transport Canada Information and Research Services, ATA Ottawa, ON, K1A 0N5
Glasgow University Library Hillhead Street Glasgow G12 8QE, Scotland, UK http://eleanor.lib.gla.ac.uk	**Lloyd's Register** http://www.lr.org
Massachusetts Institute of Technology (MIT) 77 Massachusetts Ave Cambridge, MA 02139-4307, USA http://libraries.mit.edu	**Memorial University of Newfoundland Libraries** St. John's, NF, A1B 3Y1 http://www.mun.ca/library
NASA http://www.nasa.gov	**National Library of Canada Catalogue (resAnet)** 395 Wellington Street Ottawa, ON, K1A 0N4 http://www.amicus.nlc-bnc.ca
Novanet Catalogue (consortium of Nova Scotia academic libraries) http://novanet.ns.ca	**Offshore Mechanics & Arctic Engineering (OMAE)** http://www.omae.org
Oulu University Library P.O. Box 7500 FIN-90014 UNIVERSITY OF OULU http://www.oulu.fi	**ProQuest Digital Dissertations** Bell & Howell Information and Learning (Formerly known as UMI) 300 North Zeeb Road PO Box 1346 Ann Arbor, MI 48106-1346, USA http://wwwlib.umi.com/dissertations
Springer LINK Heidelberg, Germany http://link.springer.de	**Technical Research Centre of Finland (VTT)** Vuorimiehentie 5, Espoo P.O. Box 1000, FIN-02044 VTT http://www.vtt.fi
Transport Canada 330 Sparks Street Ottawa, ON, K1A 0N5 http://www.tc.gc.ca	**University of New Brunswick Libraries** 8 Bailey Drive Fredericton, NB, E3B 5H5 http://www.unb.ca/inside/libraries.html
US Army Cold Regions Research and Engineering Laboratory (CRREL) 72 Lyme Road Hanover, NH 03755-1290, USA http://144.3.144.209/crrel	**Vaughan Memorial Library** Acadia University Wolfville, NS, B0P 1X0 http://www.acadiau.ca/vaughan

In summary, the main results of the Equivalent Standards review are:

- The basis for the equations that currently appear in the Equivalent Standards was established. As speculated, the stability equations employed in the Equivalent Standards are based on an assumed mode 1 flexural-torsional buckling mode with the entire section in compression. According to the formulation, a frame with a flange in tension will never buckle in either elastic or plastic mode. The formulation of the equations is based on coupling a formula for buckling for a beam with enforced axis of rotation (which already includes torsion about the shear centre and bending in both vertical and lateral directions) with the governing equation for vertical buckling of an unconstrained beam. It is felt that the coupling is not justified. There are also a couple of mathematical errors in the Equivalent Standards equations; however, there is insufficient time to attempt to correct these within the existing contract. [Note: Apparent errors are identified at the end of Appendix A.]

- In the proposal for this project, Martec questioned the basis behind the use of the reduced slenderness ratio ($\sigma_y/\sigma_T = 0.36$) which in essence requires a design that will not buckle until the flexural-torsional buckling stress is equal to three times the yield stress. This requirement was based on the 1984 DNV rules, which present a series of curves of reduced slenderness ratio vs. a ratio of critical buckling stress to yield stress. DNV has since changed the curves (1998 version)[15] and they no longer have the same limitation. It is unclear how the reduced slenderness is now limited but the change alters the equations in the Equivalent Standards significantly. Once again, there is not sufficient time to pursue this further but it is expected that the equations in the Equivalent Standards will not accurately reflect either linear or non-linear buckling under laterally applied loads.

5.3 Summary and Conclusions

The literature survey did not uncover any work being performed that is relevant to this project. The problem involves large displacements/rotations and large-scale, non-uniform plastic deformations in the pre-buckling range. Analytical solutions dealing with these extremely complicated situations have not yet been identified. It is highly possible that analytical solutions for this problem do not exist because of its complexity.

The stability equations in the Equivalent Standards are not expected to predict the expected "real life" response to a laterally applied load. It was decided that there would be no merit in trying to modify those equations or to try to extend the equations into the non-linear regime.

6. DESCRIPTION OF FINITE ELEMENT MODEL

6.1 Extent of the FE Model

To save time in the analysis, it was necessary to ensure that the model used was optimized from a size point of view. Non-linear runs are very computationally demanding and runs can take anywhere from several hours to several days, depending on the size of the model. One of the main factors in determining model size is the extent of the structure included in the FE model.

In the Phase I and II [18] studies, a 3x3 bay model was used for most of the work. In the Phase III study, the effectiveness of a reduced 1x3 bay model was investigated. Several analyses were conducted on two models (one 3x3 bay and one 1x3 bay) and it was found that significant differences resulted in the stress magnitudes in the main frames. Therefore, a 3x3 bay model was used to complete the Phase III study. A fairly crude mesh was used to model the outer bays and a detailed mesh was used in the centre bay. In this manner, boundary conditions were accurately imposed on the centre bay without too much of a penalty in model size. However, runtimes were very long and a run typically took over 24 hours.

For the present study, it was decided to maintain the 3x3 bay model but to take advantage of the vertical symmetry in the structure to reduce the model size to a 3x1½ bay model. Other than the hydrostatic load, all loads applied to the structure are symmetric about the longitudinal centre of the model (i.e., the waterplane). Since the hydrostatic load is small compared to the ice load, the response of the panel is expected to be very close to symmetric.

The extent of the structure included in the FE model, therefore, is the 3x3 bay section of ship side panel. It is modelled assuming symmetric response about the waterplane. Figure 6.1 shows the area of the ship included in the model, including a sketch of the 3x3 bay configuration.

It should be noted that the total ice load extends beyond the bounds of the 3x3 bay section. However, the effect of the total ice load is included in the analysis. This is discussed in detail in Sections 6.4 and 6.5.

6.2 Description of FE Model

The files and results of the Phase III work were organized and reviewed. Run 4 was selected as the run to use to perform a non-linear benchmark analysis (as described in Section 4) and the linear eigenvalue buckling analysis. There were significant time savings in utilizing the existing model from the previous phase rather than developing and testing a new model.

An angle main frame model was chosen because angle sections were found to be more susceptible to post-yield buckling. Also, previous phases of work found that angle section main frames exhibit a form of buckling where the webs displace dramatically in the lateral

direction at the point of buckling, making it easier to observe the response. The FE model is shown in Figure 6.2.

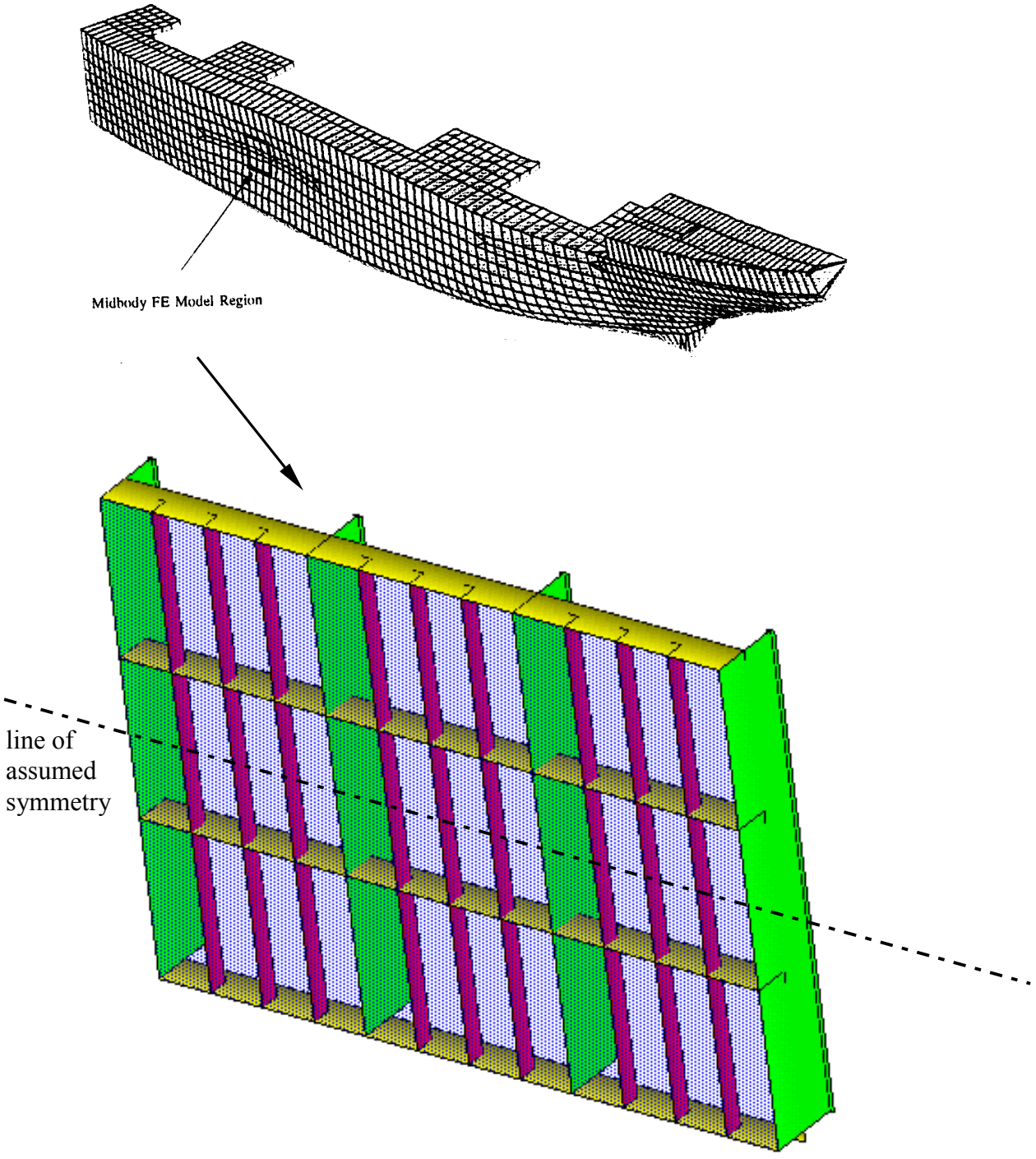

Figure 6.1 Sketch Showing Global 1/4 Model and Extent of Structure Included in Model

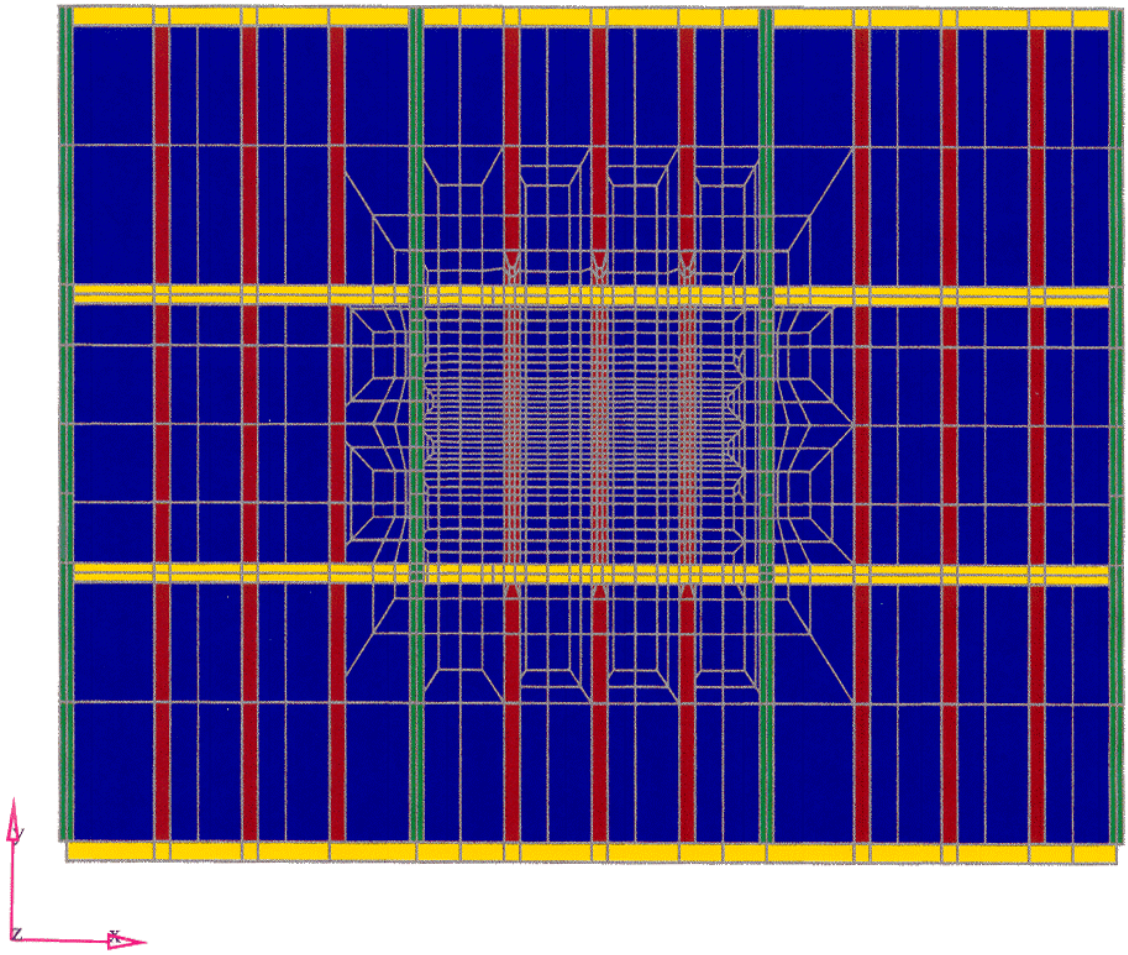

Figure 6.2 "Run 4" 3x3 Bay FE Model

The element type used for the detailed 3x3 bay FE models must be able to predict in-plane membrane and shear strains, and out-of-plane bending strains. The appropriate element for this is the 4 node shell element.

In the Phase II analysis, the 4 node ANSYS shell element was used for the analysis. This element performed very well in matching the response of the physical panel test at Carleton University. In an independent check [19], it was found that the 4 node ADINA shell element also performed well in matching these results. Based on the performance of the ADINA 4 node shell in matching actual experimental test results, this element type was selected for the FE work in Phase III of the project. The recommended ADINA default 2x2x2 integration order was used for all analyses.

As discussed in Section 6.1, the 3x3 bay model was cut in half for this study. The mesh density of the Phase III model is shown in Figure 6.2 and was retained for the 3x1½ bay model that was used in this study. The appearance of the model after reducing it by half through a symmetry assumption is shown in Figure 6.3.

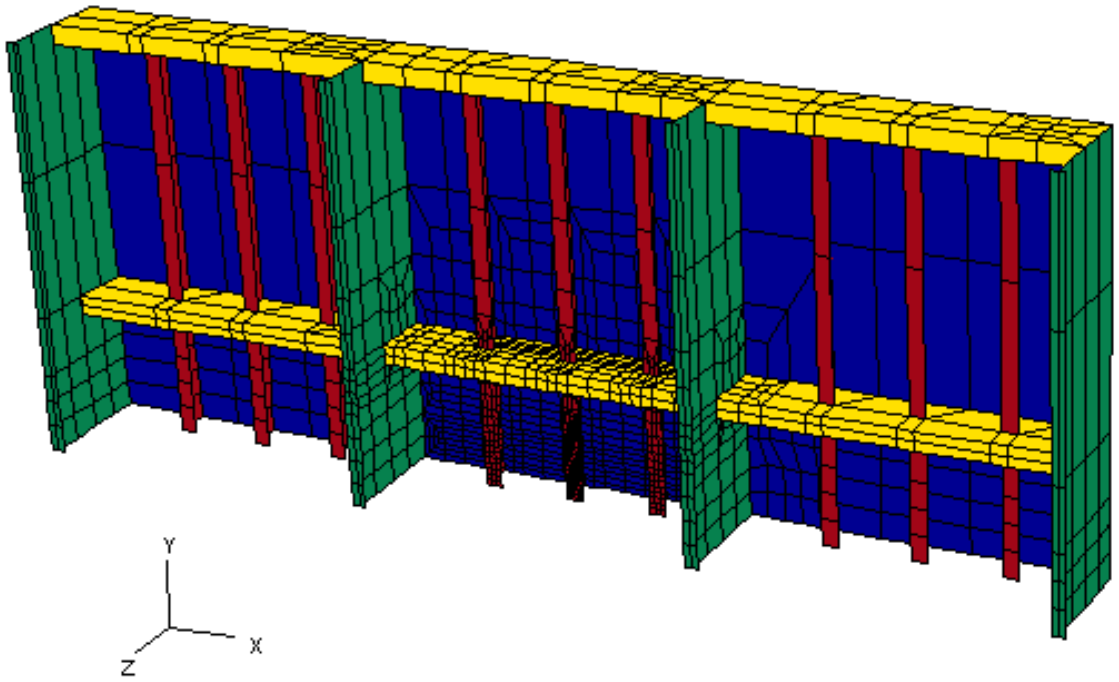

Figure 6.3 3 x 1 1/2 Bay FE Model Used in Study

As discussed in Section 3, the FE program MAESTRO/DSA was employed for this study. The 4 node shell element was employed with a 2x2x2 integration order. This was shown to produce good agreement with the previous work.

6.3 Material Properties

The material used in the model of the ship panel is steel, as in the previous phases [3, 4, 18]. The constitutive (stress/strain) relationship used was bilinear elastic plastic, and the properties were:

Yield strength:	355 MPa
Modulus of elasticity:	207,000 MPa
Strain hardening modulus:	5,175 MPa

6.4 Boundary Conditions

The boundary conditions used for the analysis were the same as those used for Run 4 in Phase III, the parametric study, modified to include symmetry boundary conditions for the reduced model, as discussed in Section 6.2.

The boundary conditions to be used on all of the 3x3 bay FE models had to be representative of the actual, "real life" constraints on the panel. In the Phase I study, the boundary conditions used were prescribed displacements that were determined from a MAESTRO analysis of the complete ship.

The benefit of modelling the boundary conditions using prescribed displacements is that the response of the overall ship is accurately included in the local 3x3 bay panel response. The disadvantage of using prescribed displacements is that a model of the complete ship must be generated and analysed to get the proper boundary conditions. In the Phase III study it was realized that this is not practical for a parametric study where the potential exists to analyse many different ship configurations. It was also concluded from the Phase I study that the prescribed displacements are not necessary if the overall ship response is included through in-plane stresses. Therefore, in the Phase III study a set of boundary conditions was defined using a combination of loads and constrained degrees of freedom that approximated the global ship response.

[Note: While the panel boundary conditions were made as realistic as possible, the Phase I study found that results for members in the centre bay were not very sensitive to the panel boundary conditions, other than in-plane stresses. The eight surrounding bays were included with a relatively coarse mesh to provide realistic boundary conditions for the centre bay.]

Figure 6.4 shows the rationale behind the selection of the boundary conditions as determined in Phase III. Figure 6.4 a) shows a sketch of the expected overall ship response to an ice load along with an outline of the local 3x3 bay region. The overall ship model is from the MAESTRO analysis of the *MV Arctic* taken from the Phase I study, where centre line symmetry was applied to the model. This means that the reaction force (not shown) was opposite to the ice force and generated no full global bending. Thus, the induced in-plane stresses indicated were minimal and could be designated as local/global.

It can be seen in Figure 6.4 that the upper and lower boundaries of the 3x3 bay panel region displace laterally at approximately the same magnitude. This is due to the fact that the ice load is applied (inward) not only to the local 3x3 bay region but also to the entire iceprint area along the side of the ship. One component of the global response in the area of the 3x3 bay model is a rigid body deflection of the panel in the lateral direction as the hull displaces inward as a result of the application of the massive ice load.

The upper and lower boundaries also rotate about a longitudinal axis. While this degree of rotation depends on the proximity of decks above and below the 3x3 bay region, the highest stresses result when the boundaries are free to rotate. In this case, higher compressive stresses are generated on the hull plating (which acts as the outer flange of the deep webs) and higher

tensile stresses are generated on the inner flanges of the deep webs (or inner skin for double hull vessels).

The forward and aft vertical edges displace concavely inward, restrained only by the structure above and below the 3x3 bay panel. There is only a small contribution from the longitudinal stringers because the structure forward and aft of the panel is displaced laterally from the ice load. Consequently, it does not put any significant lateral constraint on the 3x3 bay stiffened panel. However, the stringers have generated stresses from the local/global effect.

Based on the response of the overall ship, as shown in Figure 6.4 a), the boundary conditions used on all 3x3 bay models in Phase III are shown in Figure 6.4 b). The numbers shown on the plot indicate the global degrees of freedom that are constrained. From this it can be seen that the upper and lower panel boundaries were fixed against lateral (z) displacement. Lateral constraint is required for numerical purposes and also ensures that the top and bottom boundaries displace at the same magnitudes. Since the overall model analysis showed rotation at the top and bottom boundaries, no rotational constraints were imposed at these locations.

As previously discussed, the forward and aft vertical boundaries are considered not to be constrained laterally by the adjacent structure and displace freely. Therefore, no lateral (z) displacement boundary conditions were applied at the fore/aft boundaries.

Additional boundary conditions were imposed to satisfy numerical conditions and to permit application of the biaxial in-plane pressure loads. Nodes at the centre of the top and bottom edges were constrained in the longitudinal (x) direction only. This provided suppression of rigid body motion while permitting the structure to compress in the longitudinal direction under influence of the in-plane pressure loads. Similarly, nodes at the centre of the forward and aft edges were constrained in the vertical (y) direction such that free body motion was suppressed and the structure was still permitted to compress under the vertically applied in-plane pressure loads.

6.4.1 Boundary Conditions for the Linear Eigenvalue Analyses

The linear eigenvalue analysis is particularly demanding computationally. The finite element model was reduced in size by assuming symmetry about the centre bay in the longitudinal direction. Symmetry boundary conditions were applied on the bottom and side surfaces where the model was trimmed. Figure 6.5 shows the boundary conditions on the reduced model. Since the linear eigenvalue analysis is making gross assumptions about the behaviour of a highly non-linear structure, the inaccuracies associated with this simplification were acceptable.

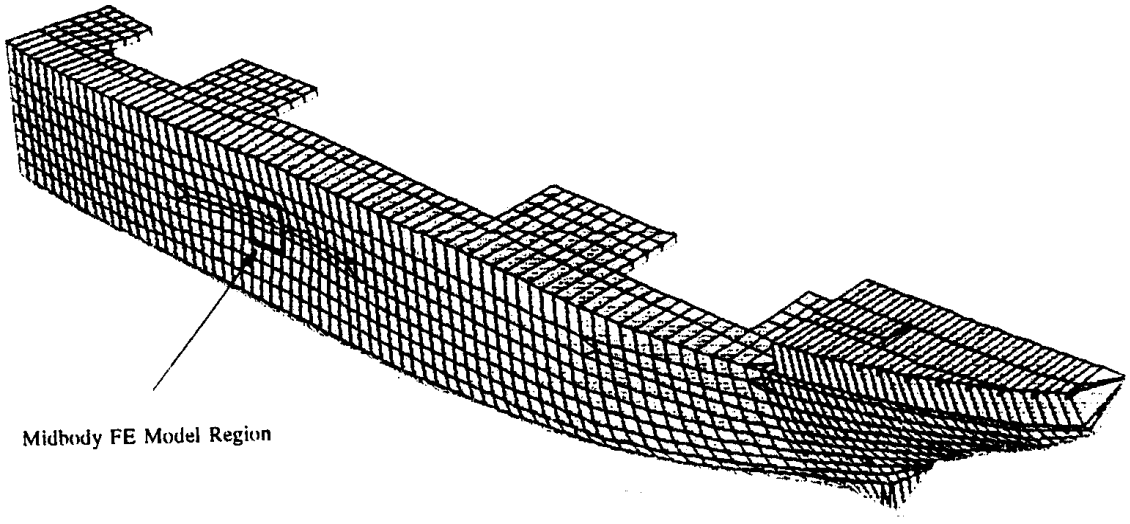

a) Overall Structure Response to Ice Load

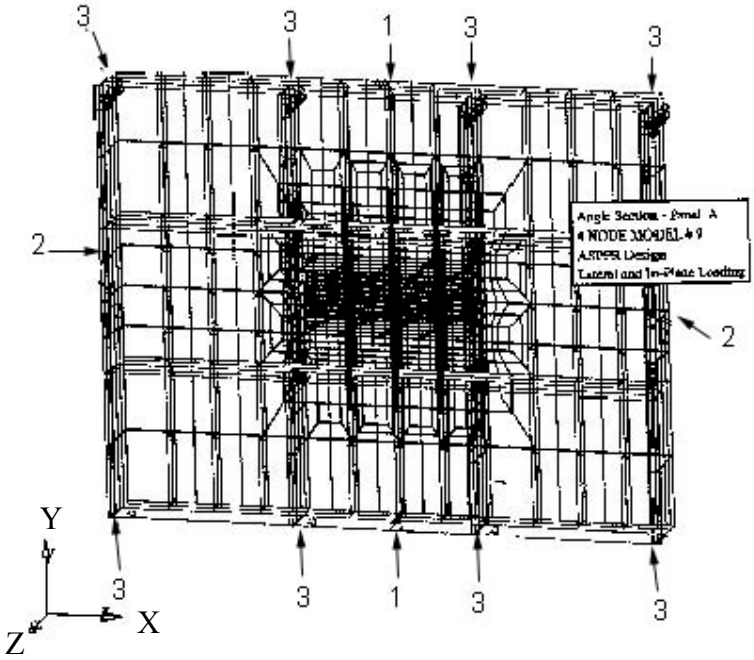

Designation	Degree of Freedom Constrained
1	δ_x
2	δ_y
3	δ_z
4	σ_x
5	σ_y
6	σ_z

b) 3x3 Bay FE Model Boundary Conditions

Figure 6.4 Selection of Boundary Conditions for Study

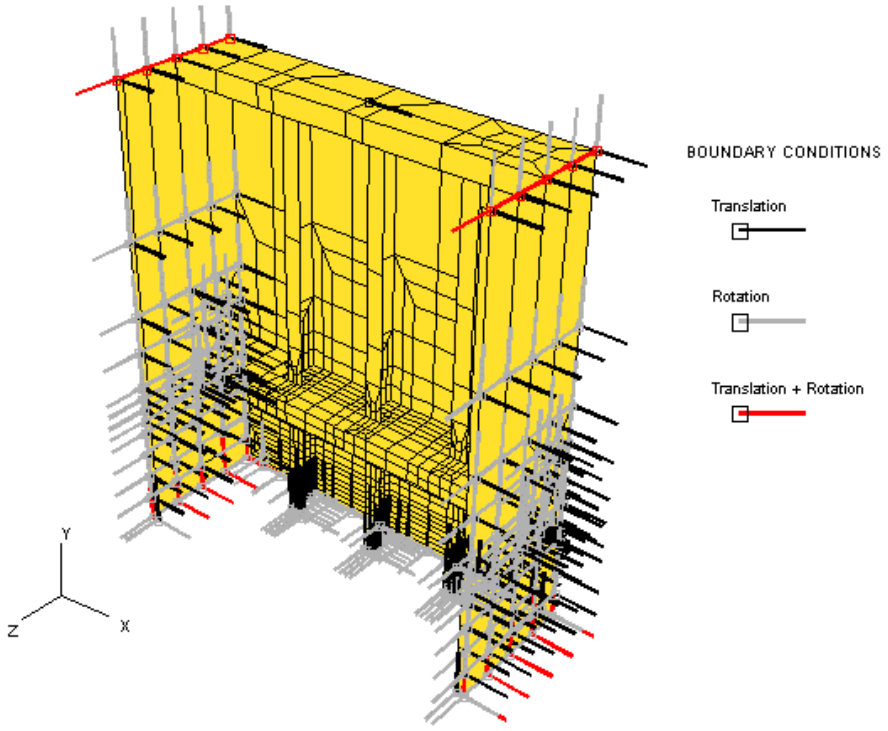

Figure 6.5 Boundary Conditions Including Symmetry

6.5 Loads

The applied load consists of two components: an in-plane load and a lateral load. The total lateral load component generated from impact with multi-year ice has a magnitude equal to "F_{max}". All applied loads are expressed as a multiplier of F_{max} (For example, 2.24 x F_{max} would be 2.24 times the load that is expected to be generated by the ship impacting the multi-year ice.). The in-plane load is generated from the global ship response. The ice load produces an overall ship response that includes a biaxial in-plane compressive load (a magnitude of 69 MPa was determined in the Phase I study as a "typical" value for the mid-body side shell of the *MV Arctic*).

In the previous phases, the in-plane compressive stresses were determined from modelling the global ship response using MAESTRO and were modelled using prescribed displacements. However, it was determined that these in-plane stresses were fairly constant, and they could be determined through simpler methods. They could also be applied to the model as in-plane forces. In this study, the in-plane stresses were applied as in-plane forces in the same manner as was used in Phase III of this work. These in-plane forces were applied as a consistent load vector along the exterior edges of the plate (i.e.,, not on the cut edges of the reduced model). The magnitude of the load was set to the "typical" value of 69 MPa, as described above. In the non-linear analyses, the in-plane loads were scaled with the application of load, along with the ice load.

The ice load is characterized by a force distributed over an area designated in the Equivalent Standards as the iceprint, with dimensions L_{DL} * V_p (length x height). Figure 6.6 (reproduced from Figure 4.9 of the ASPPR) shows the actual and idealized shape of the iceprint. This idealized distribution was used for this study. It was assumed that a triangular distribution of the pressure is acting on this iceprint.

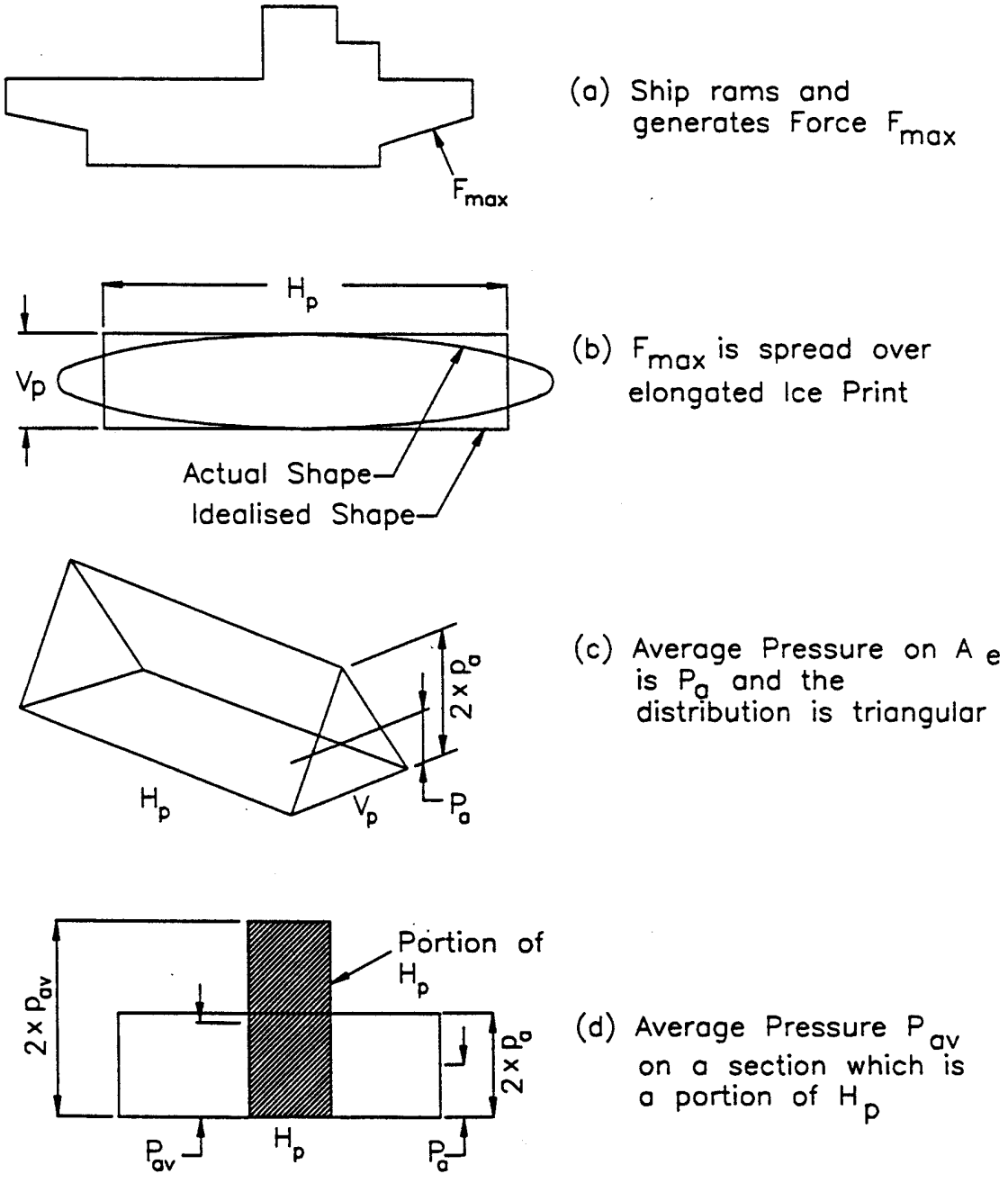

Figure 6.6 Ice Load Model (from Figure 4.9 of the ASPPR, TP 9981, Dec. 1989)

As shown in Figure 6.6, the peak of this triangle has a magnitude of 2 * P_a (where P_a is the average pressure). The pressure also varies along the length of the iceprint. This results in a higher pressure on a smaller section of the iceprint. This higher pressure is defined as P_{av} and is also shown in Figure 6.6. The value of P_{av} is calculated from Section 15 of the Equivalent Standards regulations. This value is a function of DPT, which is defined in Section 18 of the Equivalent Standards as:

$$DPT = \frac{S}{L_{DL}}$$

where S = frame spacing
L_{DL} = horizontal length of the iceprint

It should be noted that P_{av} is for a load acting at the bow area of a CAC1 ship. To achieve the proper values for different CACs and areas of the ship, these values are multiplied by appropriate class and area factors.

The size of the iceprint and ice load is based on the force developed as a result of ship-ice interaction while the vessel is engaged in icebreaking activity. To derive expressions for the ice-load parameters, several models and full-scale tests were conducted during the development of ASPPR. The effects of several parameters (i.e., speed, displacement, bow geometry, and power) on this value were examined. It was found that the ship's displacement and power had a direct influence on the ice forces. The resulting formula for the iceprint to be used in framing design, obtained from the research conducted during the development of the Equivalent Standards, is as follows:

$$L_{DL} = 2.80 \sqrt{\Delta^{0.7} + \Delta^{0.48} \cdot P^{0.33}}$$

where $V_p = L_{DL}/8$
Δ = the displacement in thousands of tonnes
P = the shaft power in megawatts

The value of F_{max} is the total applied ice load on the ship.

The magnitudes of the applied loads in this study were the same as those applied to the model in Phase III of this project. For structural models with iceprint dimensions as shown in Figure 6.7, the magnitude of the lateral ice load applied to the panel for the midbody region of the ship is illustrated in the figure. The overall iceprint is significantly larger than the area covered by the 3x3 bay panel. Therefore, only the portion of the iceprint directly applied on the panel is modelled. The effect of the ice load outside this region is represented by both the boundary conditions and the in-plane loads. The peak pressure load is centred over the centre main frame of the 3x3 bay panel.

As in the Phase III work, since the overall panel geometry did not change in this study, this ice load was used for all analyses. It should be noted that for load values not equal to F_{max}, the same proportional distribution of pressures was maintained. For the linear eigenvalue buckling runs, the lateral ice load was applied using point loads calculated in the previous phase as a consistent load vector. The magnitude of the in-plane load was set to the value of 69 MPa.

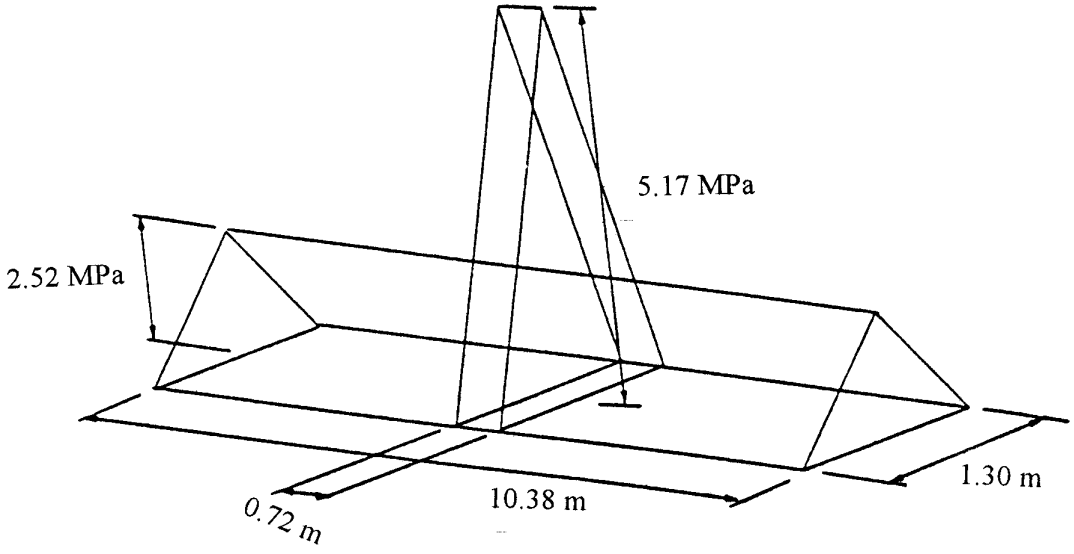

Figure 6.7 Ice Load for Midbody Region Calculating Using the Equivalent Standards (TP 12260, 1996)

7. IDENTIFICATION OF INSTABILITIES

7.1 Shear Force Difference Method

In Phase III, a methodology was developed to monitor the load being carried by a beam. It was called the "shear force difference" method and calculated the lateral load that a beam is carrying in bending and shear by determining and comparing the shear forces at selected cross sections within the beam.

When a beam supports a lateral load through flexure (bending), a shear force is developed in the beam that is directly proportional to the applied load. In a rectangular cross section, this shear force has a parabolic distribution through the depth of the beam and has a value of zero at each free surface and a maximum value at the neutral axis. Without developing this shear force, a beam is incapable of carrying a load in bending. The difference between the shear force carried at any two cross sections in a beam under a bending load gives a calculation of the applied load between the two sections. Therefore, if the shear force difference decreases, then it is because the load carried in bending by that member decreases.

Relating this to buckling, if a member that is carrying a load experiences buckling, it is no longer capable of supporting the load that it carried prior to buckling. (Note that if a member that is carrying a load yields, its ability to carry incremental load diminishes but it continues to carry the load that was present prior to yielding.) In a redundant structure, where multiple load paths exist, as scantlings in a structure buckle, the load being carried by a particular scantling will be shed to the surrounding structure until the surrounding structure is no longer capable of carrying incremental load. This is because the geometry of the buckled scantling is such that it is no longer capable of carrying the load that it supported prior to buckling. Some of the bending load shed by the buckled member will be picked up by membrane forces in the surrounding structure. Eventually, nearly all of the load will be carried by membrane stiffness.

It is therefore construed that if the load-carrying capacity of a scantling decreases, it is because of a change in geometry associated with buckling. So, if the load that a member is carrying decreases dramatically while the applied load continues to increase, it is associated with buckling.

In Phase III, the shear force difference method was used to monitor the loads being carried by members. Buckling was predicted to have initiated when the load carried by the member started to decrease while the applied load continued to increase. The method was shown to correlate well with an increase in lateral deflection (also associated with the onset of buckling) for selected frames. This provided a subjective validation of the methodology.

In this phase of the project, it was thought that the shear force difference method could be validated somewhat less subjectively by using linear eigenvalue analysis results to compare to the buckling load determined from the shear force difference curves. Details on the methodology and results of the linear validation are contained in Section 7.2.

An attempt was also made to validate the shear force difference method using the non-linear eigenvalue buckling capability contained in MAESTRO/DSA. Details on the methodology and results of this validation are contained in Section 7.3.

7.2 Validation Using Linear Eigenvalue Method

A linearized buckling analysis computes the intensity of an applied loading condition that will cause buckling. For an eigenvalue problem, the governing equations for a linear buckling analysis can be expressed as:

$$[K]\ \{\phi\} + \{\lambda\}\ [K_G]\ \{\phi\} = \{0\}$$

where: $[K]$ is the stiffness matrix;
$[K_G]$ is the geometric stiffness matrix;
$\{\phi\}$ is the buckling mode shape.

The eigenvalue function $\{\lambda\}$ is the factor by which the applied reference loading condition must be multiplied to produce buckling.

The geometric stiffness matrix $[K_G]$ is calculated using the initial stresses, which are determined from the applied load on the structure. Buckling occurs when the factored geometric stiffness $\{\lambda\}[K_G]$ equals the structural stiffness component $[K]$ associated with lateral strength. These terms basically cancel, leaving the structure with no lateral strength. The factor $\{\lambda\}$ multiplied by the applied load provides the linear buckling load.

The eigenvalue method of predicting linear buckling loads is the standard process used by FE codes and was used for the prediction of the linear buckling response of the 3x3 bay FE models in this project.

It was thought that the linear eigenvalue analysis results could be used to validate the shear force difference method, which is described in Section 7.1, somewhat less subjectively than by using load vs. lateral deflection curves. The procedure used was to select several of the linear eigenvalue models and re-analyze them by non-linear step-by-step solution under an increasing lateral load. The idea was that the run would be performed using linear material properties (i.e., no yielding) such that the same buckling load should be predicted as in the linear eigenvalue analyses, so long as the stiffness of the structure remained relatively constant. Therefore, the non-linear analysis (with linear material properties) should identify a linear buckling load that would be very close to that predicted from the linear eigenvalue buckling load analysis. The shear force difference methodology would be used to generate the buckling load level for comparison with the eigenvalue-predicted buckling loads. Correlation between the two predictions would provide a validation of the shear force difference methodology.

Unfortunately, the level of the load required to achieve linear buckling was found to be about 8* F_{max}. This is high enough to create substantial non-linear geometric effects that result in no correlation between linear and non-linear runs. Since the buckling phenomena to be predicted (which cause the changes in the shear force difference curve) were thus non-linear and could only be modelled by incorporating large displacements into the model, the run had to be conducted by including large displacement effects. Therefore, the validation using linear eigenvalue analyses was not possible.

7.3 Validation Using Non-linear Eigenvalue Method

MAESTRO/DSA, the FE program used for the project, has a non-linear option for linearized eigenvalue buckling analysis. This allows a user to perform a linearized eigenvalue buckling analysis at selected load steps during a full non-linear analysis. An excerpt from a Martec Technical Note regarding the non-linear buckling capability in MAESTRO/DSA is included in Appendix B.

A full non-linear analysis was performed using the "Run 4" configuration. Figure 7.1 shows a shear force difference curve for the analysis. From the slope of the curve, one would predict buckling at a load level of about 2.24*F_{max}. This is the point where the tangent to the curve is vertical and the frame now carries no increased bending load even though the applied load continues to increase. Subsequent to this point, the frame starts to shed load to the surrounding structure and the load carried by the frame starts to decrease.

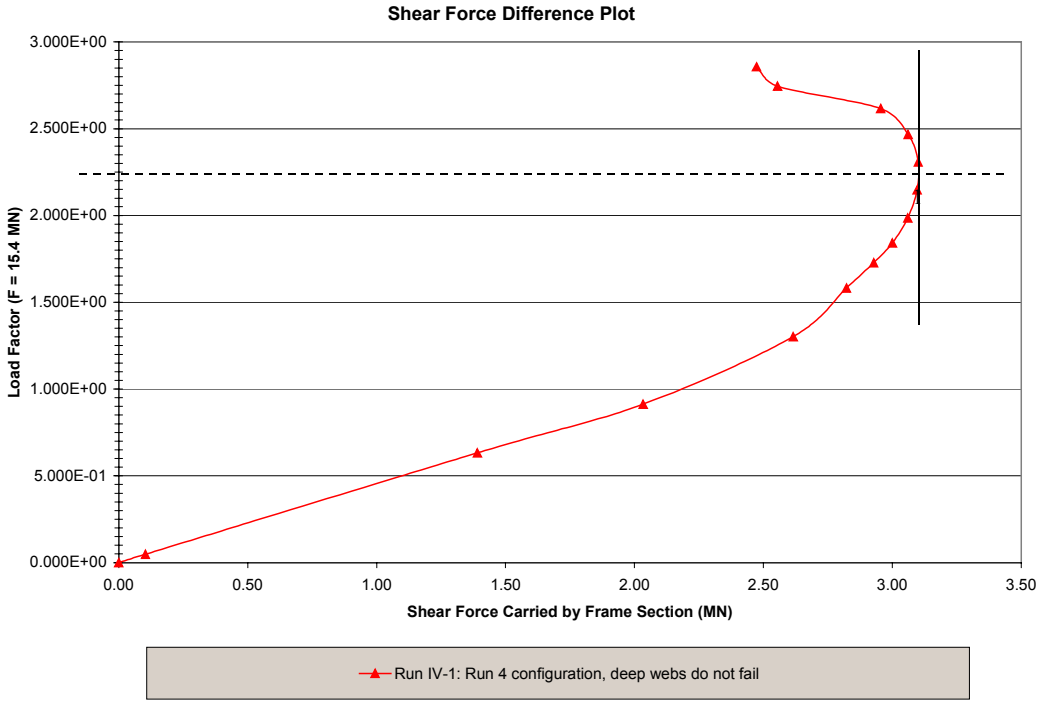

Figure 7.1 Shear Force Difference Curve for Run IV-1, "Run 4" Panel Configuration

Figure 7.2 a) shows the full-scale displaced shape of the main frame at a load level of 2.25*F_{max} and Figure 7.2 b) shows the full-scale displaced shape of the main frame at a load level of 2.86*F_{max}. From the two plots it is clearly evident that buckling of the main frame has occurred somewhere between 2.25* F_{max}. and 2.86* F_{max}.

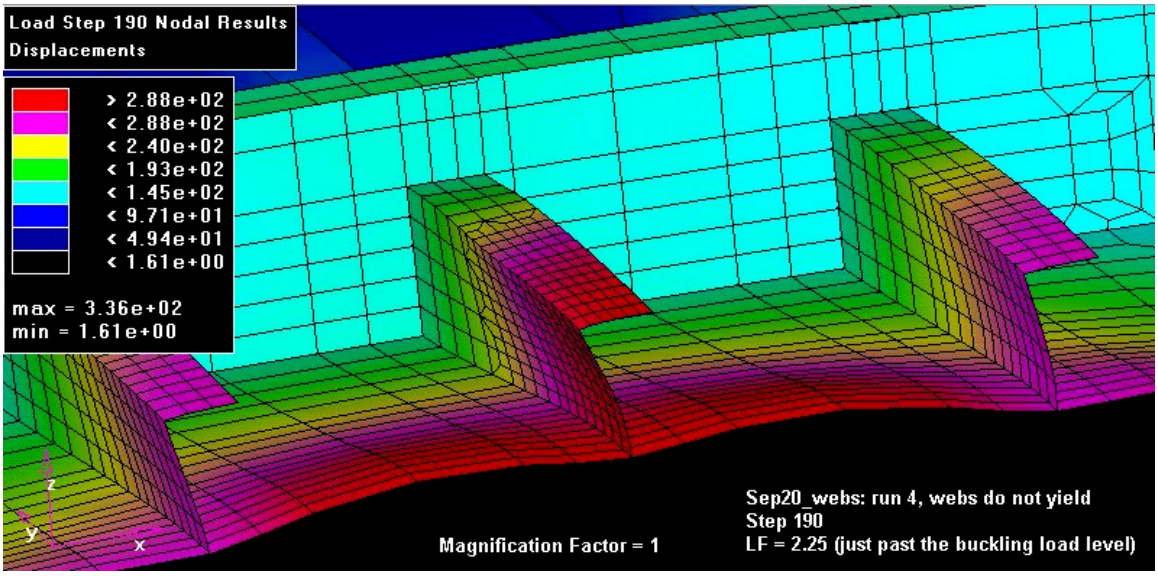

Figure 7.2 a) Deflected Shape at LF = 2.25

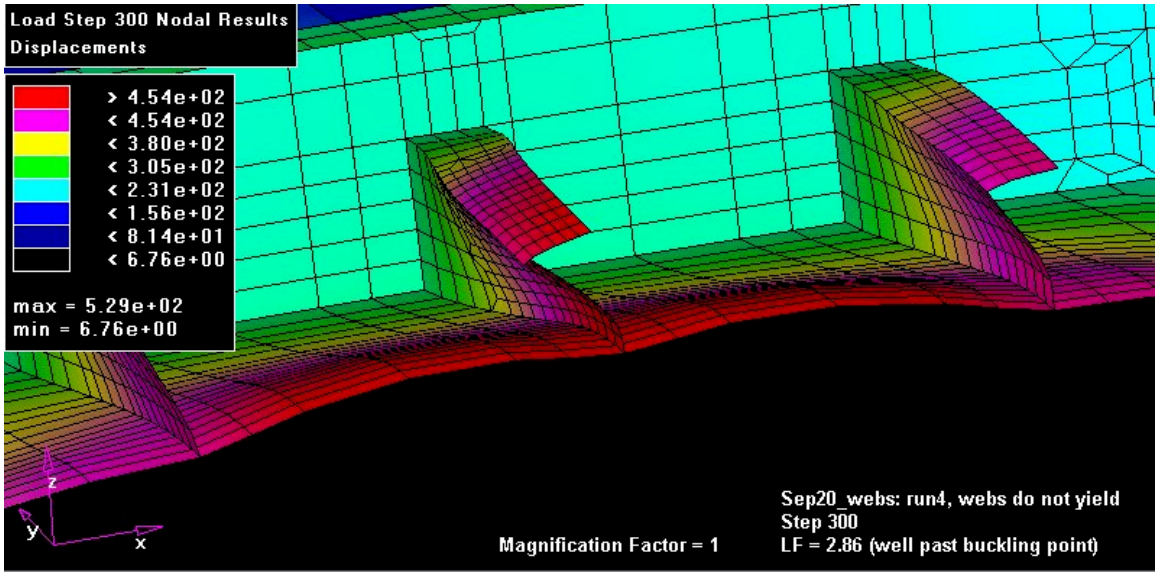

Figure 7.2 b) Deflected Shape at LF = 2.86

Figure 7.2 Run IV-1, "Run 4" Panel Configuration - Deflected Shapes at Buckling Load Level and Load Level Well Beyond Buckling

However, in the interests of providing a less subjective validation of the shear force difference method, a linearized eigenvalue buckling analysis was performed at several load steps selected from the non-linear run. If the frame is truly starting to buckle, then a linearized buckling analysis performed just before the point of buckling should predict buckling at a load level just slightly larger than the load applied at that point. This would provide confirmation that buckling is occurring, thereby validating the shear force difference method as an accurate method to predict non-linear buckling.

A linearized eigenvalue buckling analysis was performed at the load level $2.16*F_{max}$, shown as "1" just below the dashed line in Figure 7.1. Many (350) buckling modes were calculated. Review of the buckling modes indicated that the first 112 modes were very local buckling modes that were insignificant and would not result in an instability significant enough to affect the non-linear step-by-step results. Modes 113, 133 and 162 are shown in Figure 7.3. They are very similar in shape to the displaced shape plots shown in Figure 7.2 b) as predicted by the step-by-step analysis. The predicted buckling load for mode 113 is 2.197 times the applied load at that time-step, or $1.017*2.16*F_{max} = 2.197*F_{max}$. This agrees well with the more subjective prediction of $2.24*F_{max}$ from the plot in Figure 7.1.

The overall conclusion that can be drawn from the results of the linearized eigenvalue buckling analysis, performed at a load level of $2.16*F_{max}$, is that an instability exists in the structure. This instability portrays itself as a significant main frame buckling mode at a load level of $2.197*F_{max}$. This supports the graphical calculation of buckling load level described as the shear force difference method.

The shear force difference method of predicting buckling load level was used throughout the study as the methodology for calculation of buckling load.

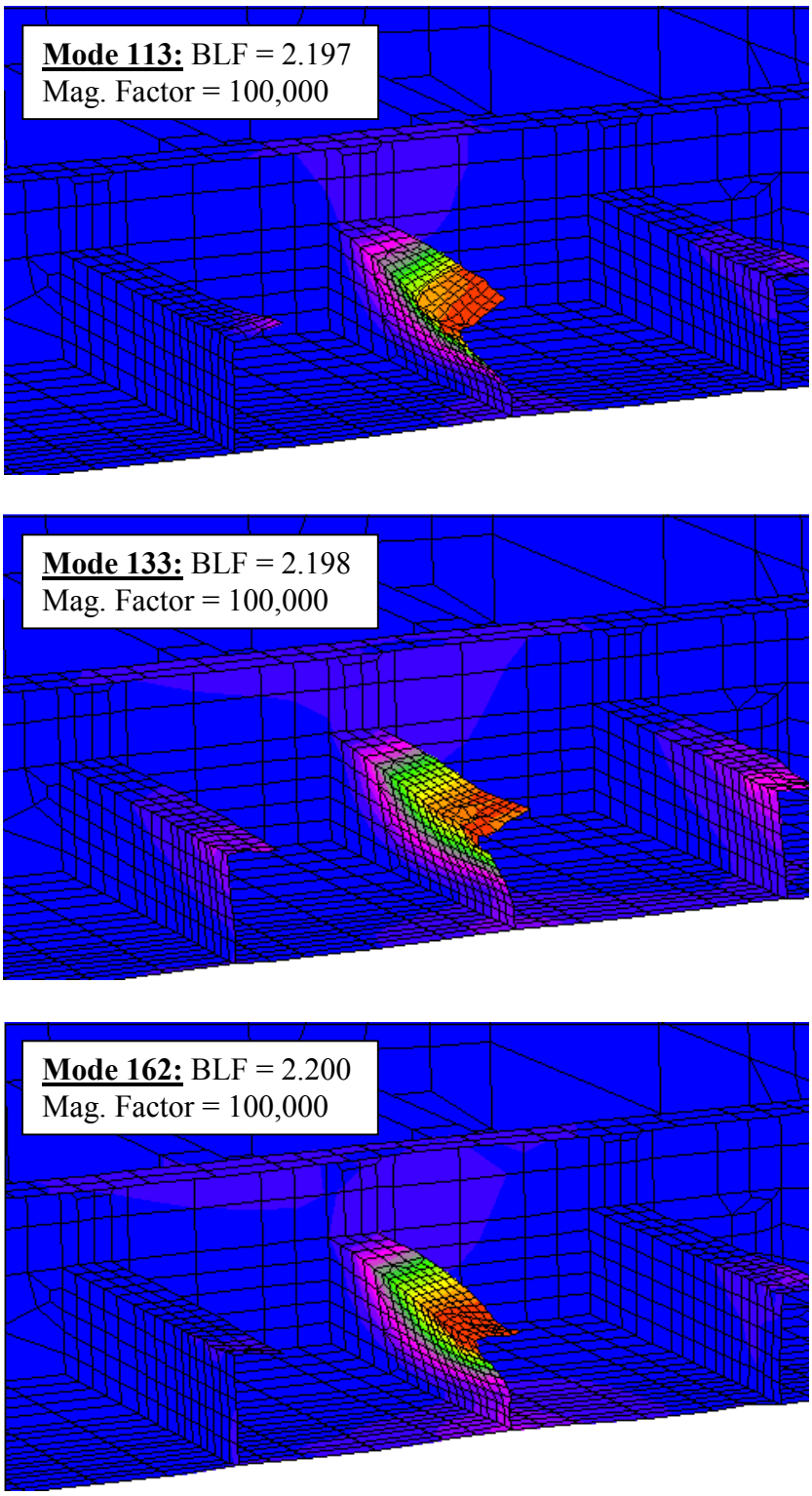

Figure 7.3 Buckling Modes Predicted by Nonlinear and Eigenvalue Analysis

8. LINEAR EIGENVALUE BUCKLING ANALYSIS

8.1 Objective of Analysis

The objective of this task was to investigate the linear buckling response of the panel using finite element analysis.

In the previous phase of this work, non-linear FEA was used to predict the post-yield response of main frames. Using the results, a relationship could not be defined between the stability equations in the Equivalent Standards and the predicted post-yield stability of the main frames. Therefore, it was proposed in this phase to take a step back and first perform an investigation of the equations in the linear range. It was thought that since the stability equations are based on linear assumptions, the FEA linear prediction of buckling might relate to the resulting prediction from the Equivalent Standards equations. Since linear eigenvalue analyses are simpler to run than non-linear analyses, the strategy was to execute a large number of linear analyses to gain an understanding of the current equations.

This validation was to be performed though a series of linear eigenvalue analyses using the FE models developed in the previous phase.

8.2 Extent of the FE Model

As described in Section 6.1, the finite element model employed for the linear eigenvalue buckling analysis represents a 3x3 bay stiffened panel section of a typical icebreaker structure at a location close to midbody.

To reduce the size of the model, the model used for the initial linear eigenvalue buckling analysis was trimmed down using symmetry. As discussed in Section 6.1, the 3x3 bay model was cut in half lengthwise, such that only the top half of the panel was included in the model while the bottom half was accounted for by applying symmetry boundary conditions on the cut edge.

There are two disadvantages to this approach, but it was felt to be acceptable for the purposes of this study. The two disadvantages are:

1) Employing a symmetric model limits the predicted eigenmodes to symmetric modes. Non-symmetric modes will not be calculated.
2) The symmetric model assumes symmetric loads. As discussed in Section 6.1, the hydrostatic loads are not symmetric.

Eigenvalue analysis is very time consuming and the 3x1½ bay model was large enough to be very inconvenient to run. It was decided to further reduce the size of the model by assuming symmetric response across bay boundaries (i.e., across deep webs). This allowed trimming of the side bays, thus leaving only 1x1½ bays from the original 3x3 bay model. Symmetry boundary conditions were again applied at the cut edges. This provided a smaller model that

simulated a 3x3 model through symmetry. Figure 6.5 shows the boundary conditions applied to the model to replicate symmetry. By applying symmetry in place of the side bays, the lateral ice load is altered, displaying three peaks (one each for the centre frame in each bay) instead of one. Although this is not a true representation of the load, the stiffness of the panel is maintained at the 3x3 bay level, and the results are expected to provide sufficient accuracy for the purposes of this study. Execution of both models independently showed good agreement in the first few significant buckling modes predicted. For the 1x1½ bay model, the horizontal in-plane load was removed and the vertical in-plane load was applied as before. This was not expected to have any significant detrimental effect on the predicted modes.

8.3 Description of FE Model and Analysis Methodology

This section of the report details the development of the FE model and the MAESTRO/DSA analysis methodology employed for the linear eigenvalue analysis.

8.3.1 FE Model Description

The FE model used for the linear eigenvalue analysis was a slightly modified version of the model that was used for the non-linear runs described in Section 6.2. As before, the model was developed for use with MAESTRO/DSA and employed the 4 node shell element.

The FE mesh density is shown in Figure 8.1. As can be seen in the figure, the model consists of a 1x1½ bay version of the 3x1½ bay model described in Section 6.2.

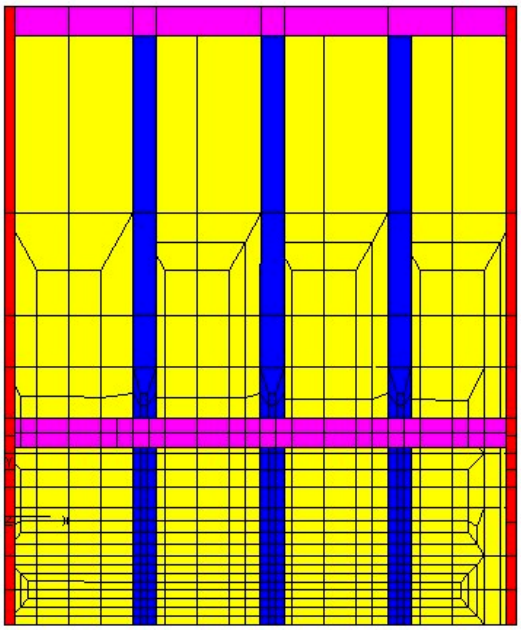

Figure 8.1 Reduced 1 x 1 1/2 Bay Model

8.3.2 Analysis Methodology

As described in Section 7.2, a linearized eigenvalue buckling analysis computes the intensity of an applied loading condition that will cause buckling. For an eigenvalue problem, the governing equations for a linear buckling analysis can be expressed as:

$$[K]\{\phi\} + \{\lambda\}[K_G]\{\phi\} = \{0\}$$

where: $[K]$ is the stiffness matrix;
$[K_G]$ is the geometric stiffness matrix;
$\{\phi\}$ is the buckling mode shape.

The eigenvalue function $\{\lambda\}$ is the factor by which the applied reference loading condition must be multiplied to produce buckling.

The geometric stiffness matrix $[K_G]$ is calculated using the initial stresses, which are determined from the applied load on the structure by completing a static analysis. Buckling occurs when the factored geometric stiffness $\{\lambda\}[K_G]$ equals the structural stiffness component $[K]$ associated with lateral strength. These terms basically cancel, leaving the structure with no lateral strength. The factor $\{\lambda\}$ multiplied by the applied load provides the linear buckling load.

The eigenvalue method of predicting linear buckling loads is the standard process used to predict buckling modes by FE codes. In this project, it is the methodology used for the prediction of the linear buckling response of the 1x1½ bay FE model.

8.4 Loads

As described in Section 8.3.2, performing an eigenvalue buckling analysis requires a previous linear static analysis to be performed. The state of stress resulting from the linear static analysis is used to calculate the geometric stiffness matrix. The load selected for the linear static analysis is similar to the load described in Section 6.5 for the non-linear analysis. It consists of a laterally applied load and an in-plane load.

The lateral load was applied as described in Section 6.5, with the exception that the load terminated at the boundaries of the model (i.e., web frames). The symmetry assumption implies that the load condition on both sides of the web frames is identical. As mentioned in Section 8.2, this is erroneous but will provide an acceptable simplification for the purposes of this analysis. The magnitude of the applied load used for the static analysis was equivalent to F_{max}. Therefore, the eigenvalues predicted were multiplied by F_{max} to give the magnitude of the buckling load.

An in-plane load of 69 MPa was applied to the model in the vertical direction only. This caused compression of the frames and was a result of the global response of the ship to the applied lateral ice load. This is described in Section 6.4. The symmetry boundary conditions applied at the web frames precluded the application of a longitudinal in-plane load.

8.5 Boundary Conditions

The overall boundary conditions used for the analysis were developed to replicate those used for Run 4 in the Phase III work. As discussed in Section 8.2, the model was reduced using symmetry for the eigenvalue analysis. Therefore, the boundary conditions had to represent the previous Run 4 and impose symmetric response on the model. Figure 6.5 in Section 6.4 shows the applied boundary conditions. Further details on the justification of the boundary conditions selected are contained in Section 6.4.

8.6 Linear Eigenvalue Analysis Results

A linear eigenvalue buckling analysis was performed for the "reduced Run 4" model. From these results, it was determined that the in-plane load was not a significant factor in the linearly predicted buckling load level. (Note: This is opposite to the effect that the in-plane load has on the post-yield buckling load level prediction as demonstrated in Section 9.3.1.) An analysis of the model with only the lateral ice load applied resulted in a buckling load level of over $8*F_{max}$. For the analysis with both load components (in-plane and lateral) applied, several of the first resulting buckling load factors (BLFs) were negative. This is because the main frames are linearly in tension when the loads are applied, while linear buckling is caused by compression of the frame.

With both load components applied, the first positive BLF (for apparent flexural-torsional buckling) was shown to occur at an applied load of about $6*F_{max}$ in a mode that was of no significance to the study. A plot of this mode shape can be seen in Figure 8.2. Even though the deflected shape for this mode looks very similar to the deflected shape for the non-linear tripping, the state of stress in the two models is entirely different.

As far as the validity of the assumed reduced model size, an analysis of the 3x3 bay model, with only the bottom half trimmed with symmetry, the side bays untouched and all loads applied as described in Section 6.5 (i.e., the original model), yielded a linear eigenvalue buckling load level of about $5*F_{max}$. This proved that the approximation using the reduced model was acceptable.

8.7 Conclusions

The philosophy behind performing these runs was to fully understand the linear equations so that they could be modified and extended into a regime where they would have the potential to be applicable to both linear and non-linear (post-yield) buckling. However, based on a review of the results, the linear equations do not reflect the non-linear flexural-torsional buckling that is observed in nature.

Performing the linear eigenvalue runs on a variety of structures as planned would not provide information that would be useful to deduce empirical relationships. It was assumed that the linear equations would have been developed to ensure that, under linear assumptions, buckling should not occur until after a load equal to F_{max} was applied. Therefore, it was expected that the linear buckling load levels would be significantly lower than observed in the eigenvalue analysis and that extrapolation of the linear results to the buckling load would give some meaningful information. However, understanding the linear response and extrapolating it to $6*F_{max}$ would not yield any insight into non-linear buckling, which will happen under a different mode at load levels below $2*F_{max}$.

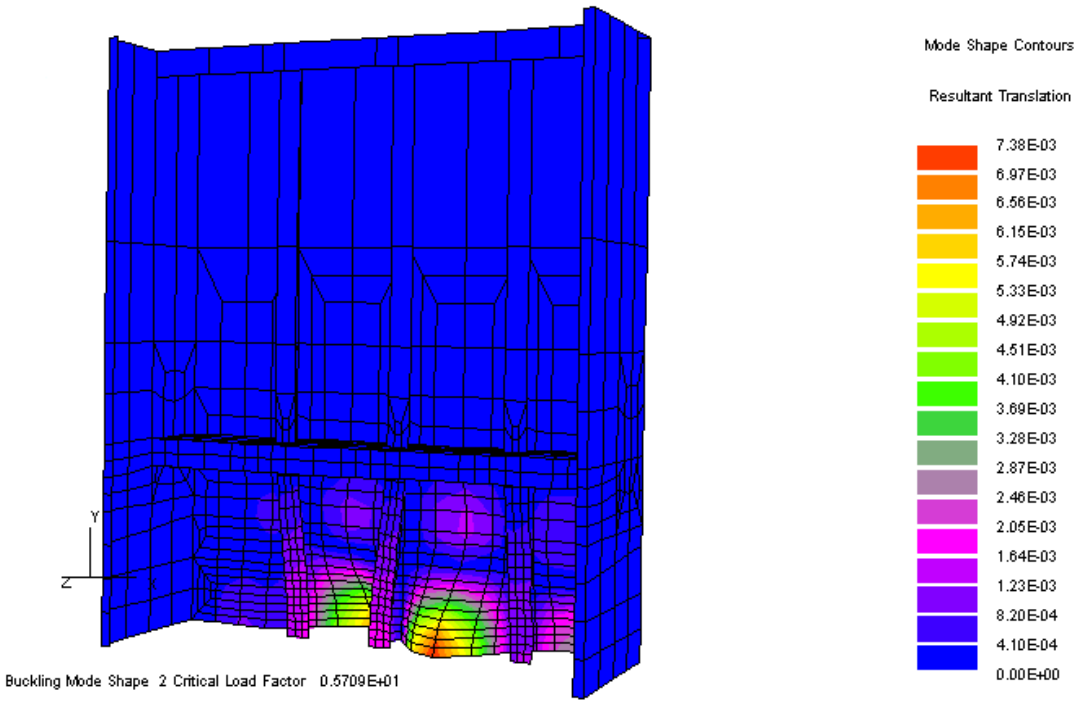

Figure 8.2 Buckling Mode for Panel with Vertical In-Plane and Lateral Ice Loads

In addition, as discussed in Section 5, there are some errors in the formulation of the linear equations and questionable assumptions have been made in their derivation. It was concluded that buckling predicted by linear equations shows no correlation with the "real life" response and little benefit would be gained by performing the linear eigenvalue runs on a variety of structures as originally intended.

With respect to the validation of the shear force difference methodology, as discussed in Sections 7.1 and 7.2, the level of the load required to achieve linear buckling was found to be high enough to create substantial non-linear effects that result in no correlation between linear and non-linear runs. Since the buckling phenomena to be predicted were non-linear and could only be modelled by incorporating large displacements into the model, the run had to be conducted by including large displacement effects. Therefore, the validation using linear eigenvalue analyses was not possible.

9. NON-LINEAR POST-YIELD ANALYSIS

9.1 Objective of Analysis

The objective of performing the non-linear post-yield analysis was to establish relationships between key parameters that describe the hull scantlings and the buckling load for main frames. The established relationships could then be used to develop equations that could be incorporated into the Equivalent Standards to control the design of icebreaker hull structures.

9.2 Analysis Methodology

9.2.1 Solution Methodology

FEA can be used to predict the "real life" response of a structure to a given set of loads. Provided that the model is developed with sufficient accuracy, FEA can give an accurate prediction of buckling response in highly non-linear, post-yield conditions. Therefore, by applying a "design" load to a given hull geometry, the response to that load can be determined with a reasonable degree of accuracy, subject to the assumptions that have been incorporated into the modelling and analysis.

The scantling geometry of a stiffened panel (representing a ship hull) can be characterized by several parameters. By selecting key parameters and altering the panel geometry by varying these independently, one can use FEA in a semi-empirical manner to study the response of the structure to these modifications. In this manner, a set of semi-empirical relationships can be developed to characterize the relationship between a selected parameter and the load at which buckling occurs.

The solution methodology for the analysis consisted of selecting several significant geometric parameters and performing series of analyses using FEA to determine the effect that varying each parameter had on the stability of the main frames. This was accomplished by varying each parameter independently while attempting to keep all other parameters constant. Details on the procedure to vary the parameters are contained in Section 9.2.2.

As described in Section 3.1, the non-linear post-yield analysis was performed using MAESTRO/DSA. The method of solution used was a procedure called the modified Load Displacement Control (LDC) method. This is the same method as was used in Phase III of this project. It was chosen because of its advantage over conventional applied force methods. When conventional applied force methods are used in the solution of large displacement non-linear analyses, the solution often fails at regions of high non-linearity (for example, at the bifurcation point of buckled structures) because of non-positive definite terms in the stiffness matrix. This results in an inability of the algorithm to converge to a unique solution.

The LDC method eliminates this problem by using displacements instead of loads to control the solution. A load vector must be provided; however, the algorithm is started at the first load step with an initial nodal displacement in the desired direction instead of a force. The program

automatically determines the load factor (a constant multiplied by the load vector) necessary to displace the structure by the initial displacement while maintaining equilibrium. The program then automatically determines the next incremental displacement and continues to the next load step. This procedure continues until either the maximum specified displacement is reached, the maximum number of time steps is reached, or the non-linearity is extreme enough to prevent convergence within four iterations of repeatedly reducing the incremental load. The advantage of using displacement control occurs when a large displacement results from a very small force (due to small stiffness). Without LDC, if a force is applied at this point, the program has difficulty converging to a displacement.

The MAESTRO/DSA program allows all of the loads and initial conditions to be incrementally increased at each load step for the LDC method. For example, the total load includes both the biaxial in-plane loads and ice loads normal to the hull plating. Therefore, at a load factor of 0.5 F_{max}, the in-plane loads and the ice load are both 50 percent of their (nominal) value at F_{max}. This provides an accurate representation of the load at all load levels. (This eliminates a problem encountered in previous studies where the in-plane load was applied with prescribed displacements that could not be scaled with applied load.)

The analysis accounts for non-linear material properties and large displacement effects, and assumes small strains.

9.2.2 Approach to Varying Parameters

As described in Section 8.7, the linear analyses did not provide any insight that would aid in the selection of relevant parameters to use for the non-linear formulations. However, based on Martec's previous analysis experience and engineering judgement, it was expected that the most important parameters affecting the buckling load for angle main frames would be: span, yield stress, flange width, flange thickness, web height (or web depth) and web thickness.

The current Equivalent Standards base the stability criteria for angles on only one parameter, span ratio. Span ratio is the ratio of the unsupported length of the frame to the width of the flange. The design is controlled by keeping this ratio below a specified value. From the results of the present study, it became apparent that the stability in the post-yield regime is adversely affected by both increasing span (LU) and by increasing flange width (WF). This means that the ratio LU/WF cannot be used to control stability since a proportional increase in both parameters would maintain the same span ratio but adversely affect stability. It is more likely that the product of LU*WF could be maintained at a given value to ensure stability. That is, as the span is increased, the flange width could be decreased to maintain the product. In the limit, this would lead to the elimination of the flange (resulting in a flat bar main frame) if post-yield buckling were the only consideration in the design. This indicates that the current parametric ratio, span ratio, is inadequate for controlling post-yield stability. Section 9.4.7 presents the results of an investigation of the relationship between span ratio and stability.

In this study, non-linear runs were conducted to determine the relationships between span and stability, and flange width and stability, independently. The most desirable way to vary the models to study the effects of changing individual parameters is to vary one parameter independently of all others. Therefore, to study the effect of increasing span, it was desirable to simply stretch out the panel while keeping all other dimensions the same. The drawback to this approach was that it produced a frame that does not meet the strength criteria of the Equivalent Standards and yielding would occur at a lower load level than in the original design. This yielding effect would, in itself, alter the buckling load levels and could mask the effect of increasing span. To offset this effect, the yield strength of the material was increased proportionally to the increase in span. Since the applied moment is linearly proportional to span, this compensated for the changed span and yielding should occur at the same applied load as the original design.

A similar approach was taken for varying the flange and web width and thickness, with the exception that the yield strength was modified proportionally to the moment of inertia of the equivalent section (i.e., combination of effective width of hull plating, web and flange). This approach maintained the original level of stress for a given load and hence yielding occurred at the original yielding load level.

Table 9.1 contains a sample calculation of the modified yield strength for one of the web thickness analyses. Table 2.1 in Section 2.2 contains a summary of the scantling dimensions used in the study. It also shows the modified yield strengths in MPa that were used for each of the runs.

9.2.3 Prediction of Buckling

As described in Section 7, buckling is predicted when the calculated value of the shear force difference decreases during increasing load application. This is determined by plotting the shear force difference (for a main frame) versus the total applied load. The load at which buckling occurs is found by selecting the value of the applied load corresponding to the point where the tangent to the curve is vertical. As described in Section 7, this methodology is found to give values that agree well with other characteristics that are indicative of buckling.

9.2.4 Methodology for Presentation of Results

The empirical/analytical approach for the evaluation of the non-linear FEA results was based on data visualization and relationship determination.

The data visualization step is important in understanding how the variables/parameters affect the stability of the structure in a post-yield condition. This step was a pattern recognition procedure that established patterns of behaviour from the non-linear analysis results. Microsoft Excel was used to visualize the data.

Once the data was plotted, regression analysis tools were used to develop the relationships between the significant variables and the limiting condition (i.e., the plastic buckling load). The regression analysis tools fit a curve through a set of observations. This enabled the determination of how a single dependent variable (plastic buckling load) is affected by the values of one or more independent variables.

To define the relationships, Microsoft Excel was used to fit the necessary type of equations to the non-linear FEA results. The options available through MS Excel are linear, polynomial, logarithmic, power or exponential. MS Excel also provides various regression statistics that were used to determine the accuracy of the curve fit for each of the parameters.

9.3 Non-linear Modelling Requirements

9.3.1 Effect of In-plane Loads on Main Frame Stability

In the non-linear solution algorithm (see Section 9.2.1), all of the loads and load-related "initial" conditions are incrementally increased at each load step in direct proportion to each other. The total load includes both a biaxial in-plane load and ice loads (applied normal to the plate). Both of these load components are scaled in the solution process. Since the in-plane load is a direct result of the local/global response of the ship to the ice load, this representation is accurate at all load levels. However, it creates some confusion when the load factor is greater than one and all loads are scaled accordingly.

The effect of the in-plane load was studied by varying the "nominal" level of the in-plane load. The nominal in-plane load is defined as the magnitude of the in-plane load at an applied ice load equal in magnitude to F_{max}. Note that for a load factor of less than one the in-plane load will be less than its nominal value, and at load factors greater than one it will be greater.

The results of the study are shown in Figure 9.1. From this figure, it can be seen that as the nominal in-plane load is increased, buckling occurs at a lower load level. Note, however, that buckling at a load level less than F_{max} would mean that the value of the in-plane load at buckling is less than the nominal level. This effect is shown in Figure 9.1, which plots the BLF vs. the magnitude of the in-plane load at the point of buckling. As shown in the figure, it is evident that as the magnitude of the in-plane load is increased, the BLF is decreased, and that the trend is virtually linear. Therefore, as the proportion of in-plane load to lateral ice load is increased, the structure buckles at a lower overall load level.

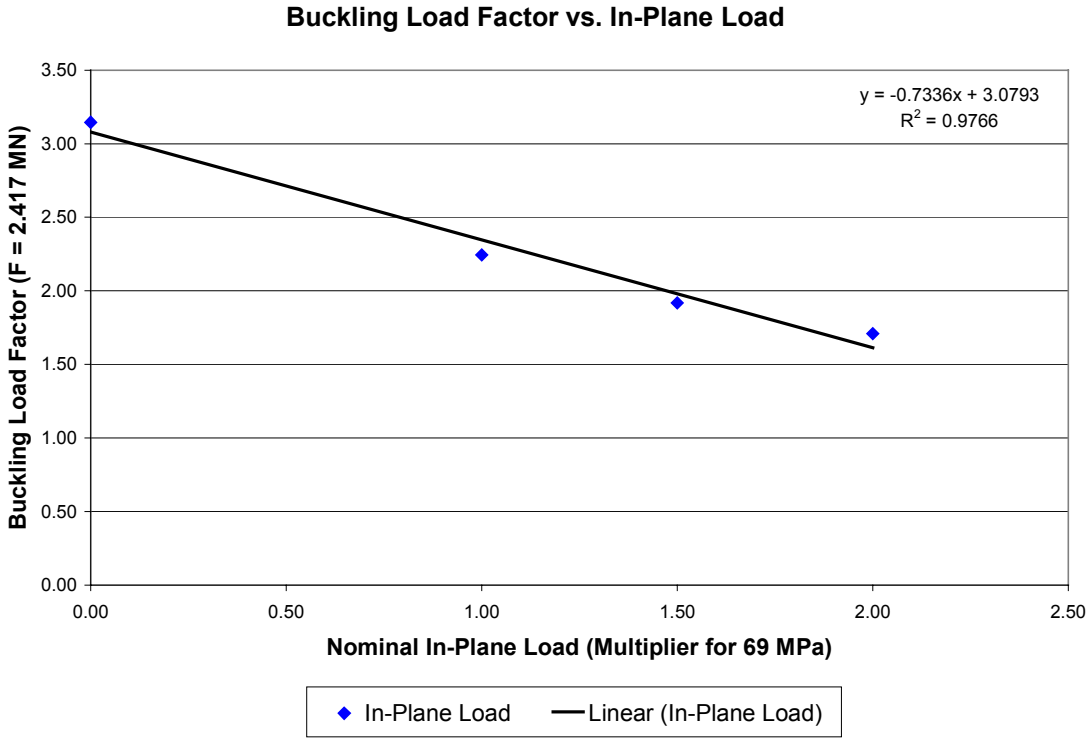

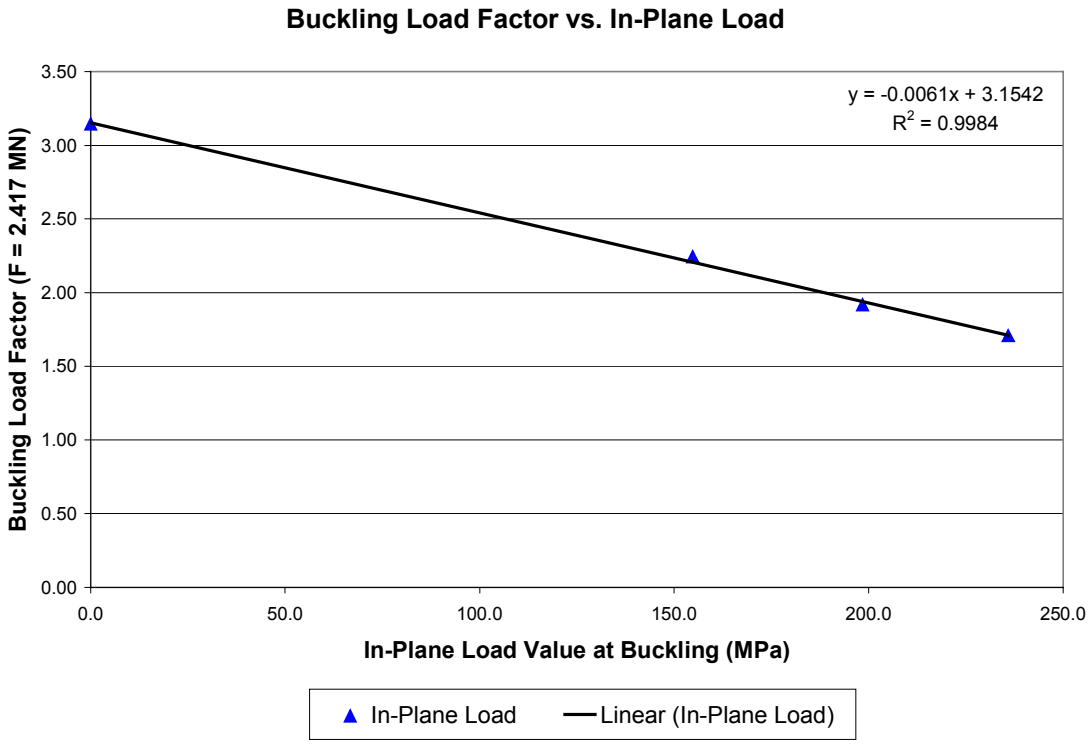

Figure 9.1 Buckling Load Factors vs. In-Plane Loads

9.3.2 Effect of Deep Web Failure on Main Frame Stability

During the course of the initial non-linear investigation, it was found that the extent of yielding in the deep web frames greatly affected the stability of the main frames. Figure 9.2 shows the shear force difference curves of the benchmark analysis (DSA Run 4) and the base run for the current parametric study (Run IV-1). The two models are essentially identical, with the exception of the strain-hardening modulus in the deep webs. In Run IV-1, this modulus is set equal to the modulus of elasticity, E, and as a result the deep webs behave linearly throughout the analysis and do not yield.

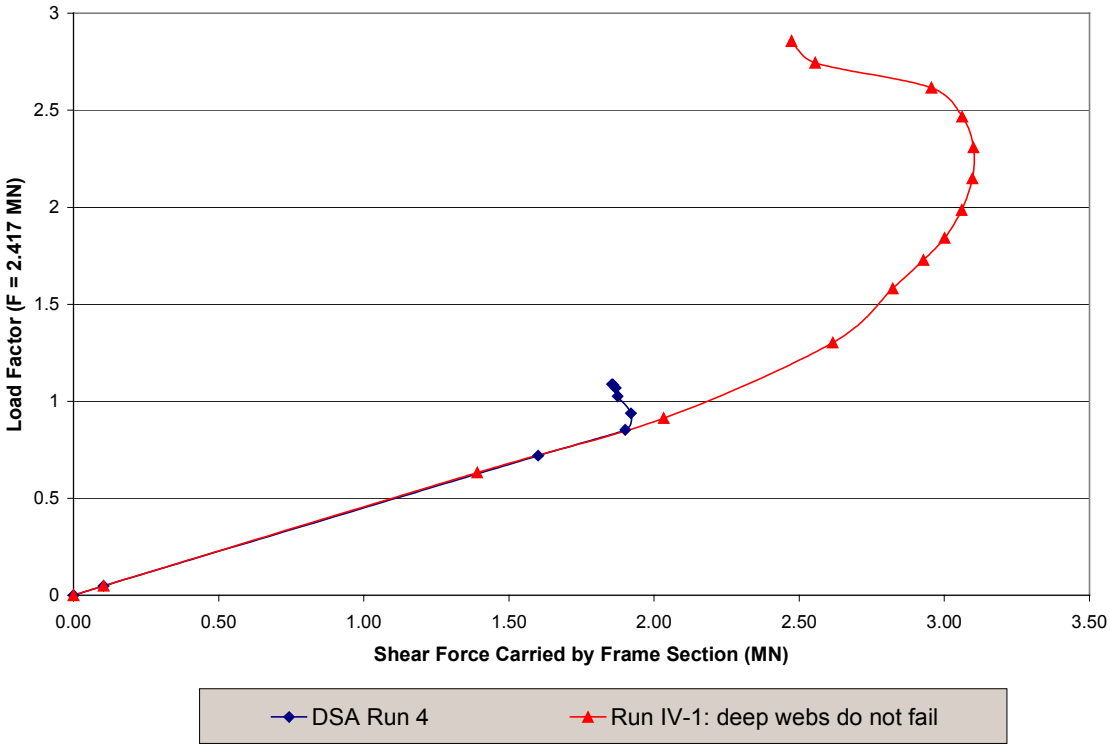

Figure 9.2 Shear Force Difference Plot Comparing Runs with Linear and Nonlinear Response in the Deep Webs

It can be seen that the response in the main frames is very different between the two runs. The main frames in the benchmark analysis (see Section 4) buckle at a significantly lower load level than those in Run IV-1. Upon an investigation of this occurrence, it was found that the deep webs in the benchmark analysis fail prior to main frame buckling. Thus the response in the main frames is influenced by the failure of the tertiary supporting structure.

To study the buckling stability of the main frames, it was necessary to eliminate the failure of the deep web frames. This was accomplished by increasing the strain-hardening modulus of the deep web frames to the value of the elastic modulus, E, effectively creating a linear response in the deep web frames.

In justifying this modification on a physical, "real life" level, one must look at the physical implications of the modification. The fact that the deep web frames buckle prior to the main frames would indicate that the either the deep web frames are underdesigned or the main frames are overdesigned, based on a post-yield buckling design requirement. If the structure is optimally designed for post-yield buckling, the structure will remain stable until just after F_{max} and then the deep web frames and main frames would become unstable at approximately the same load level. Although this is unlikely to occur (since other design constraints will likely result in one or the other structure being overdesigned for buckling), the performance of the main frames should not be influenced by the prior buckling of the deep web frames. This concern is eliminated by requiring the material in the deep web frames to remain linear.

9.4 Test Matrix

9.4.1 Effect of Yield Strength on Stability

In Section 9.2.2 it was explained that the yield strength of the panel was modified for the non-linear runs in order for all the new panel configurations to yield at the same applied load level. In the previous phases of this project, it was found that main frame stability is heavily affected by the magnitude of the material yield strength.

To determine the effect of yield strength on stability, a series of runs was completed where only the yield strength was modified. This investigation showed that the material yield strength has an important effect on the stability of the main frames. The relationship between the yield strength and the BLF was found to be linear, as can be seen in Figure 9.3. The panel becomes more stable in the post-yield regime as the yield strength is increased.

This relationship, in the form of the equation displayed in the figure, was used to adjust the results of the other runs to take into account the change in yield strength. It is important to notice that for this particular panel, the curve does not go below F_{max} until the yield strength of the material is reduced to a value too small to be practical in design. Therefore, for this geometry, non-linear buckling will not result from yield strength modifications alone.

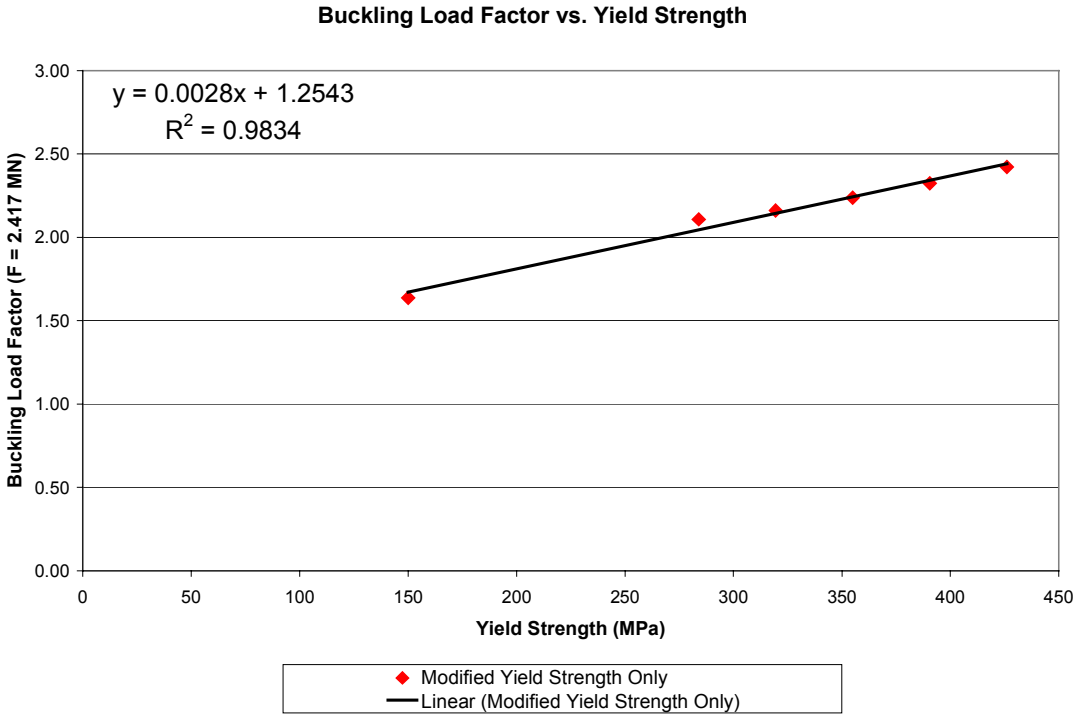

Figure 9.3 Buckling Load Factor vs. Yield Strength

9.4.2 Effect of Span on Stability

In the linear regime, span is very important to stability. Linearly, the buckling load depends on the inverse of span squared. Thus, as the unsupported length (or span), increases, the buckling load decreases. A similar relationship was anticipated in the case of the non-linear runs. Seven analyses were performed to investigate the effect of varying span on non-linear main frame stability. The values of span that were considered in the analyses are shown below. Also shown below are the load levels corresponding to the initiation of buckling as determined from each of the analyses.

	Span		Increase/Run IV-1 of Buckling	Load Level for Initiation
Run IV-1	2300.0 mm	–	00.0% increase	2.24 * F_{max}
Run IV-2	2530.0 mm	–	10.0% increase	2.40 * F_{max}
Run IV-3	2760.0 mm	–	20.0% increase	2.67 * F_{max}
Run IV-4	2070.0 mm	–	10.0% decrease	2.20 * F_{max}
Run IV-5	1840.0 mm	–	20.0% decrease	2.13 * F_{max}
Run IV-6	1533.3 mm	–	33.0% decrease	2.21 * F_{max}
Run IV-7	1298.0 mm	–	43.6% decrease	Did not buckle

Other than the changes made to the span, all other scantlings remained unchanged from the Run 4 panel configuration. The yield strength of the panel was modified for each of the analyses in order for all the new panel configurations to yield at the same applied load level. To achieve this, the yield strength was adjusted proportionally with span. This was done to account for the increase in bending moment (and therefore the relevant stress) as the span was increased. For example, when span was increased by 10 percent, the yield strength was also increased by 10 percent.

The buckling load level is plotted versus the span in Figure 9.4. (Note: In the plot of Figure 9.4 and subsequent plots, polynomials are used to fit the data points generated from the analyses. These are the "best fit" curves and are identified as the "Poly." of the particular data set that is being plotted.)

As can be seen from Figure 9.4 and the numbers presented above, the relationship found is rather counter-intuitive. Initially, as one might expect, the stability of the panel decreases as the span is increased. However, for spans greater than about 2 m, this trend reverses and the stability begins to increase as the span is increased. The curve shows a change in buckling load as span is varied, but it appears to be bounded by a horizontal line at BLF = 2. That is, regardless of the dimension of the span, the main frames do not experience buckling below a load level of $2*F_{max}$.

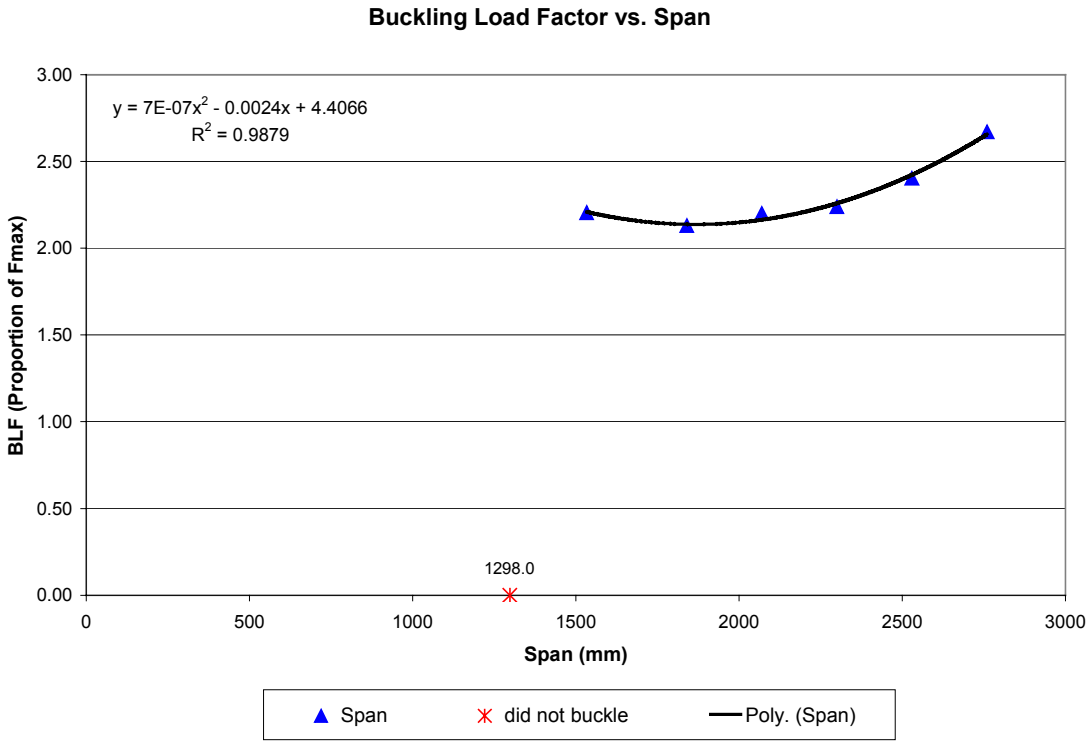

Figure 9.4 Buckling Load Factor vs. Span

In Section 9.4.1 the effect of changing the yield strength on stability was investigated. This relationship proved to be linear and the resulting relationship was used to determine what the response of the various panels would have been if the yield strength had not been changed. The comparison of the results from the actual analyses and the results with the yield strength effect accounted for is shown in Figure 9.5. It can be seen that the effect of changing the yield strength is not particularly dramatic, and that the two curves are similar and exhibit the same type of polynomial shape.

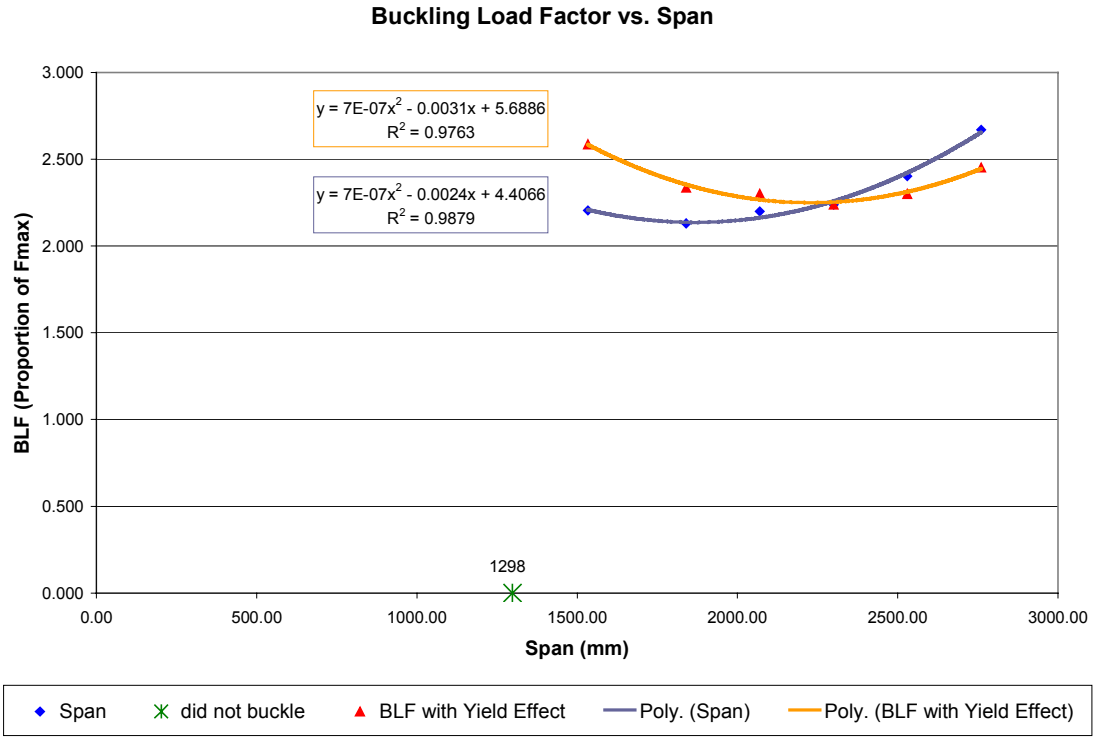

Figure 9.5 Buckling Load Factor vs. Span, Including Yield Effect

9.4.3 Effect of Main Frame Flange Width on Stability

The flange width is important to stability in more than one way. First, the flange increases the bending stiffness of the section, so increasing its width (while maintaining constant flange thickness) should increase the load at which buckling occurs. Counteracting this effect, however, is the added eccentricity of the section as the flange width is increased. In the previous phase of this project, it was thought that this eccentricity contributed to non-linear tripping, and therefore increasing the flange width should, in this respect, lower the post-yield buckling load.

In addition to Run IV-1, five analyses were performed to investigate the effect of flange width on non-linear main frame stability. The values of flange width considered for the analyses are shown below, as are the load levels corresponding to the initiation of buckling as determined from each of the analyses.

	Main Frame Flange Width		Load Level for Increase/Run IV-1	Initiation of Buckling
Run IV-1	132 mm	–	00.0% increase	2.24 * F_{max}
Run IV-8	165 mm	–	25.0% increase	2.11 * F_{max}
Run IV-9	198 mm	–	50.0% increase	2.10 * F_{max}
Run IV-10	250 mm	–	89.4% decrease	2.31 * F_{max}
Run IV-11	99 mm	–	25.0% decrease	2.50 * F_{max}
Run IV-12	66 mm	–	50.0% decrease	No buckling

Other than the changes made to the flange width, all other scantlings remained unchanged from the Run 4 panel configuration. Again, the yield strength of the panel was modified for each of the analyses in order for all the new panel configurations to yield at the same applied load level. To achieve this, the yield strength was adjusted according to the change in section modulus. A sample calculation is provided in Table 9.1.

The post-yield buckling load level is plotted versus the flange width in Figure 9.6.

As can be seen from Figure 9.6 and the numbers presented above, the relationship found is similar in shape to that found for span. Initially, the stability of the panel decreases as the flange width is increased, then at one point the response alters such that the stability begins to increase as the flange width is increased. The curve is again bounded by a horizontal line at BLF = 2. That is, regardless of the dimension of the flange width, the main frames do not experience buckling below a load level of 2*F_{max}.

To determine what the response of the various panels would have been if the yield strength had not been changed, the relationship from Section 9.4.1 was applied. The comparison of the results from the actual analyses and the results with the yield strength effect accounted for is shown in Figure 9.7. It can be seen that the effect of changing the yield strength is again quite unimportant, and that the two curves are very similar and exhibit the same type of polynomial shape.

Table 9.1 Sample Calculation of Adjustment of Yield Strength Based on Section Modulus

ORIGINAL (RUN 4, webs do not yield)					
b1 (flange width) =	132	**A1 =** b1*h1	**x1 =** 0.5*h1+h2+h3	**I1 =** (1/12)b1*h1^3	**d1 =** x1-xbar
h1 (flange thickness) =	15.875	= **2095.5**	= **312.1005**	= **44008.2**	= **243.7974**
b2 (web thickness) =	23.81	**A2 =** b2*h2	**x2 =** 0.5*h2+h3	**I2 =** (1/12)b2*h2^3	**d2 =** x2-xbar
h2 (web depth) =	274	= **6523.94**	= **167.163**	= **40815943.3**	= **98.860**
b3 (included plating length) =	720	**A3 =** b3*h3	**x3 =** 0.5*h3	**I3 =** (1/12)b3*h3^3	**d3 =** x3-xbar
h3 (plate thickness) =	30.163	= **21717.36**	= **15.0815**	= **1646549.7**	= **-53.2216**
		Atotal = A1+A2+A3	**xbar =** $\frac{(A1*x1+A2*x2+A3*x3)}{Atotal}$	**Ixbar =** $\Sigma\,(I_n+A_n*d_n^2)$	**xbar/Ixbar =** **2.33649E-07**
		= **30336.8**	= **68.30**	= **292332649.7**	
			Yield stress 1 = **355**		

DECREASE WEB THICKNESS BY 10%					
b1 (flange width) =	132	**A1 =** b1*h1	**x1 =** 0.5*h1+h2+h3	**I1 =** (1/12)b1*h1^3	**d1 =** x1-xbar
h1 (flange thickness) =	15.875	= **2095.5**	= **312.1005**	= **44008.2**	= **245.9701**
b2 (web thickness) =	21.429	**A2 =** b2*h2	**x2 =** 0.5*h2+h3	**I2 =** (1/12)b2*h2^3	**d2 =** x2-xbar
h2 (web depth) =	274	= **5871.55**	= **167.163**	= **36734349.0**	= **101.033**
b3 (included plating length) =	720	**A3 =** b3*h3	**x3 =** 0.5*h3	**I3 =** (1/12)b3*h3^3	**d3 =** x3-xbar
h3 (plate thickness) =	30.163	= **21717.36**	= **15.0815**	= **1646549.7**	= **-51.0489**
		Atotal = A1+A2+A3	**xbar =** $\frac{(A1*x1+A2*x2+A3*x3)}{Atotal}$	**Ixbar =** $\Sigma\,(I_n+A_n*d_n^2)$	**xbar/Ixbar =** **2.34726E-07**
		= **29684.406**	= **66.13**	= **281734899.7**	
	% Diff in xbar/Ixbar = **0.460967**		**Yield stress 2 =** **356.6**	= [1+(% Diff/100)]*YS1	

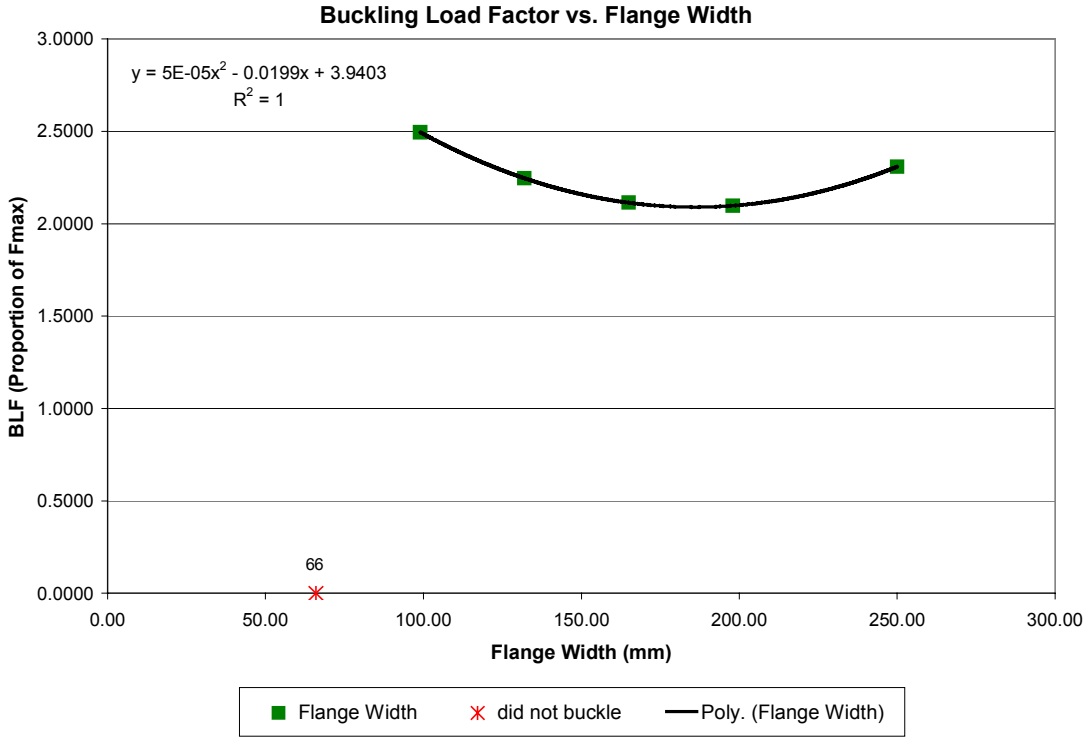

Figure 9.6 Buckling Load Factor vs. Flange Width

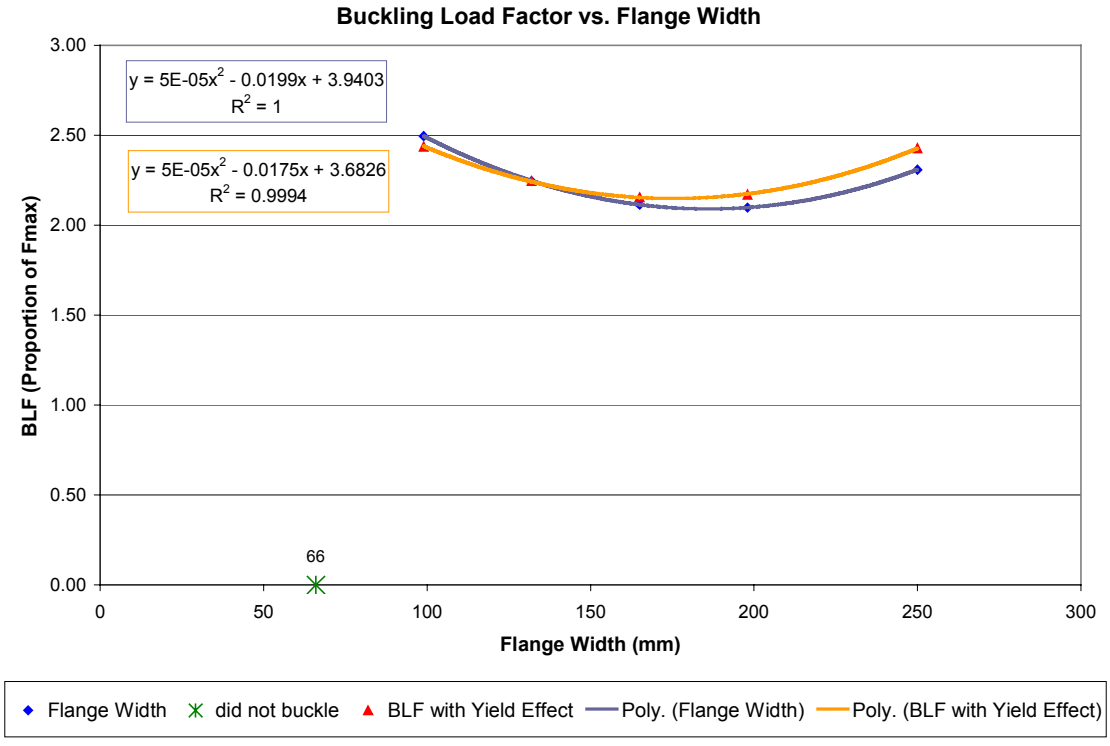

Figure 9.7 Buckling Load Factor vs. Flange Width, Including Yield Effect

9.4.4 Effect of Main Frame Web Depth on Stability

Linearly, increasing the main frame web depth would have an adverse affect on main frame stability. As the web depth is increased, the section centroid moves farther from the plating, increasing the potential for tripping of the frame. Counteracting this effect, the section modulus increases in proportion to the web depth, increasing the bending stiffness.

In addition to Run IV-1, five analyses were performed to investigate the effect of web depth on non-linear, post-yield main frame stability. The values of web depth considered in the analyses are shown below, as are the load levels corresponding to initiation of buckling.

	Main Frame Flange Width		Increase/Run IV-1	Load Level for Initiation of Buckling
Run IV-1	274.0 mm	–	00% increase	2.24 * F_{max}
Run IV-13	328.8 mm	–	20% increase	2.04 * F_{max}
Run IV-14	356.2 mm	–	30% increase	2.01 * F_{max}
Run IV-15	400.0 mm	–	46% decrease	2.04 * F_{max}
Run IV-16	246.6 mm	–	10% decrease	2.50 * F_{max}
Run IV-17	219.2 mm	–	20% decrease	3.11 * F_{max}

Other than the changes made to the web depth, all other scantlings remained unchanged from the Run 4 panel configuration. Again, the yield strength of the panel was modified according to the change in section modulus for each of the analyses in order for all the new panel configurations to yield at the same applied load level.

The buckling load level is plotted versus the web depth in Figure 9.8.

As can be seen from Figure 9.8 and the numbers presented above, the relationship found is again similar in shape to that found for span and flange width. Initially, as one might expect, the stability of the panel decreases as the web depth is increased, but at one point the response alters such that the stability begins to increase as the web depth is increased. The curve is again bounded by a horizontal line close to BLF = 2. That is, regardless of the dimension of the web depth, the main frames do not experience buckling below a load level of around 2*F_{max}.

To determine what the response of the various panels would have been if the yield strength had not been changed, the relationship from Section 9.4.1 was again applied. The comparison of the results from the actual analyses and the results with the yield strength effect accounted for is shown in Figure 9.9. It can be seen that the effect of changing the yield strength is again relatively unimportant, and that the two curves are similar.

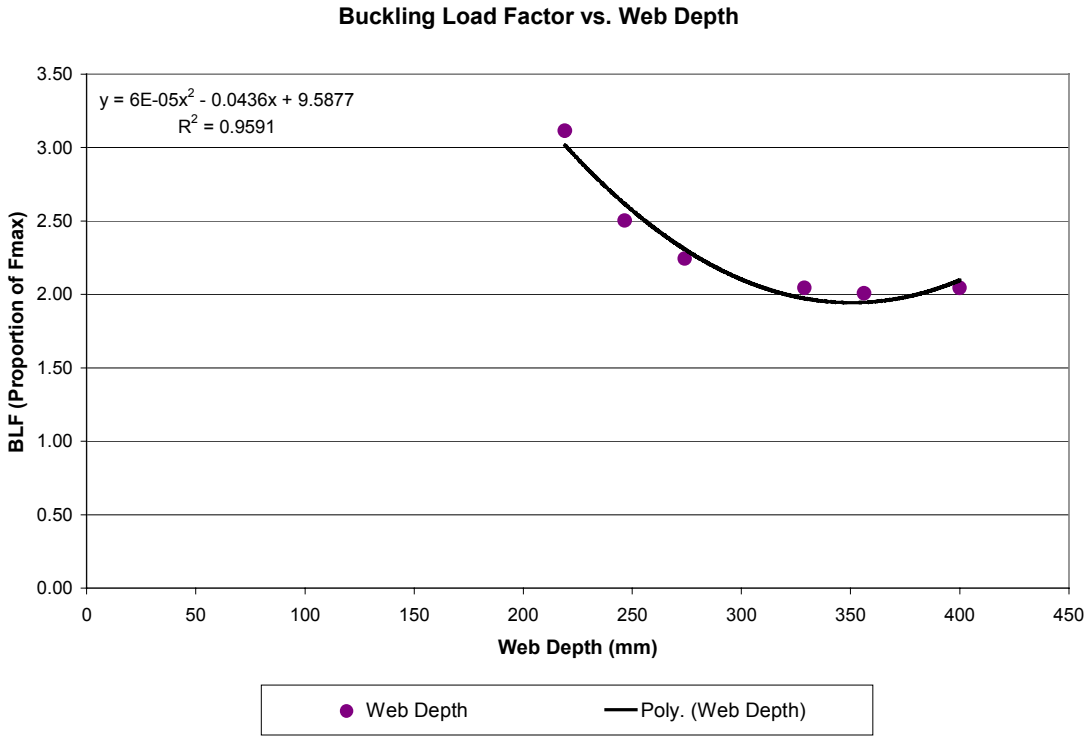

Figure 9.8 Buckling Load Factor vs. Web Depth

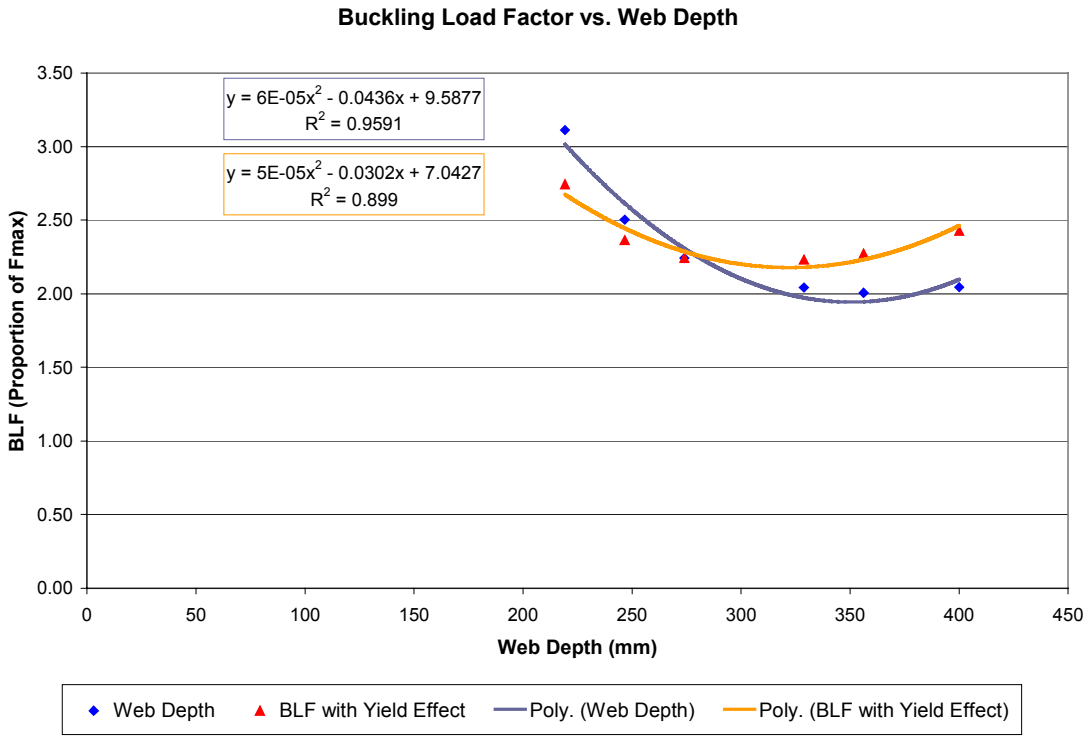

Figure 9.9 Buckling Load Factor vs. Web Depth, Including Yield Effect

9.4.5 Effect of Main Frame Flange Thickness on Stability

One would expect that the flange thickness would have a similar effect on stability as flange width, in that an increase in the flange width increases the bending stiffness of the section. Thus, intuitively, it is expected that increasing its thickness should increase the buckling load. Also similar to increasing the flange width, increasing the flange thickness increases the eccentricity of the centroid of the section.

In addition to Run IV-1, five analyses were performed to investigate the effect of flange thickness on non-linear main frame stability. The values of flange thickness are shown below for each of the runs. The load level corresponding to the initiation of buckling is also shown below.

	Main Frame Flange Thickness		Increase/Run IV-1	Load Level for Initiation of Buckling
Run IV-1	15.875 mm	–	00% increase	2.24 * F_{max}
Run IV-18	19.050 mm	–	20% increase	2.18 * F_{max}
Run IV-19	23.813 mm	–	50% increase	2.13 * F_{max}
Run IV-20	30.000 mm	–	89% decrease	2.13 * F_{max}
Run IV-21	12.700 mm	–	20% decrease	2.36 * F_{max}
Run IV-22	7.938 mm	–	50% decrease	2.89 * F_{max}

Other than the changes made to the flange thickness, all other scantlings remained unchanged from the Run 4 panel configuration. Again, the yield strength of the panel was modified according to the change in section modulus for each of the analyses in order for the new panel configurations to yield at the same applied load level.

The buckling load level is plotted versus the flange thickness in Figure 9.10.

As can be seen from Figure 9.10 and the numbers presented above, the relationship found is again somewhat similar in shape to those found for the preceding parameters. The stability of the panel decreases as the flange thickness is increased. The data does not change to indicate that the stability would at some point increase as the flange thickness is further increased, but it may be that this would occur if further analyses were performed. A best-fit curve indicates that this is the case. Further analysis was not deemed necessary, as the curve is again bounded by a horizontal line at BLF = 2. That is, regardless of the dimension of the flange thickness, the main frames do not experience buckling below a load level of 2*F_{max}.

To determine the response of the various panels if the yield strength had not been changed, the relationship from Section 9.4.1 was applied. The comparison of the results from the actual analyses and the results with the yield strength effect accounted for is shown in Figure 9.11. It can be seen that the effect of changing the yield strength is minimal, and that the two curves are very similar and exhibit the same type of polynomial shape.

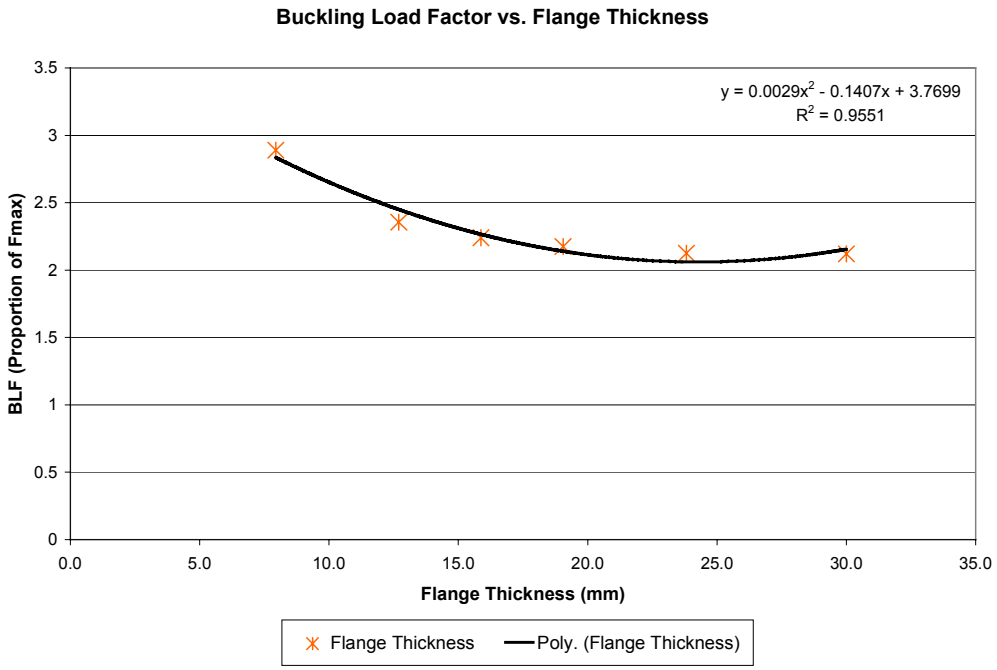

Figure 9.10 Buckling Load Factor vs. Flange Thickness

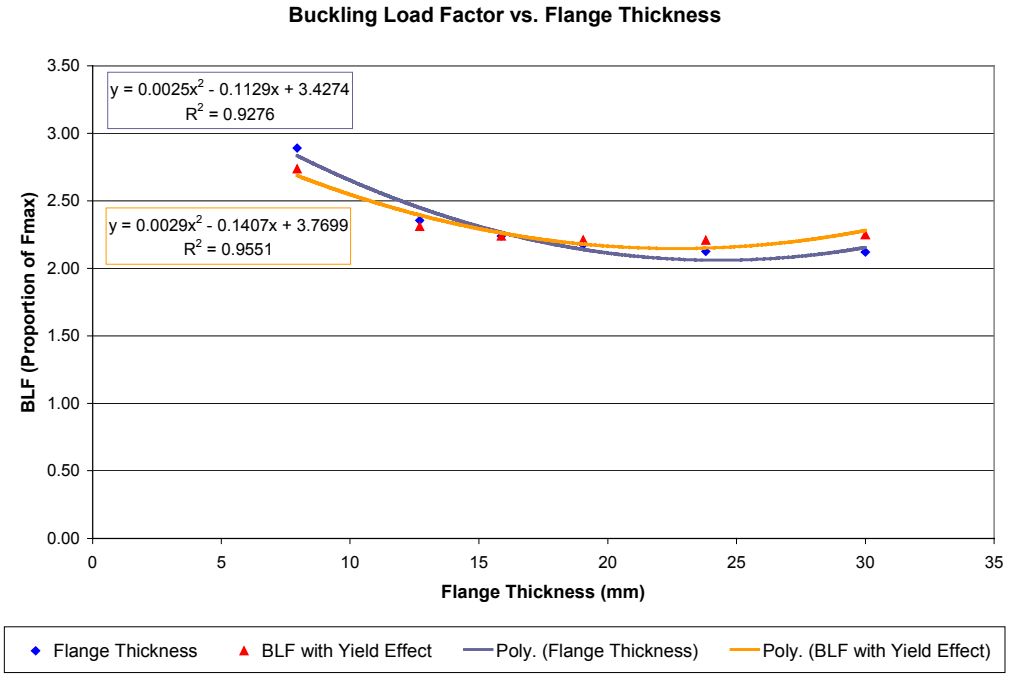

Figure 9.11 Buckling Load Factor vs. Flange Thickness, Including Yield Effect

9.4.6 Effect of Main Frame Web Thickness on Stability

In addition to Run IV-1, six analyses were performed to investigate the effect of web thickness on non-linear main frame stability. The values of web thickness are shown below for each of the runs together with the load level corresponding to the initiation of buckling.

	Web Thickness		Increase/Run IV-1	Load Level for Initiation of Buckling
Run IV-1	23.810 mm	–	00% increase	2.24 * F_{max}
Run IV-23	26.191 mm	–	10% increase	2.64 * F_{max}
Run IV-24	28.570 mm	–	20% increase	2.85 * F_{max}
Run IV-25	21.429 mm	–	10% decrease	1.95 * F_{max}
Run IV-26	19.048 mm	–	20% decrease	1.70 * F_{max}
Run IV-27	15.000 mm	–	37% decrease	1.37 * F_{max}
Run IV-28	10.000 mm	–	58% decrease	0.84 * F_{max}

Other than the changes made to the web thickness, all other scantlings remained unchanged from the Run 4 panel configuration. Again, the yield strength of the panel was modified according to the change in section modulus for each of the analyses in order for all the new panel configurations to yield at the same applied load level.

The buckling load level is plotted versus the web thickness in Figure 9.12.

As can be seen from Figure 9.12 and the numbers presented above, there is a linear dependence of buckling load on frame web thickness. The stability of the panel increases as the web thickness is increased.

To determine what effect the change in yield strength had on the response of the various panels, the relationship from Section 9.4.1 was applied again. The comparison of the results from the actual analyses and the results with the yield strength effect accounted for is shown in Figure 9.13. It can be seen that the effect of changing the yield strength is again minimal, and that the two curves are virtually identical.

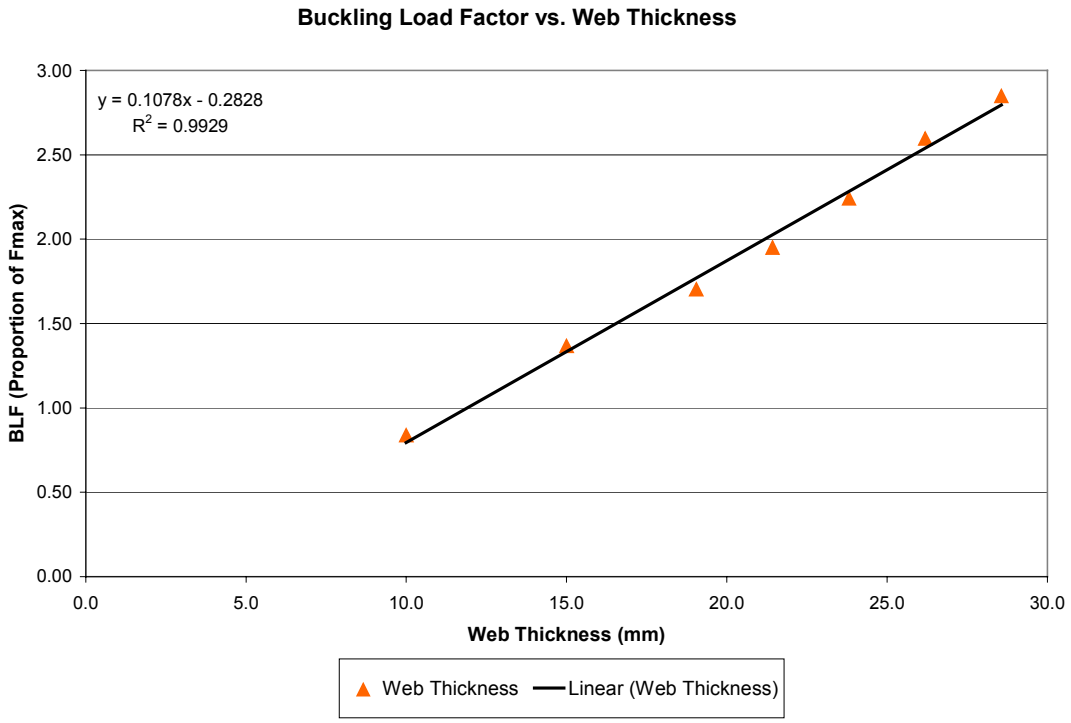

Figure 9.12 Buckling Load Factor vs. Web Thickness

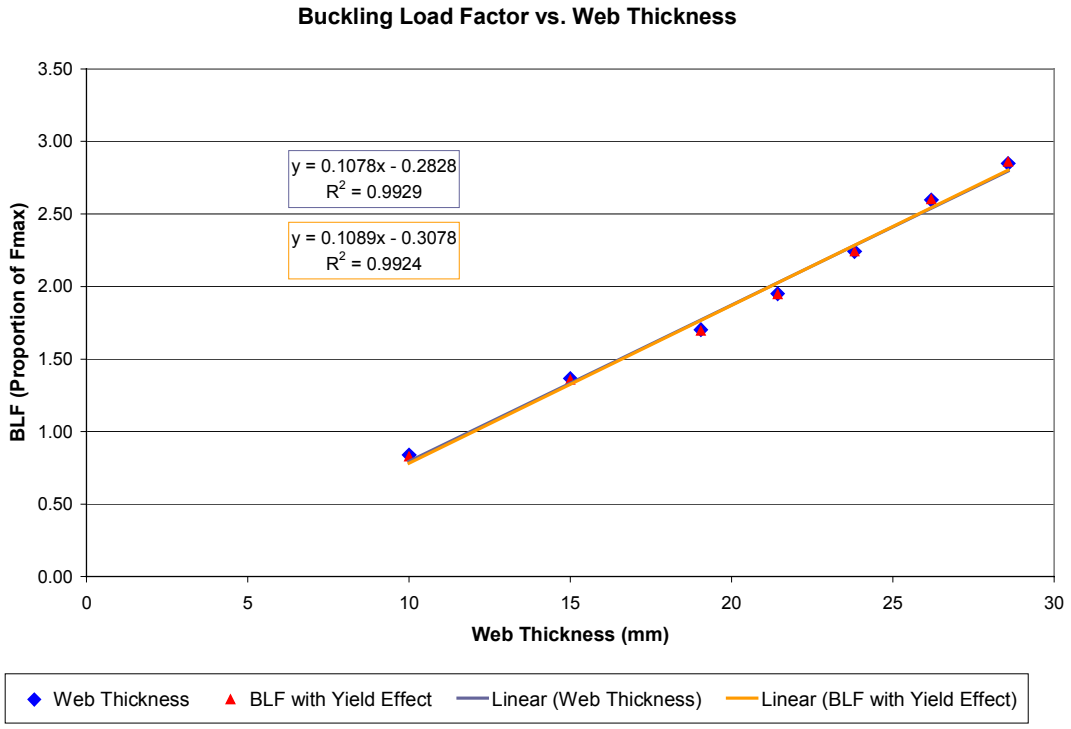

Figure 9.13 Buckling Load Factor vs. Web Thickness, Including Yield Effect

9.4.7 LU/WF versus Buckling Load

As discussed in Section 9.2.2, LU/WF is used in the Equivalent Standards to control stability. The Equivalent Standards require that LU/WF be maintained below a specified value and indicate that any increase in LU/WF would result in a decrease in stability. Using the results of the analyses presented in Sections 9.4.2 through 9.4.6, a curve of Span/Flange Width (LU/WF) was generated and can be seen in Figure 9.14. It shows a relationship between LU/WF and BLF. The curve is still bounded by a horizontal line BLF = 2, as was the case with the separate flange width and span curves. Figure 9.15 compares the LU/WF curves for the actual analysis results and the results altered by including the yield strength effect as described in Section 9.4.1. Again, the curves are bounded by a horizontal line BLF = 2.

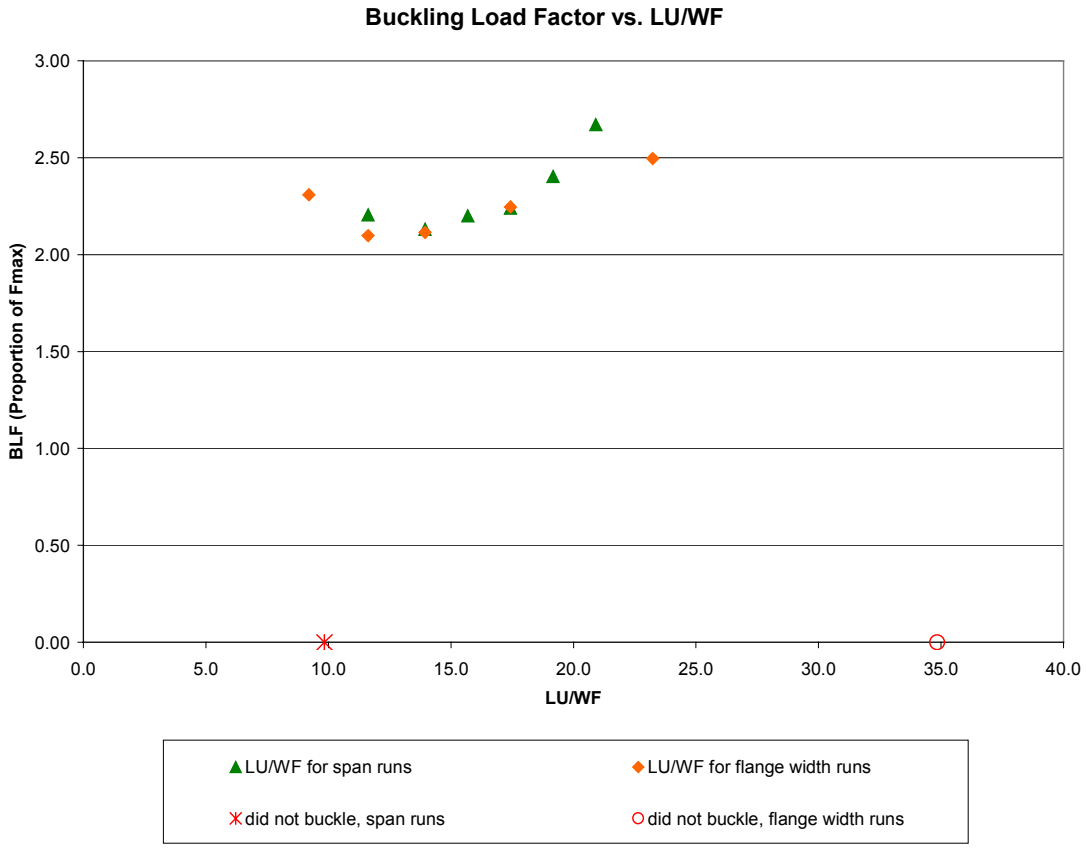

Figure 9.14 Buckling Load Factor vs. LU/WF

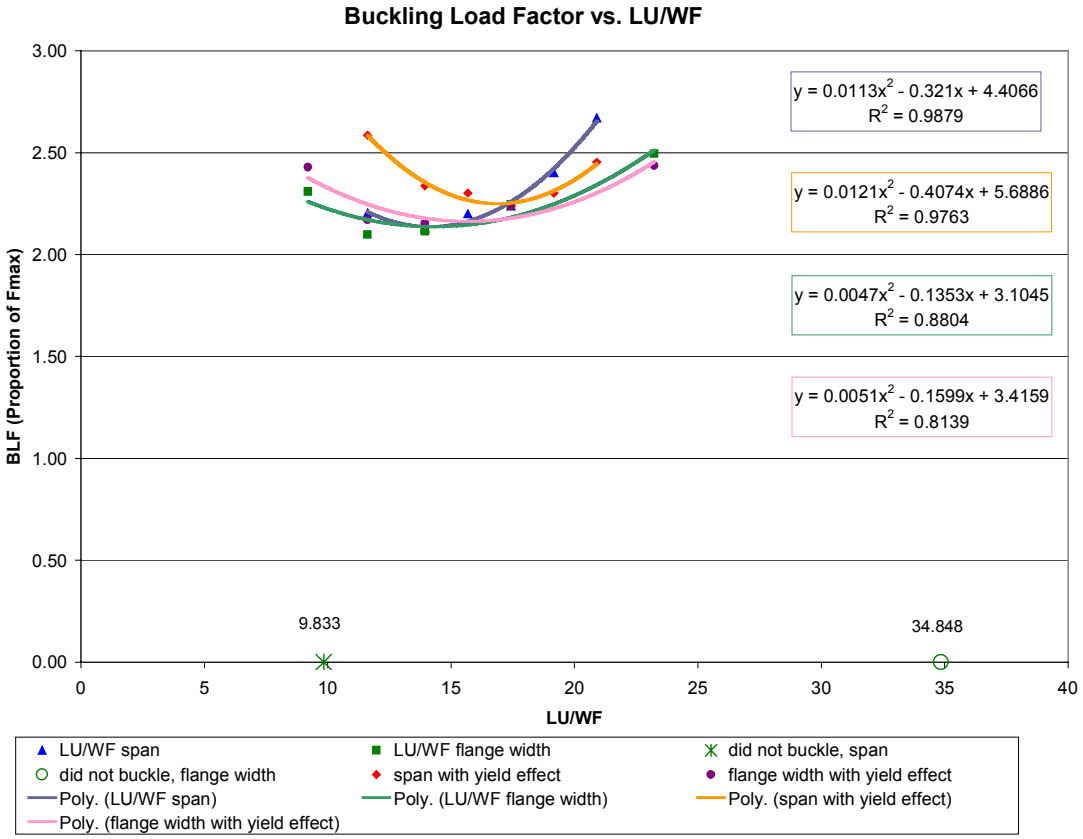

Figure 9.15 Buckling Load Factor vs. LU/WF, Including Yield Effect

9.5 Results and Conclusions from the Non-linear Analyses

For each of span, web depth, flange thickness and flange width, the curves of BLF vs. dimension are bounded by a horizontal line at BLF = 2. That is, regardless of the dimensions of the span, web depth or flange, the main frames do not experience buckling below a load level of $2*F_{max}$.

Therefore, in summary, only two parameters affect the frame stability at the load levels of interest: web thickness and material yield strength.

It must be understood that all of the information generated in this study is based on one ship configuration (i.e., displacement and power). Dimensions have been varied extensively for this ship and there is a high level of confidence that, for this ship, the relationships defined in Sections 9.4.1 to 9.4.7 are accurate and that post-yield buckling will not be a problem except for frames with very thin webs. However, whether this will hold for all ships of varying displacement and power has yet to be determined and is beyond the scope of this project.

Typically, current restrictions imposed on designers to control buckling are very conservative and result in a structure that is overdesigned. This is because the equations describing buckling do not reflect the structural response and employ large factors of safety (3 or 4) to account for their inaccuracies. Upon completion of this study, it appears that it would probably not be practical (or perhaps even possible) to identify analytical relationships that would accurately predict post-yield buckling because the response is too complicated. It is quite possible that the approach taken in the future will be that ship designers will use formulae only to provide an initial design that will then be verified and optimized by non-linear FEA.

In summary, based on the results of this study, it could be concluded that post-yield buckling is a concern only when determining the web thickness for main frames.

10. OVERALL PROJECT CONCLUSIONS AND RECOMMENDATIONS

The literature survey did not uncover any new work relevant to the post-yield buckling response of ship structure. No analytical solutions dealing with large displacements/rotations and large-scale non-uniform plastic deformations in the pre-buckling range were identified. Because of its complexity, it is likely that analytical solutions for this problem do not exist.

The stability equations in the Equivalent Standards are not expected to predict the expected "real life" response to a laterally applied load. It was decided that there would be no merit in trying to modify those equations or to try to extend the equations into the non-linear regime.

It is concluded that the shear force difference method for predicting the post-yield buckling load level is a valid process. A linear eigenvalue buckling analysis, performed within a non-linear analysis at a load level of $2.16*F_{max}$, demonstrated a main frame instability in the structure at a load level of $2.197*F_{max}$. This supported the graphical calculation of buckling load level at $2.24*F_{max}$ determined using the shear force difference method.

Although the purpose of the study was to review post-yield buckling criteria that would be independent of ship geometry, the study was conducted with one global ship configuration. For this specific configuration, it is concluded that only two parameters affect the frame stability at the load levels of interest: web thickness and material yield strength. It was determined that post-yield buckling will not occur unless the frame webs are very thin. Whether this will hold for all ships of varying displacement and power is unknown at this point as all studies were conducted with one ship geometry.

It was shown that for variations in span, web depth, flange thickness and flange width, main frames do not experience buckling for this ship below a load level of $2*F_{max}$. Therefore, it is concluded that post-yield buckling is not a concern unless frame web thicknesses are very small.

Upon completion of this study, it appears that it is not practical (or perhaps even possible) to identify analytical relationships that would accurately control post-yield buckling because the response is too complicated. It is quite possible that the approach taken in the future will be that ship designers use such formulas only to provide an initial design that will then be verified and optimized by non-linear finite element analysis.

It is therefore recommended that designers use the current Equivalent Standards rules for developing ship scantling sizes. Based on the results of this and previous studies, main frames designed using the current rules show no trend toward post-yield buckling below F_{max}. In fact, most designs fail above $2* F_{max}$.

It is also recommended that, where critical, non-linear finite element analysis be performed to determine the specific post-yield buckling response of the designed structure. It is further recommended that procedures/guidelines be developed for performing the non-linear analyses. These analyses are very complicated and a set procedure should be followed by qualified personnel to assure accurate results.

11. REFERENCES

1. *Equivalent Standards for the Construction of Arctic Class Ships*, Ship Safety, Transport Canada, TP 12260, 1996.

2. Canadian Coast Guard, *Proposed Revisions to the Arctic Shipping Pollution Prevention Regulations*, TP 9981, December 1989.

3. DesRochers, C.G., E.J. Crocker, R. Kumar, et al., *Post-Yield Strength of Icebreaking Ship Structural Members*, Transportation Development Centre, Transport Canada, TP 11837E, February 1994.

4. DesRochers, C., J. Crocker, R. Kumar, et al., *Parametric Review of Post-Yield Buckling*, Transportation Development Centre, Transport Canada, TP 13016E, March 1997.

5. *MAESTRO v.8, Method for Analysis Evaluation and Structural Optimization*, Proteus Engineering, Stevensville, MD, USA, 1999.

6. *DSA-GP, Graphics System User's Manual*, Martec Limited, Halifax, NS, June 2000.

7. *VAST v8.2, Vibration and Strength Analysis Program: User's Manual*, Martec Limited, Halifax, NS, 2000.

8. *ANSYS*, ANSYS, Inc., Houston, PA, USA, 1995.

9. *ADINA 6.1, A Finite Element Program for Automatic Dynamic Incremental Non-linear Analysis*, K.J. Bathe, ADINA Engineering Inc., Watertown, MA, USA, 1992.

10. HyperMesh 3.1, Altair Engineering Inc., Troy, MI, USA, 1999.

11. Microsoft Excel v97, Microsoft Corporation, 1997.

12. Bleich, F., *Buckling Strength of Metal Structures*, McGraw-Hill, New York, 1952.

13. Danielson, D.A., "Analytical Tripping Loads for Stiffened Plates", *Int. J. Solids Structures,* Vol. 32, No. 8/9, pp. 1319-1328, 1995.

14. Daley, C. and C. Ferregut, *Strength and Stability of Framing for Ice Strengthening*, Fleet Technology, Ottawa, Ontario, June 1988.

15. *DNV Rules for Classification of Ships*, Det norske Veritas, Oslo, Norway, January 1998.

16. Ferregut, C. and C. Daley, *Towards an Understanding of Stiffener Tripping Under External Lateral Loading*, Fleet Technology, Ottawa, Ontario, January 1989.

17. Timoshenko, S.P. and J.M. Gere, *Theory of Elastic Stability (2nd Edition),* McGraw-Hill, New York, NY, USA, 1961.

18. MIL Systems, *Finite Element and Physical Modelling of Post Yield Stability of Icebreaker Structure*, Transportation Development Centre, Transport Canada, TP 12528E, July 1995.

19. Crocker, E.J., *Finite Element Analysis of Physical Panel Using ADINA*, Martec Limited, Halifax, NS, Martec Technical Report No. TR-95-17, 1995.

APPENDIX A

A Note on Design Equations for Stiffener Tripping

By: Lei Jiang

1 Derivation of Torsional Buckling Stress for Beams with Enforced Axis of Rotation and Under Uniform Axial Compression

The design equations for stiffener tripping in the CASPPR Hull Structure Regulations were obtained as special cases of the torsional-flexural buckling stress of stiffeners with enforced axis of rotation.

This buckling stress can be derived using an energy approach (Bleich, 1952), which involved construction of potential energy expression for axially loaded thin-walled beam structures. The potential energy equation obtained by Bleich (presented in Equation (4.5) in Daley and Ferregut's report, 1988 and reproduced as Equation 1 below) was quite general and included bending deformations about both principal axes and torsion about the shear centre. It should be noted that the displacement components, *u* and *v,* were measured with respect to the shear centre and θ denoted rotation about the shear centre.

Equation 1:

$$Y = \frac{1}{2}\int_0^l [EI_y u''^2 + EI_x v''^2 + E\Gamma\theta''^2 + GJ\theta'^2 - \sigma A(u'^2 + v'^2) - 2\sigma A y_o u'\theta' + 2\sigma A x_o v'\theta' - \sigma I_p \theta'^2]dz$$

This potential energy expression was derived based on the following assumptions:

1. The cross section of the beam is constant along the axial direction;
2. The geometry of the cross section remains unchanged during deformation;
3. The stresses due to the external load are in linear elastic range;
4. The pre-buckling displacements are negligibly small so that the potential energy expression can be derived based on the original configuration of the beam;
5. The axial pre-stresses are uniformly distributed over the beam cross section, so that the resultant of these stresses is through the centroid of the cross section. Lateral load and transverse bending moment were not considered.

For beams with enforced axis of rotation, the displacements at shear centre can be expressed in terms of the rotation about the enforced axis. For cross section that is symmetric about one of the principal axes, such as the Tee section, displacement components can be expressed as in Equations (4.3) and (4.4) in Daley and Ferregut (1988) (shown as Equations 2 and 3 below) where the assumption of small rotation had been utilized. Substituting this kinematic relation into the potential energy function resulted in a simplified expression that contained only one variable: the rotation about the enforced axis.

Equation 2: $u = a\,\theta$

Equation 3: $v = 0$

Once the potential energy was established, the buckling stress could be obtained in various ways. One method was to derive the governing differential equation of the problem, which

was Euler's equation in the calculus of variation. (Please note: this is different from Euler's formula for lateral buckling of beam columns.) The other approach was to use the Ritz method, which involved direct substitution of an assumed displacement field into the potential energy function and then minimizing the potential energy by differentiating with respect to the coefficient in the displacement function. With proper selected displacement field, these two methods should yield identical solutions.

The assumed half sine wave displacement pattern implied the following boundary conditions:

a) along the enforced axis of rotation, u=v=0 and no restraint on θ (like a hinge).
b) at both ends, simply supported boundary conditions were assumed so that u=θ=0 and u''=θ''=0.

Timoshenko and Gere (1961) considered the same problem using a slightly different approach. Instead of constructing potential energy function, they derived the system of governing differential equations for coupled torsional-flexural buckling of thin-walled beams. This system of equations included flexural deformations in vertical and lateral directions and torsional deformation about shear centre. For buckling with enforced axis of rotation, the use of the kinematic relations between displacements and rotation simplified the governing system of equations and reduced it to a single equation about θ, which was identical to Euler's equation obtained by Bleich using the energy method. Timoshenko and Gere (1961) presented their result in a more general form that did not require any symmetry of the beam cross section. The equation of Timoshenko and Gere was presented as Equation (4.31) in Daley and Ferregut's report (1988) and is reproduced as Equation 4 below.

Equation 4:

$$\sigma_T = \frac{\left[\Gamma + EI_y\left(y_o - y_c\right)^2 + EI_x\left(x_o - x_c\right)^2\right]\pi^2/\left(LU\right)^2 + GJ}{A\left[y_c^2 + x_c^2 - x_o^2 - y_o^2\right] + I_o}$$

where: I_x, I_y = moment of inertia with respect to principal axis of the section

x_o, y_o = coordinates of the shear centre with respect to centroid

x_c, y_c = coordinates of the enforced axis of rotation with respect to centroid

I_o = Polar moment of inertia about the shear centre

As mentioned above, the formula for buckling stress for beam with enforced axis of rotation was obtained from a single equation that was derived by substituting the kinematic relations into the governing system of equations. This reduced equation already includes torsion about the shear centre and bending in both vertical and lateral directions. In Daley and Ferregut (1988), however, this equation was coupled with the governing equation for vertical buckling of unconstrained beam and no detail was given. In my opinion, this coupling is not justified.

The torsional-flexural buckling formula obtained by Bleich and Timoshenko, et al. could be over-conservative because in their derivation, no rotational restraints were assumed along the enforced axis of rotation. Several attempts had been made to account for this effect by Adamchak (1979), Faulkner (1973, 1975, 1991, 1996) and Hughes (1983), among others.

2 Derivation of Critical Stress $\sigma_T \geq \sigma_y / 0.36$ and the Design Equations

From the formula for buckling stress, it is readily recognized that the reduced slenderness λ only depends on the geometric and material properties of the stiffener. In other words, for a given stiffener, this parameter can be uniquely determined. If σ_T is the true critical stress, we should then obtain the curve marked as "EULER" in Figure A-1, reproduced from Daley and Ferregut's report (1988) below.

However, the relationship between the true (experimentally measured?) critical stress σ_{CR} and the reduced slenderness parameter λ was shown as curve "e". To ensure that no buckling occurred prior to the complete yielding of the cross section (form of plastic hinge), σ_{CR} must be greater than or equal to the yield stress σ_y. This results in $\lambda \geq 0.6$ or equivalently $\sigma_T \geq \sigma_y / 0.36$.

To gain a better understanding of this relation, we could consider the intersection of curve "e" and vertical line corresponding to $\lambda = 1$. At this intersection, we have $\sigma_T = \sigma_y$, however, $\sigma_{CR} < \sigma_y$.

However, in the 1998 version of the *DNV Rules for Classification*, the critical buckling stress was determined as:

$$\sigma_{CR} = \begin{cases} \sigma_T, & when\ \ \sigma_T < \sigma_Y / 2 \\ \sigma_Y \left(1 - \dfrac{\sigma_Y}{4\sigma_T} \right), & when\ \sigma_T > \sigma_Y / 2 \end{cases}$$

Based on this equation, σ_{CR} never exceeds the yield stress.

Figure A-1

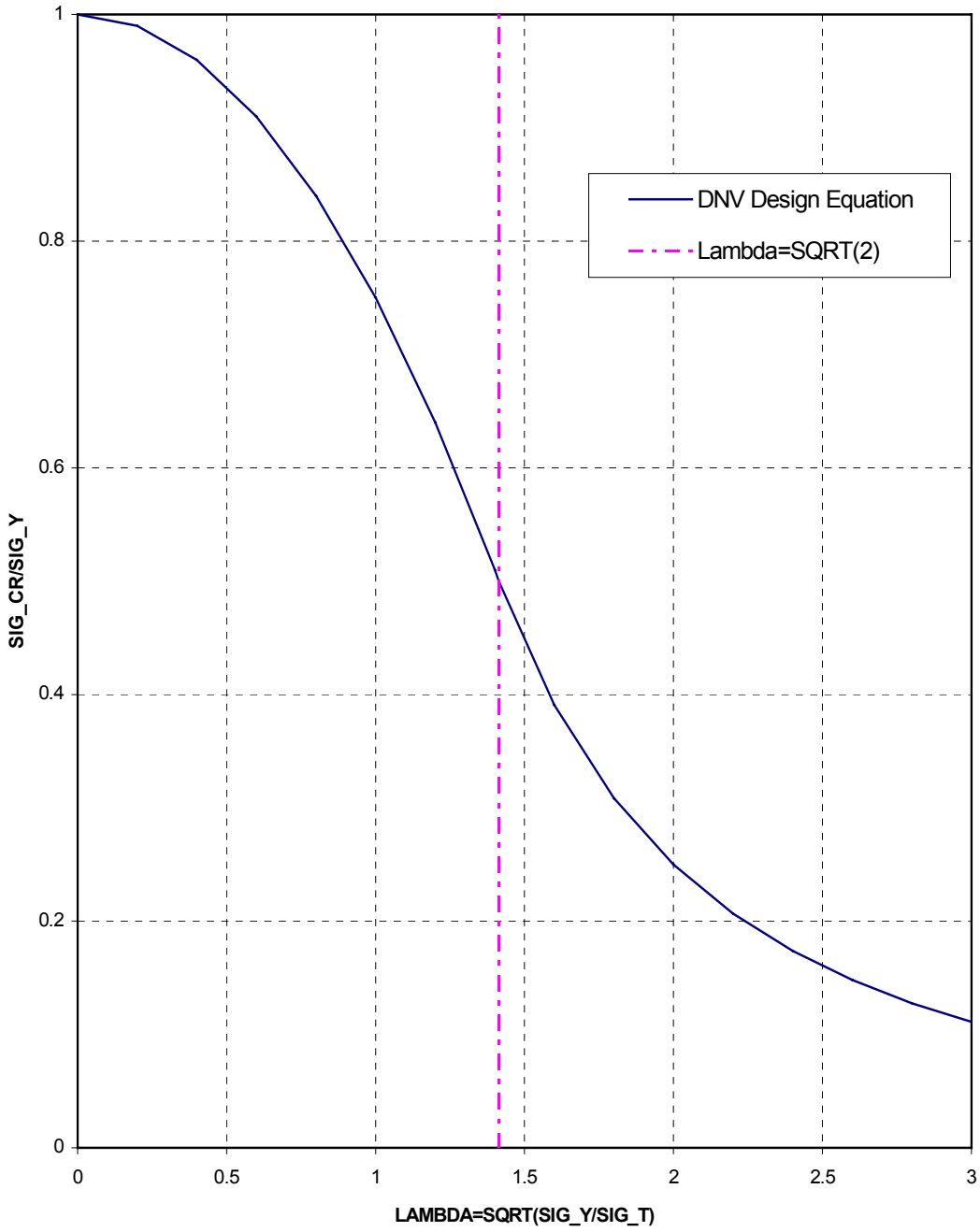

The design equations in the ASPPR standards were derived by combining the torsional-flexural buckling stress and the requirement $\sigma_T \geq \sigma_y / 0.36$. Two extreme cases covered by the buckling equation were considered. If the section is a shallow thick section, the torsional strength would predominate, whereas if the section is deep and thin, the warping and lateral bending strength would be predominate. To obtain design equations in their simplest form,

average values of geometric parameters of the beam cross section, such as the ratio of the flange width and the web height and the ratio of the flange and web thicknesses for Tee section, have been utilized.

Some errors were identified in Daley and Ferregut's report (1988) in the treatment of the flat bar cross section. [Note: Apparent errors are identified in this Appendix, following Section 4.]

3 Stiffener Tripping Under Lateral Loads

Stiffener tripping under lateral loads and vertical bending moments were also considered by Bleich and Timoshenko, et al. Some of the results were summarized by Ferregut and Daley (1989).

The potential energy function obtained by Bleich considered axial compressions (acting on the shear centre), vertical bending moments and distributed load acting in the mid-plane of the web. The assumptions used in this derivation were similar to those presented earlier, with one additional assumption stating that the direction of the vertical load remains constant and does not change to follow the displaced shape of the structure.

For beams with enforced axis of rotation subjected to a constant bending moment, this theory predicted that only moments caused by compressive stress in flange can lead to buckling of the stiffener.

Ferregut and Daley (1989) had attempted to solve the tripping buckling problem with flange in tension. However, this attempt was unsuccessful.

Danielson (1995) has recently considered buckling of stiffened plate under combined axial compressive stress, uniform lateral pressure and uniform bending moment. An energy method was utilized based on the von Karman plate equation and a non-linear beam theory developed previously by the author. The potential energy expression was obtained using a number of assumptions including:

1. The plate and stiffener material was elastic, linear and isotropic;
2. The bases of the stiffeners were clamped to the plate along the line of attachment;
3. The pre-buckling displacements were less than the maximum thickness of the structure;
4. The plate and stiffeners were think and slender.

Critical axial stress was found as a function of the magnitudes of the lateral pressure, bending moment, initial geometric imperfection and residual stress. It is very interesting to note that the first three parameters all have stabilization effects on the stiffened plate structure.

The problem that we are facing involves large displacements/rotations and large-scale, non-uniform plastic deformations in the pre-buckling range. Analytical solutions dealing these extremely complicated situations have not been identified at the present time. A more detailed literature search should be conducted. However, it is highly possible that analytical solutions for this problem do not exist because of its complexity.

4 References

Bleich, F., *Buckling Strength of Metal Structures,* McGraw-Hill, New York, 1952.

Danielson, D.A., "Analytical Tripping Load for Stiffened Plates", *Int. J. Solids Structures*, Vol. 32, No. 8/9, pp. 1319-1328, 1995.

Daley, C. and C. Ferregut, *Strength and Stability of Framing for Ice Strengthening*, Fleet Technology, June 1988.

DNV Rules for Classification of Ships, January 1998.

Ferregut, C. and C. Daley, *Towards an Understanding of Stiffener Tripping Under External Lateral Loading*, Fleet Technology, January 1989.

Timoshenko, S.P. and J.M. Gere, *Theory of Elastic Stability (2nd Edition)*, McGraw-Hill, New York, 1961.

Errors identified in Daley and Ferregut's report (1988) in the treatment of the flat bar cross section:

In the report by Daley and Ferregut (1988), Equation (4.29) should be:

$$\sigma_T = \frac{\pi^2 E}{(LU)^2}\left[\frac{a^2 I_y + \Gamma}{I_{pc}}\right]$$

where I_{pc} is the polar moment of inertia of the cross section with reference to the enforced centre of rotation (as defined on page 11 of the same report). For a flat bar with centre of rotation at the toe, we have:

$$I_{pc} = \frac{(HW)^3 \times TW}{3}.$$

However, the equation shown in the report is:

$$\sigma_T = \frac{\pi^2 E}{(LU)^2}\left[\frac{a^2 I_y + \Gamma}{I_p}\right]$$

where

$$I_p = (HW)^3 \times TW\ .$$

No further explanation of variable I_p is given in the report.

APPENDIX B

Excerpt from FURTHER ENHANCEMENT AND VERIFICATION

OF THE NONLINEAR BUCKLING CAPABILITY IN DSA-VAST

By: Lei Jiang

(Martec Technical Note No. TN-00-06, Martec Limited, November 2000)

INTRODUCTION

In most finite element programs, linearized buckling analysis capabilities are associated with the solution of an eigenvalue problem formulated by linearizing the non-linear equilibrium equations at the stress-free reference configuration. It is well known that this buckling analysis algorithm can only predict critical buckling loads with acceptable accuracy for problems with an almost linear response in the pre-buckling regime. For problems showing a strong non-linearity prior to buckling, the linearized buckling analysis often results in significant overestimation of the critical buckling load level. This is obviously undesirable in practical engineering analysis.

One way to solve this difficulty is to formulate a linearized buckling (eigenvalue) problem in terms of the current tangent stiffness matrices around a converged equilibrium point along the non-linear solution path. Since the tangent stiffness matrices contain information on the non-linearities involved in this problem, these eigen solutions can provide more accurate predictions to the critical load level. Such an analysis option has been implemented in the VAST program [1], in which the user is permitted to terminate a non-linear run in the pre-buckling range and perform a linearized buckling analysis. This capability in VAST is referred to as Advanced Buckling Analysis [2].

The VAST advanced buckling analysis capability has been verified previously using two buckling problems with known analytical solutions [1]. The first problem is the buckling of a beam column subjected to an axial compression, and the second is the buckling of a simply supported plate subjected to uniform biaxial in-plane stresses. The verification results are documented in Reference [1]. However, since its development, it has been discovered that this buckling analysis capability produces spurious numerical results for some non-linear problems, especially for those having significantly non-linear pre-buckling responses. In order to gain an improved understanding of the performance and limitations of this numerical algorithm, its theoretical derivation and computer implementation have been reconsidered in the present study. Additional numerical verifications have also been conducted by using non-linear benchmark problems involving non-linear pre-buckling responses. These problems include clamped-clamped shallow arch and hinged shallow spherical shell subjected to centre point loads. After modifying a number of details on the implementation of the advanced buckling algorithm, VAST produced excellent results for all of the test problems.

SOME FURTHER CONSIDERATIONS ON THEORETICAL DERIVATIONS

The advanced buckling capability in VAST was developed based on an algorithm proposed by Bathe and Dvorkin [3] using a linear extrapolation of the tangent stiffness matrix. Denoting the tangent stiffness matrices of a structure at the end of the current and previous equilibrium points as ${}^{t}\boldsymbol{K}_{T}$ and ${}^{t-\Delta t}\boldsymbol{K}_{T}$, and the corresponding load parameters as ${}^{t}\lambda$ and ${}^{t-\Delta t}\lambda$, respectively, the tangent stiffness matrix at an arbitrary load level λ was assumed as:

$$\boldsymbol{K}_{T}(\lambda) = {}^{t-\Delta t}\boldsymbol{K}_{T} + \mu \left({}^{t}\boldsymbol{K}_{T} - {}^{t-\Delta t}\boldsymbol{K}_{T} \right) \tag{1a}$$

where

$$\mu = \frac{\lambda - {}^{t-\Delta t}\lambda}{{}^{t}\lambda - {}^{t-\Delta t}\lambda}. \tag{1b}$$

Let λ indicate the load level at which buckling or collapse would occur in an incremental analysis, we then have:

$$det\left(\boldsymbol{K}_T(\lambda)\right) = 0. \tag{2}$$

Substituting Equation (1a) into (2) leads to an eigenvalue problem as:

$${}^{t-\Delta t}\boldsymbol{K}_T\boldsymbol{\phi} = -\mu\left({}^{t}\boldsymbol{K}_T - {}^{t-\Delta t}\boldsymbol{K}_T\right)\boldsymbol{\phi}. \tag{4}$$

In Reference [3], Bathe and Drovkin have suggested rearranging the terms in Equation (4) to establish an equivalent eigenvalue problem as:

$${}^{t}\boldsymbol{K}_T\boldsymbol{\phi} = -\gamma\ {}^{t-\Delta t}\boldsymbol{K}_T\,\boldsymbol{\phi} \tag{5a}$$

where

$$\gamma = \frac{1-\mu}{\mu}. \tag{5b}$$

Once the eigenvalue γ is obtained, the buckling load parameter can be readily computed using Equations (5b) and (1b).

Although the above algorithm is effective in evaluating structural instability of non-linear systems, it also has a number of disadvantages. We first consider the effect of the change of variable defined in Equation (5b). The relation between μ and γ is displayed graphically in Figure 1. It was observed that when μ is greater than 1.0, the eigenvalues of eigenvalue problem (5a) become very closely spaced and approach –1.0. This fact indicates a number of potential numerical problems: (1) a small error in eigenvalue γ may be amplified to a huge error in μ and eventually in the predicted load parameter λ, (2) the convergence rate of the eigen solver may be extremely slow, and (3) the eigen solutions may be extremely sensitive to the accuracy of the arithmetic operations. Based on Figure 1, it was also realized that the best performance of the eigenvalue problem solver can be reached when $\mu \to 1$. This occurs when critical load parameter λ is close to ${}^{t}\lambda$. As an attempt to avoid using the change of variable in (5b), an alternative eigenvalue problem has been implemented and tested. This eigenvalue problem was formulated directly in terms of the load parameter λ as:

$$\left({}^{t}\lambda^{\,t-\Delta t}\boldsymbol{K}_T - {}^{t-\Delta t}\lambda\,{}^{t}\boldsymbol{K}_T\right)\boldsymbol{\phi} = -\lambda\left({}^{t}\boldsymbol{K}_T - {}^{t-\Delta t}\boldsymbol{K}_T\right)\boldsymbol{\phi}. \qquad (6)$$

Unfortunately, numerical experiments indicated that this formulation was less effective than the one defined in (5a). This is probably because in (6) the matrices are too sensitive to the accuracy of arithmetic operations and a small round-off error may cause completely incorrect eigen solutions.

Another limitation of this advanced buckling analysis algorithm is associated with the linear approximation of the tangent stiffness matrix as defined in Equation (1a). This approximation is obviously not applicable to the extreme cases where the structure has either a very stiff or a very highly non-linear pre-buckling response. In addition, it should be realized that this buckling analysis algorithm is based on an overall measure of the properties of the tangent stiffness matrix. Because plastic deformations can also cause a reduction of the structural tangent stiffness, the eigenvalues and eigenvectors obtained in the buckling analysis may not always be interpreted as critical load levels and buckling mode shapes. This point will be further demonstrated later using a numerical example.

NUMERICAL VERIFICATIONS

Test Case 1 : Buckling of a Simply-Supported Plate Under Uniform In-Plane Stresses

In this test problem, buckling of a simply-supported square plate compressed by uniform stresses in two directions was considered. The problem is depicted in Figure 2. The in-plane dimension of the plate is 10×10, and the thickness is 0.1. The elastic isotropic material properties are $E=1.2\times10^8$ and $\nu=0.3$. The reference uniform stress is $\sigma_0=10^3$. Due to symmetry, one quarter of the plate was modelled by using a 10×10 mesh of 4-noded quadrilateral shell elements.

The analytical solution to the buckling stress for this problem has been given by Timoshenko [4] as:

$$\sigma_X = \sigma_Y = \frac{\pi^2 E h^2}{6\left(1-\nu^2\right)a^2}$$

where *a* and *h* denote the edge length and thickness of the plate, respectively. Substitution of the geometry and material properties defined above into this formula results in a buckling stress of 21.6914×10^3, which corresponds to a load parameter of 21.6914.

In the present study, a fully non-linear analysis was first performed to obtained a complete non-linear solution to this problem. In order to trigger the desired buckling mode, a small vertical force was applied at the plate centre in the non-linear run. The load-centre deflection curve predicted by the non-linear analysis is displayed in Figure 3. Once the non-linear analysis was completed, five advanced buckling analyses were performed by restarting VAST from the fifth, fourth, third, second and first solution step, respectively. The first critical load

parameters predicted by these analyses are summarized in Table 1, along with the load parameters at the end of these solution steps. An excellent convergence property of the advanced buckling analysis algorithm is observed. The deformed shape predicted by non-linear analysis at the end the fifth load step and the first buckling mode predicted by advanced buckling analysis performed at the end of the third step are compared in Figure 4. The close agreement between these deformed shapes indicates the ability of the advanced buckling analysis algorithm to predict the correct failure mode of structures. The buckling load was also obtained using the regular linearized buckling analysis and the result is also included in Table 1. For this particular problem, the buckling stress predicted by the regular buckling analysis is in good agreement with those obtained using the advanced buckling algorithm.

Table 1: Comparison of Critical Loads of the Simply-Supported Plate Under Uniform In-Plane Stresses Predicted by Various Buckling Analysis Methods

Solution Methods	Load Step No.	Critical Load Parameter λ_{CR}	Load Parameter at which advanced buckling analysis is performed, ${}^{t}\lambda$
Advanced Buckling	1	21.796	11.191
Advanced Buckling	2	21.779	16.309
Advanced Buckling	3	21.734	18.477
Advanced Buckling	4	21.664	19.614
Advanced Buckling	5	21.603	20.309
Regular Buckling		21.799	
Analytical [4]		21.691	

[Tests cases 2, 3 and 4 were removed to abbreviate this appendix.]

CONCLUSIONS

In this technical note, the theoretical derivation of the advanced buckling analysis algorithm and its implementation in VAST have been seriously reconsidered. A number of potential problems and limitations of this algorithm were investigated and the computer program was enhanced. This capability has been verified using a number of example problems involving different types of non-linearities and excellent results have been obtained for all test problems. The numerical verification indicates the effectiveness of the advanced buckling analysis capability, but also suggested that the results of the advanced buckling analyses must be interpreted with caution!

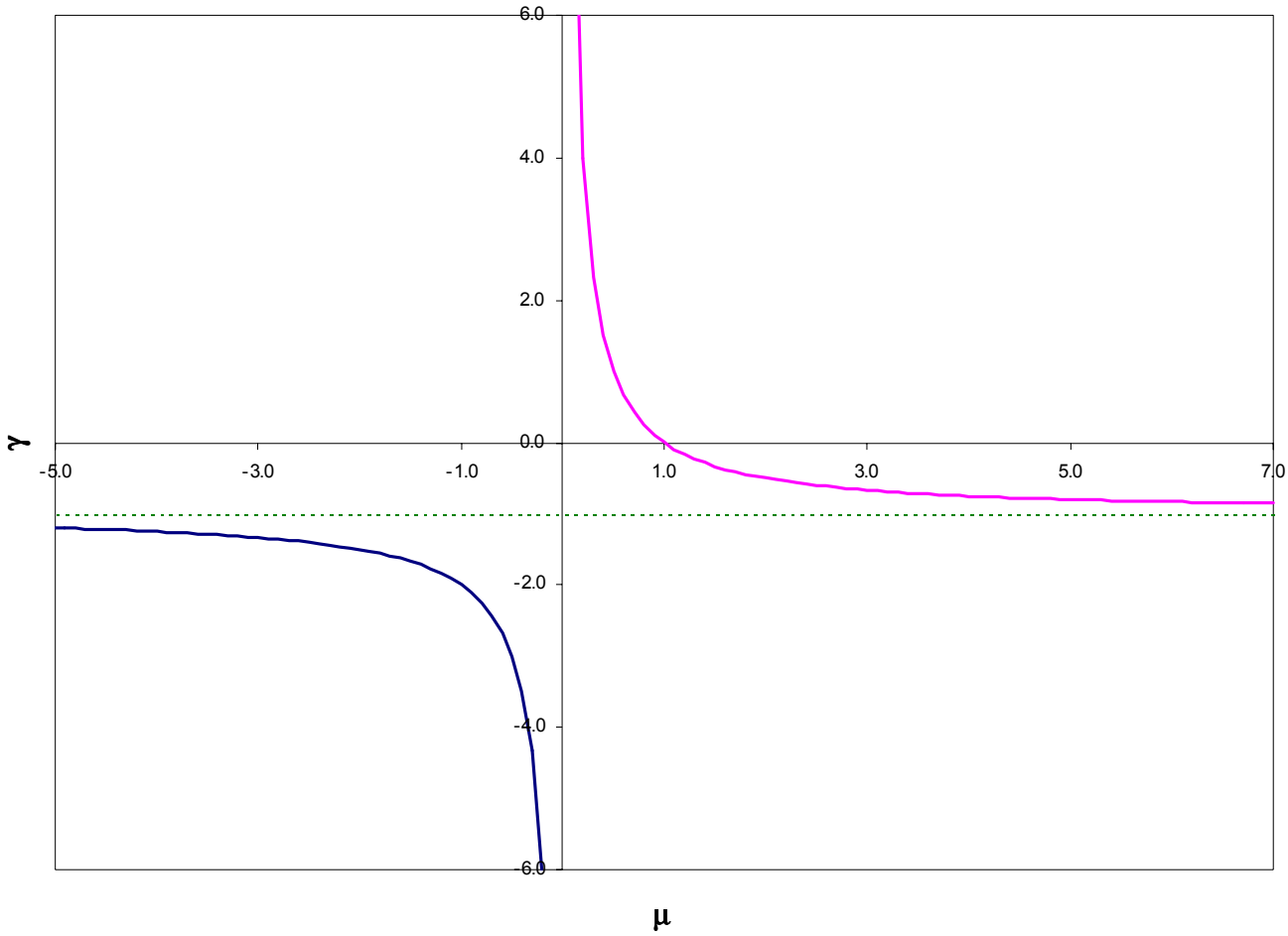

Figure 1: Relationship Between Load Parameter Ratio μ and Eigenvalue γ.

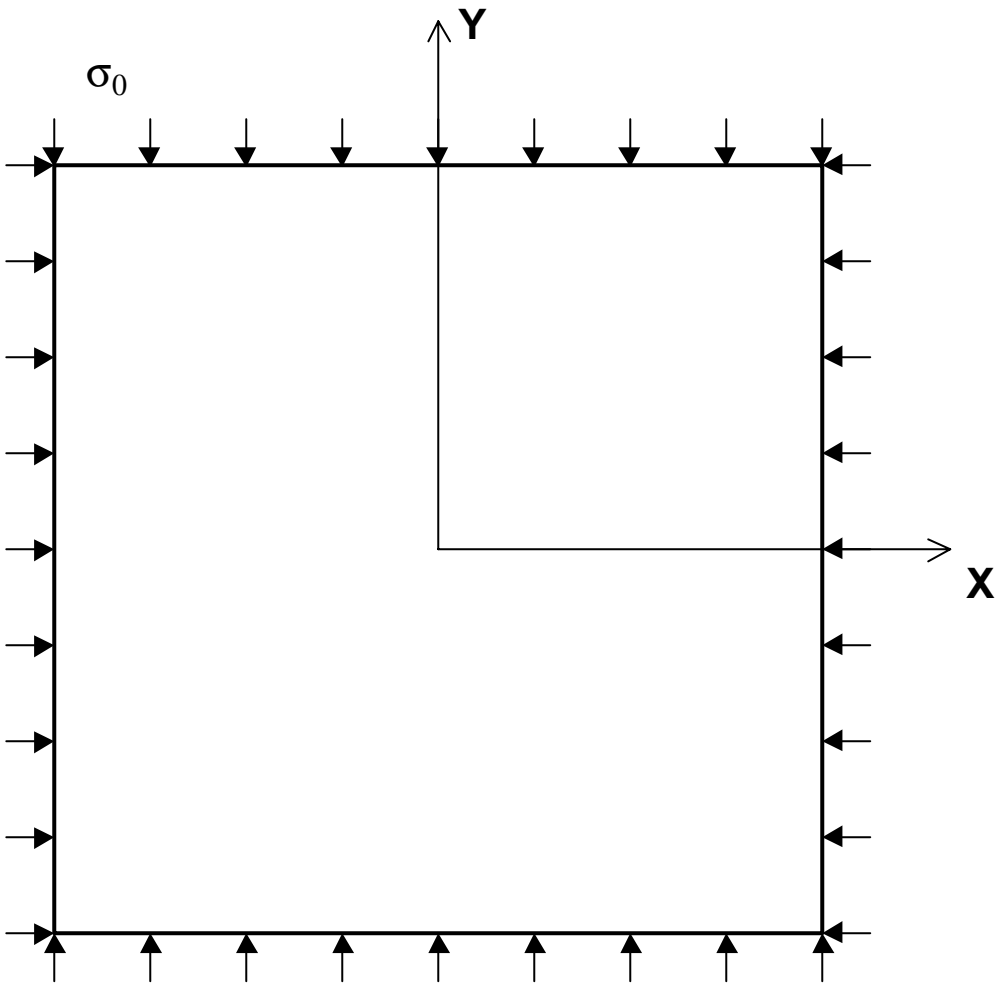

Figure 2: A Simply-Supported Plate Subjected to Uniform Bi-Axial In-Plane Stresses.

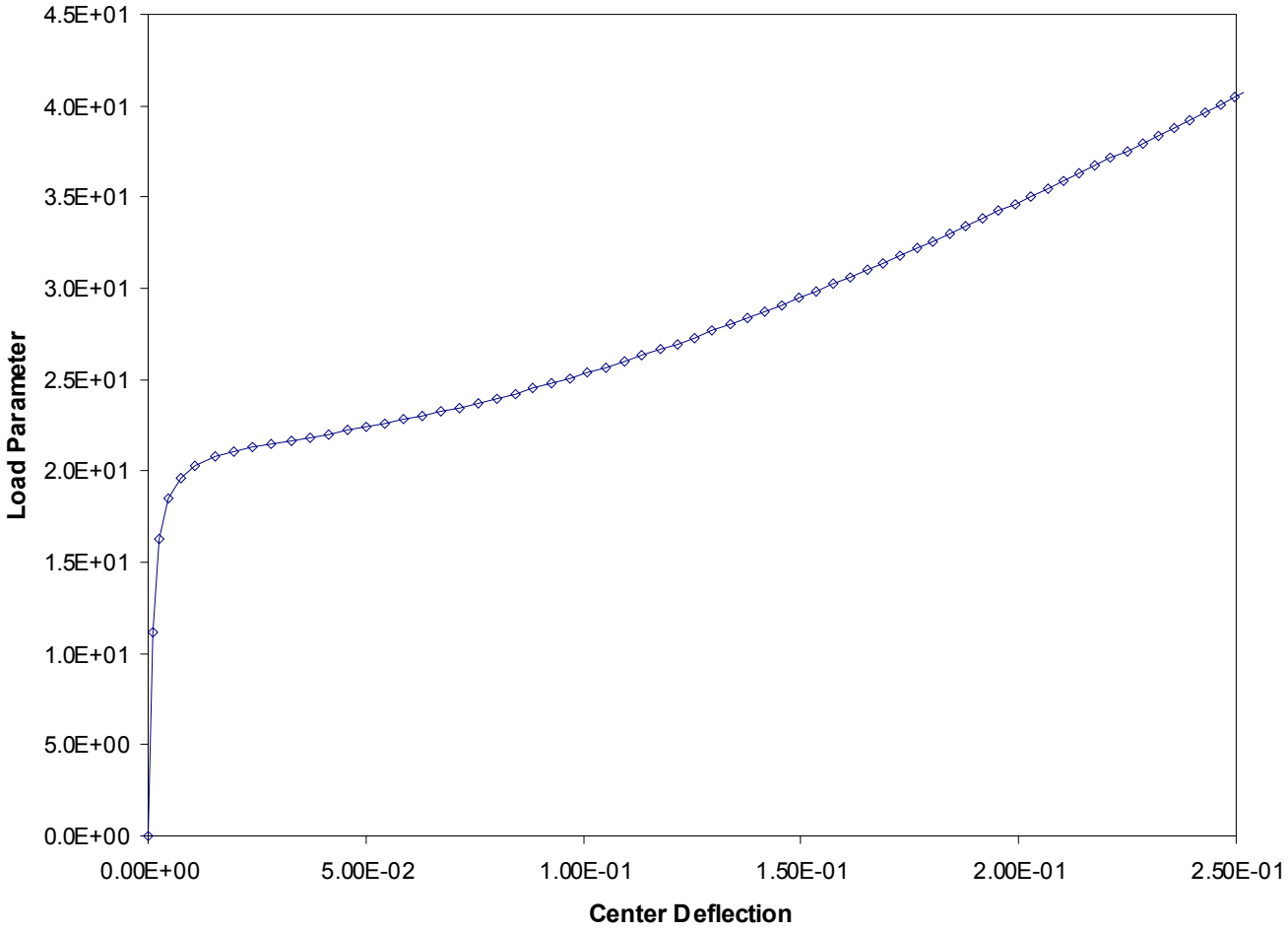

Figure 3: Load-Center Deflection Curve of the Simply-Supported Plate Subjected to Uniform Bi-Axial In-Plane Stresses Obtained by Fully Nonlinear Analysis.

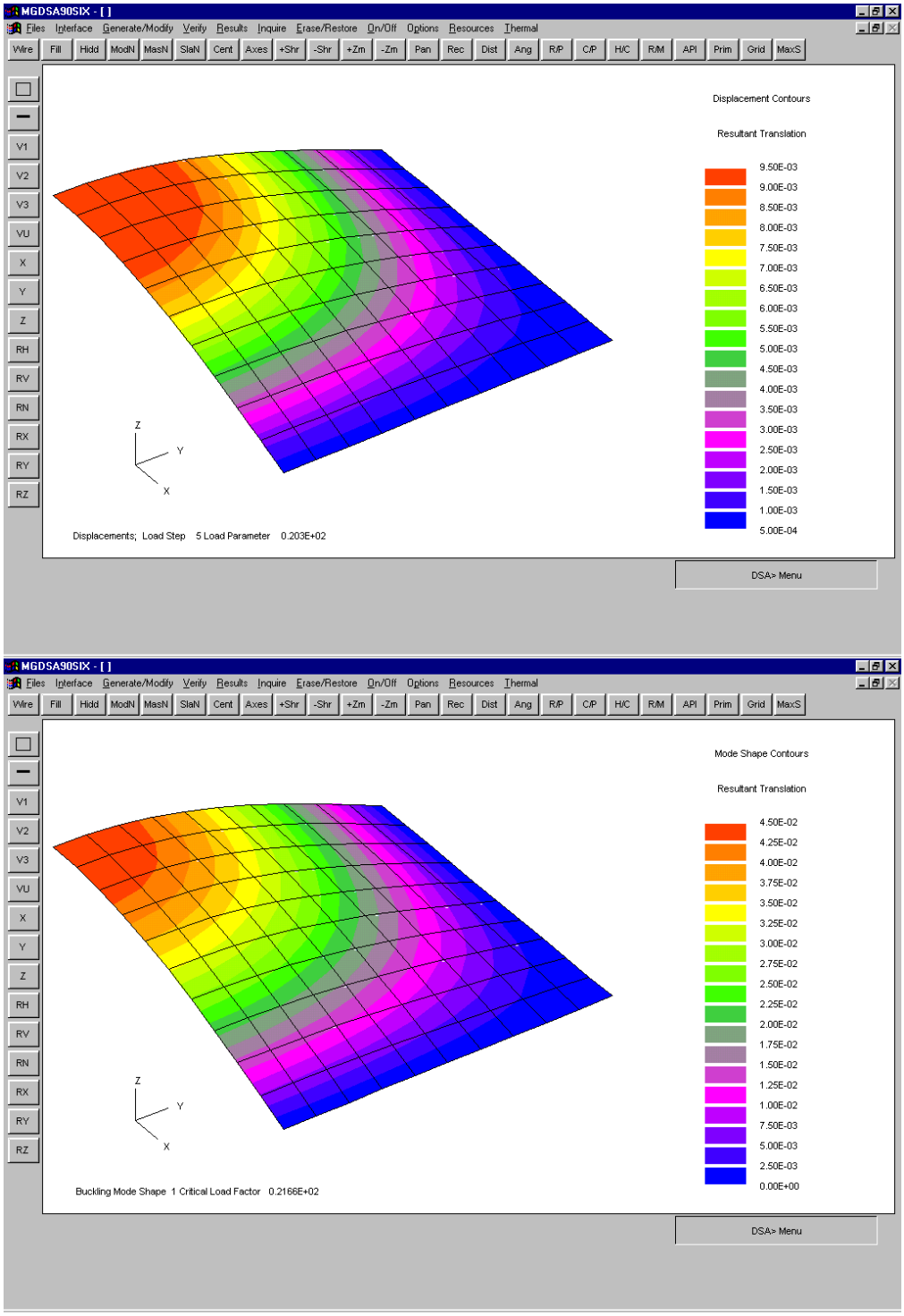

Figure 4: Comparison of Deformed Configuration Predicted by Nonlinear Analysis and Eigenmode Predicted by Advanced Buckling Analysis for the Simply-Supported Plate.

REFERENCES

[1] L. JIANG and M.W. CHERNUKA, *Implementation of a Large Displacement Capability for VAST – Phase II*, Martec Technical Report TR-93-14, April 1993.

[2] *VAST User's Manual*, Version 8.1, Martec Limited, Halifax, 2000.

[3] K.J. BATHE and E.N. DVORKIN, "On the Automatic Solution of Non-linear Finite Element Equations", *Computers & Structures*, Vol. 17, pp. 871-879, 1983.

[4] S. TIMOSHENKO, *Theory of Elastic Stability*, McGraw-Hill, New York, 1936.

[5] R.H. LEICESTER, "Finite Deformations of Shallow Shells", *Proc. ASCE*, Vol. 94 (EM6), pp. 1409-1423, 1968.

[6] K.J. BATHE and L.W. HO, "A Simple and Effective Element for Analysis of General Shell Structures", *Computers & Structures*, Vol. 13, pp. 673-681, 1981.